5
Results & Discussion

5.1 OPTIMIZATION OF PHYSICOCHEMICAL AND THERMOPHYSICAL PROPERTIES

In this chapter discussion about development of regression models on the basis of various physicochemical and thermophysical properties of fluxes obtained during experimentation for basic, rutile-basic and rutile-acidic flux systems has been carried out. Adequacy of developed regression models were checked using analysis of variance (ANOVA).

5.1.1 Development and analysis of physicochemical and thermophysical responses for fluxes

Development and analysis of various physicochemical and thermophysical properties such as density, grain fineness number, percentage weight change, change in enthalpy, thermal conductivity, thermal diffusivity, and specific heat in terms of individual, binary and ternary flux components for three flux systems was conducted. Table 5.1-5.2 shows the results of various physicochemical and thermophysical properties. Results of density, grain fineness number, percentage weight change, and change in enthalpy for basic, rutile-basic, and rutile-acidic flux systems shown in table 5.1. Table 5.2 shows the results for thermal conductivity, thermal diffusivity, and specific heat for three flux systems.

5.1.1.1 Regression model of density, grain finesses number, weight loss, change in enthalpy, thermal conductivity, thermal diffusivity and specific heat for three flux systems

Quadratic, cubic, special cubic, and reduced special cubic regression models of density, grain fineness number, percentage weight change, change in enthalpy, thermal conductivity, thermal diffusivity, and specific heat were developed in terms of individual, binary and ternary flux components. Equations A1-A7, A8-A14, and A15-A21 show the regression model equations for basic, rutile-basic, and rutile-acidic flux systems. Regression equations (A1-A21) given in Appendix 1.

Table 5.1: Density, grain fineness number, weight loss and change in enthalpy for basic, rutile-basic and rutile-acidic flux systems

S.No	*Density (g/cm^3)*			*Grain finesse number*			*Percentage weight change*			*Change in enthalpy*		
Flux	Basic system	Rutile-basic system	Rutile-acidic system	Basic system	Rutile-basic system	Rutile-acidic system	Basic system	Rutile-basic system	Rutile-acidic system	Basic system	Rutile-basic system	Rutile-acidic system
F1	1.312	1.401	1.422	9.152	8.968	6.111	0.924	4.21	1.253	-5535.23	-2969.61	-6821.89
F2	1.372	1.399	1.685	7.699	8.218	6.415	1.828	5.422	1.353	-6490.00	-4073.69	-7149.10
F3	1.398	1.423	1.490	7.231	8.885	6.053	1.388	0.416	0.802	-6001.11	-2963.80	-7873.04
F4	1.421	1.344	1.598	8.120	7.733	6.474	0.615	1.178	0.399	-5320.71	-5849.76	-7409.08
F5	1.511	1.376	1.687	7.934	7.985	6.718	0.495	7.032	1.568	-6001.11	-3312.89	-7486.81
F6	1.411	1.389	1.591	7.195	8.405	6.356	4.261	6.015	0.899	-6113.70	-4336.06	-6523.53
F7	1.571	1.422	1.471	7.296	7.477	6.359	1.688	1.739	1.627	-6501.24	-4733.41	-7528.41
F8	1.537	1.351	1.455	7.191	8.052	6.631	1.028	8.979	1.650	-5005.47	-9171.25	-7318.79
F9	1.492	1.321	1.501	7.207	7.681	5.986	4.060	7.022	1.631	-4769.69	-7128.73	-8062.63
F10	1.500	1.361	1.622	7.622	8.069	6.411	0.320	0.790	0.373	-4817.67	-6699.48	-6485.05
F11	1.521	1.299	1.662	7.368	7.627	6.190	0.461	0.312	1.098	-5694.51	-5411.13	-6620.23
F12	1.565	1.351	1.552	7.475	7.536	5.945	0.567	0.546	1.414	-6209.34	-5824.77	-6512.30
F13	1.581	1.400	1.588	8.013	7.853	6.211	1.470	1.289	0.883	-7601.35	-9417.02	-8386.16
F14	1.531	1.451	1.578	7.423	8.387	6.502	1.258	1.170	1.533	-6473.88	-7673.85	-7703.58
F15	1.510	1.331	1.672	7.501	8.865	6.023	1.181	0.916	0.567	-5338.42	-6518.27	-8381.59
F16	1.580	1.388	1.499	7.222	8.626	6.721	0.823	1.064	1.637	-7126.64	-8082.02	-9210.19
F17	1.544	1.377	1.662	7.825	8.931	6.431	1.088	1.058	0.633	-6759.15	-7009.27	-8183.23
F18	1.590	1.399	1.599	7.923	8.282	6.602	0.569	0.813	1.518	-5103.70	-6030.13	-7019.96
F19	1.600	1.366	1.699	7.124	8.301	6.712	0.794	1.092	0.563	-5667.12	-6662.12	-7239.31
F20	1.580	1.388	1.677	7.932	7.923	6.751	0.645	1.152	0.725	-6020.21	-6861.95	-10728.8
F21	1.522	1.411	1.621	7.862	7.865	6.333	0.578	2.616	0.612	-5094.21	-7922.35	-8388.26

Table 5.2: Thermal conductivity, thermal diffusivity and specific heat for basic, rutile-basic and rutile-acidic flux systems

S.No	*Thermal conductivity (W/mK)*			*Thermal diffusivity (mm^2/s)*			*Specific heat (MJ/m^3K)*		
Flux	Basic system	Rutile-basic system	Rutile-acidic system	Basic system	Rutile-basic system	Rutile-acidic system	Basic system	Rutile- basic system	Rutile-acidic system
F1	0.145	0.145	0.239	0.207	0.266	0.327	0.702	0.678	0.731
F2	0.122	0.138	0.243	0.221	0.244	0.297	0.551	0.604	0.821
F3	0.139	0.127	0.221	0.245	0.361	0.272	0.568	0.458	0.813
F4	0.134	0.137	0.236	0.190	0.196	0.320	0.705	0.713	0.739
F5	0.150	0.152	0.232	0.273	0.393	0.275	0.549	0.519	0.845
F6	0.135	0.148	0.246	0.206	0.289	0.240	0.656	0.651	0.926
F7	0.138	0.167	0.222	0.219	0.417	0.250	0.629	0.448	0.619
F8	0.157	0.146	0.211	0.329	0.20	0.220	0.478	0.741	0.958
F9	0.141	0.140	0.250	0.195	0.287	0.363	0.725	0.477	0.688
F10	0.207	0.147	0.235	0.403	0.181	0.326	0.513	0.704	0.720
F11	0.195	0.153	0.233	0.322	0.405	0.303	0.605	0.411	0.767
F12	0.247	0.151	0.241	0.365	0.222	0.286	0.677	0.620	0.842
F13	0.166	0.187	0.237	0.295	0.303	0.397	0.564	0.504	0.597
F14	0.172	0.165	0.233	0.410	0.304	0.304	0.419	0.499	0.765
F15	0.189	0.177	0.215	0.507	0.193	0.260	0.373	0.758	0.830
F16	0.178	0.188	0.225	0.297	0.261	0.281	0.598	0.578	0.801
F17	0.175	0.173	0.215	0.338	0.242	0.299	0.519	0.713	0.718
F18	0.161	0.180	0.236	0.293	0.279	0.320	0.549	0.635	0.739
F19	0.173	0.194	0.237	0.257	0.159	0.302	0.674	0.912	0.782
F20	0.183	0.173	0.217	0.351	0.248	0.256	0.523	0.698	0.848
F21	0.158	0.204	0.238	0.278	0.278	0.326	0.568	0.698	0.729

5.1.1.2 Analysis of variance for density grain finesses number, weight loss, change in enthalpy, thermal conductivity, thermal diffusivity and specific heat for three flux systems

There were many insignificant terms observed in the models during the regression analysis of different physicochemical and thermophysical properties. So to improve the physicochemical & thermophysical properties of each model, a backward elimination procedure used in A1-A21 equations. Backward elimination is a model reduction method used to eliminate the insignificant terms present in the existing models. The hierarchy of models adjusted by removing the irrelevant terms in the backward analysis. ANOVA results after backward elimination shown in table 5.3-5.5 for three flux systems.

Table 5.3: ANOVA results of various physicochemical and thermophysical properties for basic flux system

Properties	*Source*	*SS*	*DF*	*MS*	*F value*	*P value*	R^2 *value*	*Status*
GFN	Model	3.48	9	0.39	4.29	0.0133	0.77	Significant
	Linear	0.33	3	0.11	1.20	0.3548		Not Significant
	$CaO.SiO_2$	0.71	1	0.71	7.86	0.0172		Significant
	$CaO.CaF_2$	0.13	1	0.13	1.42	0.2578		Not Significant
	$CaO.Al_2O_3$	0.059	1	0.059	0.65	0.4357		Not Significant
	$SiO_2.CaF_2$	1.07	1	1.07	11.85	0.0055		Significant
	$SiO_2.Al_2O_3$	0.45	1	0.45	5.00	0.0471		Significant
	$CaF_2.Al_2O_3$	0.17	1	0.17	1.84	0.2024		Not Significant
	Residual	0.99	11	0.090				
	Total	4.48	20					
Density	Model	0.041	13	3.189E-003	3.59	0.0487	0.86	Significant
	Linear	2.592E-003	3	8.640E-004	0.97	0.4579		Not Significant
	$CaO.SiO_2$	1.924E-003	1	1.924E-003	2.17	0.1846		Not Significant

	$CaO.CaF_2$	0.011	1	0.011	12.05	0.0104		Significant
	$CaO.Al_2O_3$	2.761E-003	1	2.761E-003	3.11	0.1213		Not Significant
	$SiO_2.CaF_2$	9.378E-003	1	9.378E-003	10.55	0.0141		Significant
	$SiO_2.Al_2O_3$	8.626E-003	1	8.626E-003	9.71	0.0169		Significant
	$CaF_2.Al_2O_3$	5.028E-003	1	5.028E-003	5.66	0.0490		Significant
	$CaO.SiO_2.CaF_2$	9.221E-005	1	9.221E-005	0.10	0.7568		Not Significant
	$CaO.SiO_2.Al_2O_3$	8.144E-004	1	8.144E-004	0.92	0.3703		Not Significant
	$CaO.CaF_2.Al_2O_3$	0.016	1	0.016	17.45	0.0041		Significant
	$SiO_2.CaF_2.Al_2O_3$	4.59E-003	1	4.59E-003	5.17	0.572		Not Significant
	Residual	6.220E-003	7	8.886E-004				
	Total	0.048	20					
Weight loss	Model	20.03	9	2.23	10.59	0.0003	0.89	Not Significant
	Linear	7.54	3	2.51	11.96	0.0009		Significant
	$CaO.SiO_2$	2.76	1	2.76	13.12	0.0040		Significant
	$CaO.CaF_2$	0.18	1	0.18	0.87	0.3707		Not Significant
	$CaO.Al_2O_3$	0.88	1	0.88	4.20	0.0649		Not Significant
	$SiO_2.CaF_2$	0.46	1	0.46	2.19	0.1667		Not Significant

	SiO_2. Al_2O_3	2.66	1	2.66	12.67	0.0045		Significant
	CaF_2.Al_2O_3	0.37	1	0.37	1.75	0.2126		Not Significant
	Residual	2.31	11	0.21				
	Total	22.34	20					
Thermal Conductivity	Model	0.014	10	1.391E-003	4.33	0.0149	0.81	Significant
	Linear	5.680E-003	3	1.893E-003	5.90	0.0139		Significant
	$CaO.SiO_2$	3.332E-004	1	3.332E-004	1.04	0.3323		Not Significant
	$CaO.CaF_2$	1.287E-004	1	1.287E-004	0.40	0.5408		Not Significant
	$CaO.Al_2O_3$	6.795E-004	1	6.795E-004	2.12	0.1763		Not Significant
	$SiO_2.CaF_2$	1.476E-003	1	1.476E-003	4.60	0.0576		Not Significant
	$SiO_2.Al_2O_3$	3.197E-003	1	3.197E-003	9.96	0.0102		Significant
	$CaO.SiO_2.CaF_2$	9.341E-004	1	9.341E-004	2.91	0.1188		Not Significant
	$CaO.SiO_2$. Al_2O_3	1.822E-003	1	1.822E-003	5.68	0.0384		Significant
	Residual	3.210E-003	10	3.210E-003				
	Total	0.017	20					

Thermal Diffusivity	Model	0.10	9	0.012	4.34	0.0127	0.78	Significant
	Linear	0.051	3	0.017	6.33	0.0094		Significant
	$CaO.SiO_2$	0.026	1	0.026	9.58	0.0102		Significant
	$CaO.CaF_2$	4.294E-003	1	4.294E-003	1.60	0.2318		Not Significant
	$CaO.Al_2O_3$	0.011	1	0.011	4.02	0.0701		Not Significant
	$SiO_2.CaF_2$	8.786E-004	1	8.786E-004	0.33	0.5785		Not Significant
	$SiO_2.Al_2O_3$	3.516E-003	1	3.516E-003	1.31	0.2764		Significant
	$CaF_2.Al_2O_3$	0.010	1	0.010	3.78	0.0778		Not Significant
	Residual	0.029	11	2.681E-003				
	Total	0.13	20					
Specific Heat	Model	0.12	7	0.017	3.92	0.0162	0.67	Significant
	Linear	0.026	3	8.712E-003	2.04	0.1581		Not Significant
	$CaO.SiO_2$	0.051	1	0.051	11.89	0.0043		Significant
	$CaO.CaF_2$	7.895E-003	1	7.895E-003	1.85	0.1971		Significant

	$SiO_2.CaF_2$	9.184E-004	1	9.184E-004	0.21	0.6506		Not Significant
	$CaO.SiO_2.CaF_2$	0.065	1	0.065	15.25	0.0018		Significant
	Residual	0.056	13	4.272E-003				
	Total	0.17	20					
Change in Enthalpy (ΔH)	Model	1.053E-007	13	8.098E+005	4.59	0.0256	0.89	Significant
	Linear	3.233E+006	3	1.078E+006	6.11	0.0229		Significant
	$CaO.SiO_2$	22050.58	1	22050.58	0.12	0.7341		Not Significant
	$CaO.CaF_2$	2.193E+005	1	2.193E+005	1.24	0.3017		Not Significant
	$CaO.Al_2O_3$	1395.95	1	1395.95	7.909 E-003	0.9316		Not Significant
	$SiO_2.CaF_2$	1.626E+006	1	1.626E+006	9.21	0.0190		Significant
	$SiO_2.Al_2O_3$	20261.14	1	20261.14	0.11	0.7447		Not Significant
	$CaF_2.Al_2O_3$	1.886E+005	1	1.886E+005	1.07	0.3357		Not Significant
	$CaO.SiO_2.CaF_2$	5.921E+005	1	5.921E+005	3.35	0.1097		Not Significant

	$CaO.SiO_2.Al_2O_3$	1.591E+006	1	1.591E+006	9.01	0.0199		Significant
	$CaO.CaF_2.Al_2O_3$	4.784E+005	1	4.784E+005	2.71	0.1437		Not Significant
	$SiO_2.Al_2O_3.(SiO_2 - Al_2O_3)$	9.420E+005	1	9.420E+005	5.34	0.0542		Not Significant
	Residual	1.235E+006	7	1.765E+005				
	Total	1.176E+007	20					

Table 5.4: ANOVA results of various physicochemical and thermophysical properties for rutile-basic flux system

Properties	*Source*	*SS*	*DF*	*MS*	*F value*	*P value*	R^2 *value*	*Status*
GFN	Model	3.56	9	0.40	4.78	0.0089	0.79	Significant
	Linear	0.57	3	0.19	2.29	0.1344		Not Significant
	TiO_2.SiO_2	0.28	1	0.28	3.36	0.0939		Not Significant
	TiO_2.CaO	0.37	1	0.37	4.51	0.0573		Not Significant
	SiO_2.CaO	9.264E-003	1	9.264E-003	0.11	0.7443		Not Significant
	SiO_2. Al_2O_3	0.043	1	0.043	0.52	0.4869		Not Significant
	CaO.Al_2O_3	0.53	1	0.53	6.40	0.0280		Significant
	SiO_2.CaO. Al_2O_3	0.72	1	0.72	8.65	0.0134		Significant
	Residual	0.91	11	0.91				
Density	Model	7.249E-003	4	1.812E-003	3.78	0.0239	0.84	Significant
	Linear	5.238E-004	3	1.746E-004	0.36	0.7797		Not Significant
	TiO_2.CaO	6.725E-003	1	6.725E-003	14.03	0.0018		Significant
	Residual	7.670E-003	16	4.794E-004				
	Total	0.015	20					

Weight loss	Model	119.18	11	10.83	4.41	0.0170	0.84	Significant
	Linear	25.30	3	8.43	3.44	0.0655		Not Significant
	$TiO_2.SiO_2$	2.54	1	2.54	1.03	0.3359		Not Significant
	$TiO_2.CaO$	0.94	1	0.94	0.38	0.5523		Not Significant
	$TiO_2.Al_2O_3$	20.51	1	20.51	8.36	0.0179		Significant
	$SiO_2.CaO$	9.58	1	9.58	3.90	0.0796		Not Significant
	$SiO_2.Al_2O_3$	30.11	1	30.11	12.27	0.0067		Significant
	$CaO.Al_2O_3$	14.90	1	14.90	6.07	0.0359		Significant
	$TiO_2.SiO_2.Al_2O_3$	28.49	1	28.49	11.61	0.0078		Significant
	$TiO_2.CaO.Al_2O_3$	18.45	1	18.45	7.52	0.0228		Significant
	Residual	22.09	9	2.45				
	Total	141.27	20					
Thermal Conductivity	Model	7.067E-003	10	7.067E-004	3.50	0.0304	0.77	Significant
	Linear	1.658E-003	3	5.526E-004	2.74	0.0994		Not Significant
	$TiO_2.SiO_2$	3.463E-005	1	3.463E-005	0.17	0.6876		Not Significant
	$TiO_2.CaO$	1.797E-004	1	1.797E-004	0.89	0.3678		Not Significant
	$TiO_2.Al_2O_3$	2.315E-004	1	2.315E-004	1.15	0.3095		Not

								Significant
	SiO_2.CaO	4.642E-004	1	4.642E-004	2.30	0.1605		Not Significant
	SiO_2. Al_2O_3	1.851E-003	1	1.851E-003	9.16	0.0127		Significant
	TiO_2.SiO_2.CaO	6.171E-004	1	6.171E-004	3.06	0.1111		Not Significant
	TiO_2.SiO_2.Al_2O_3	5.750E-004	1	5.750E-004	2.85	0.1225		Not Significant
	Residual	2.020E-003	10	2.020E-004				
	Total	9.087E-003	20					
Thermal Diffusivity	Model	0.073	8	9.176E-003	3.28	0.0317	0.68	Significant
	Linear	5.863E-003	3	1.954E-003	0.70	0.5711		Not Significant
	TiO_2.CaO	9.197E-004	1	9.197E-004	0.33	0.5772		Not Significant
	TiO_2.Al_2O_3	0.028	1	0.028	10.04	0.0081		Significant
	SiO_2.Al_2O_3	0.031	1	0.031	11.12	0.0059		Significant
	CaO.Al_2O_3	0.020	1	0.020	6.97	0.0216		Significant
	TiO_2.CaO.Al_2O_3	0.014	1	0.014	4.85	0.0480		Significant
	Residual	0.034	12	2.800E-003				
	Total	0.11	20					
Specific Heat	Model	0.31	14	0.022	11.06	0.0037	0.96	Significant
	Linear	7.692E-003	1	2.564E-003	1.29	0.3612		Not Significant

	TiO_2.SiO_2	0.013	1	0.013	6.56	0.0428		Significant
	TiO_2.CaO	3.084E-004	1	3.084E-004	0.15	0.7076		Not Significant
	TiO_2.Al_2O_3	3.323E-004	1	3.323E-004	0.17	0.6971		Not Significant
	SiO_2.CaO	3.236E-003	1	3.236E-003	1.62	0.2495		Not Significant
	SiO_2. Al_2O_3	6.805E-003	1	6.805E-003	3.42	0.1140		Not Significant
	CaO.Al_2O_3	4.606E-005	1	4.606E-005	0.023	0.8841		Not Significant
	TiO_2.SiO_2.CaO	5.601E-003	1	5.601E-003	2.81	0.1445		Not Significant
	TiO_2.SiO_2.Al_2O_3	0.036	1	0.036	17.89	0.0055		Significant
	TiO_2.CaO.Al_2O_3	0.054	1	0.054	27.28	0.0020		Significant
	SiO_2.CaO. Al_2O_3	0.042	1	0.042	21.03	0.0037		Significant
	SiO_2.Al_2O_3. (SiO_2- Al_2O_3)	0.070	1	0.070	34.97	0.0010		Significant
	Residual	0.012	6	1.991E-003				
	Total	0.32	20					
Change in Enthalpy (ΔH)	Model	6.731E+007	13	5.178E+006	11.12	0.0019	0.95	Significant
	Linear	1.487E+007	3	4.957E+006	10.64	0.0053		Significant
	TiO_2.SiO_2	1.285E+007	1	1.285E+007	27.60	0.0012		Significant
	TiO_2.CaO	4.376E+006	1	4.376E+006	9.40	0.0182		Significant

	$TiO_2.Al_2O_3$	1.032E+007	1	1.032E+007	22.15	0.0022		Significant
	$SiO_2.CaO$	2.120E+005	1	2.120E+005	0.46	0.5216		Not Significant
	$SiO_2.Al_2O_3$	1.016E+007	1	1.016E+007	21.81	0.0023		Significant
	$CaO.Al_2O_3$	1.959E+006	1	1.959E+006	4.21	0.0794		Not Significant
	$TiO_2.SiO_2.CaO$	1.151E+007	1	1.151E+007	24.70	0.0016		Significant
	$TiO_2.SiO_2.Al_2O_3$	6.357E+006	1	6.357E+006	13.65	0.0077		Significant
	$TiO_2.CaO.Al_2O_3$	2.356E+006	1	2.356E+006	5.06	0.0593		Not Significant
	$SiO_2.CaO.Al_2O_3$	318.41	1	318.41	6.836 E-004	0.9799		Not Significant
	Residual	3.260E+006	7	4.658E+005				
	Total	7.057E+007	20					

DF: degree of freedom

Table 5.5: ANOVA results of various physicochemical and thermophysical properties for rutile-acidic flux system

Properties	*Source*	*SS*	*DF*	*MS*	*F value*	*P value*	R^2 *value*	*Status*
GFN	Model	1.20	13	0.092	4.77	0.0231	0.89	Significant
	Linear	0.12	3	0.039	1.99	0.2049		Not Significant
	$TiO_2.SiO_2$	0.027	1	0.027	1.38	0.2785		Not Significant
	$TiO_2.MgO$	5.850E-003	1	5.850E-003	0.30	0.6000		Not Significant
	$TiO_2.Al_2O_3$	3.424E-003	1	3.424E-003	0.18	0.6870		Not Significant
	$SiO_2.MgO$	0.16	1	0.16	8.35	0.0233		Significant
	$SiO_2.Al_2O_3$	9.085E-003	1	9.085E-003	0.47	0.5158		Not Significant
	$MgO.Al_2O_3$	3.318E-008	1	3.318E-008	1.710 E-006	0.9990		Not Significant
	$TiO_2.SiO_2.Al_2O_3$	0.14	1	0.14	7.06	0.0326		Significant
	$TiO_2.MgO.Al_2O_3$	0.054	1	0.054	2.79	0.1390		Not Significant
	$SiO_2.MgO.\ Al_2O_3$	0.21	1	0.21	10.86	0.0132		Significant
	$TiO_2.Al_2O_3.$ $(TiO_2\text{-}\ Al_2O_3)$	0.078	1	0.078	4.02	0.0851		Not Significant
	Residual	0.14	7	0.019				
	Total	1.34	20					
Density	Model	0.057	13	4.375E-003	4.21	0.0322	0.88	Significant

	Linear	0.029	3	9.772E-003	9.40	0.0075		Significant
	$TiO_2.SiO_2$	1.769E-003	1	1.769E-003	1.70	0.2333		Not Significant
	$TiO_2.MgO$	2.579E-003	1	2.579E-003	2.48	0.1592		Not Significant
	$TiO_2.Al_2O_3$	3.574E-003	1	3.574E-003	3.44	0.1061		Not Significant
	$SiO_2.MgO$	2.221E-003	1	2.221E-003	2.14	0.1872		Not Significant
	$SiO_2.Al_2O_3$	6.660E-003	1	6.660E-003	6.41	0.0392		Significant
	$MgO.Al_2O_3$	0.013	1	0.013	12.03	0.0104		Significant
	$TiO_2.SiO_2.MgO$	1.199E-003	1	1.199E-003	1.15	0.3184		Not Significant
	$TiO_2.SiO_2.Al_2O_3$	4.654E-003	1	4.654E-003	4.48	0.0721		Not Significant
	$TiO_2.MgO.Al_2O_3$	5.201E-004	1	5.201E-004	0.50	0.5022		Not Significant
	$SiO_2.MgO.\ Al_2O_3$	9.921E-003	1	9.921E-003	9.55	0.0176		Significant
	Residual	7.276E-003	7	1.039E-003				
	Total	0.064	20					
	$TiO_2.CaO.Al_2O_3$							
	Residual							
	Total							

Weight loss	Model	2.85	8	0.36	2.89	0.0478	0.65	Significant
	Linear	0.95	3	0.32	2.58	0.1025		Not Significant
	TiO_2.MgO	0.80	1	0.80	6.45	0.0260		Significant
	SiO_2.MgO	0.025	1	0.025	0.20	0.6588		Not Significant
	SiO_2.Al_2O_3	0.072	1	0.072	0.59	0.4585		Not Significant
	MgO.Al_2O_3	0.30	1	0.30	2.45	0.1433		Not Significant
	SiO_2.MgO.Al_2O_3	0.29	1	0.29	2.35	0.1513		Not Significant
	Residual	1.48	12	0.12				
	Total	4.33	20					
Thermal Conductivity	Model	1.153E-003	4	2.882E-004	3.67	0.0264	0.74	Significant
	Linear	6.406E-004	4	2.135E-004	2.72	0.0790		Not Significant
	TiO_2.Al_2O_3	5.124E-004	1	5.124E-004	6.53	0.0212		Significant
	Residual	1.256E-003	16	7.852E-005				
	Total	2.409E-003	20					
Thermal Diffusivity	Model	0.035	1	3.173E-003	4.57	0.0152	0.84	Significant

	Linear	3.511E-003	3	1.170E-003	1.69	0.2387		Not Significant
	$TiO_2.SiO_2$	9.175E-003	1	9.175E-003	13.22	0.0054		Significant
	$TiO_2.Al_2O_3$	0.014	1	0.014	19.64	0.0016		Significant
	$SiO_2.MgO$	4.585E-004	1	4.585E-004	0.66	0.4373		Not Significant
	$SiO_2.Al_2O_3$	0.015	1	0.015	21.31	0.0013		Significant
	$MgO.Al_2O_3$	0.020	1	0.020	28.54	0.0005		Significant
	$TiO_2.SiO_2.Al_2O_3$	8.860E-003	1	8.860E-003	12.77	0.0060		Significant
	$SiO_2.MgO.\ Al_2O_3$	9.724E-003	1	9.724E-003	14.01	0.0046		Significant
	$SiO_2.Al_2O_3.$ $(SiO_2- Al_2O_3)$	6.643E-003	1	6.643E-003	9.57	0.0128		Significant
	Residual	6.245E-003	9	6.939E-004				
	Total	0.041	20					
Specific Heat	Model	0.13	12	0.011	4.31	0.0231	0.86	Significant
	Linear	0.021	3	6.938E-003	2.68	0.1182		Not Significant
	$TiO_2.SiO_2$	0.029	1	0.029	11.15	0.0102		Significant
	$TiO_2.MgO$	8.461E-003	1	8.461E-003	3.26	0.1085		Not Significant
	$TiO_2.Al_2O_3$	0.044	1	0.044	16.91	0.0034		Significant
	$SiO_2.MgO$	9.503E-004	1	9.503E-004	0.37	0.5617		Not Significant
	$SiO_2.Al_2O_3$	0.039	1	0.039	15.16	0.0046		Significant
	$MgO.Al_2O_3$	0.063	1	0.063	24.37	0.0011		Significant

	$TiO_2.SiO_2.Al_2O_3$	0.034	1	0.034	13.00	0.0069		Significant
	$SiO_2.MgO.Al_2O_3$	0.027	1	0.027	10.52	0.0118		Significant
	$TiO_2.Al_2O_3.(TiO_2-Al_2O_3)$	0.018	1	0.018	7.08	0.0287		Significant
	Residual	0.021	8	2.593E-003				
	Total	0.15	20					
Change in Enthalpy (ΔH)	Model	1.881E+007	13	1.447E+006	3.74	0.0438	0.87	Significant
	Linear	4.415E+006	3	1.472E+006	3.80	0.0661		Not Significant
	$TiO_2.SiO_2$	1.273E+006	1	1.273E+006	3.29	0.1126		Not Significant
	$TiO_2.MgO$	939.56	1	939.56	2.428 E-003	0.9621		Not Significant
	$TiO_2.Al_2O_3$	1.328E+005	1	1.328E+005	0.34	0.5763		Not Significant
	$SiO_2.MgO$	2.035E+006	1	2.035E+006	5.26	0.0555		Not Significant
	$SiO_2.Al_2O_3$	9.907E+005	1	9.907E+005	2.56	0.1536		Not Significant
	$MgO.Al_2O_3$	88493.15	1	88493.15	0.23	0.6471		Not Significant
	$TiO_2.SiO_2.MgO$	3.279E+006	1	3.279E+006	8.48	0.0226		Significant
	$TiO_2.SiO_2.Al_2O_3$	2.620E+006	1	2.620E+006	6.77	0.0353		Significant
	$TiO_2.MgO.Al_2O_3$	1.824E+005	1	1.824E+005	0.47	0.5145		Not Significant
	$SiO_2.MgO.Al_2O_3$	2.180E+005	1	2.180E+005	0.56	0.4773		Not Significant

	Residual	2.708E+006	7	3.869E+005				
	Total	2.152E+007	20					

For all physicochemical and thermophysical properties (Table 5.3-5.5), the p values less than 0.005 indicate that the models are significant, and very lesser chances of error due to noise. The difference between predicted and experimental results is not high due to moderate R^2 value for all properties. Figure 5.1, 5.2, and 5.3 (for three flux systems) shows the variation of predicted values from actual responses for different physicochemical and thermophysical properties.

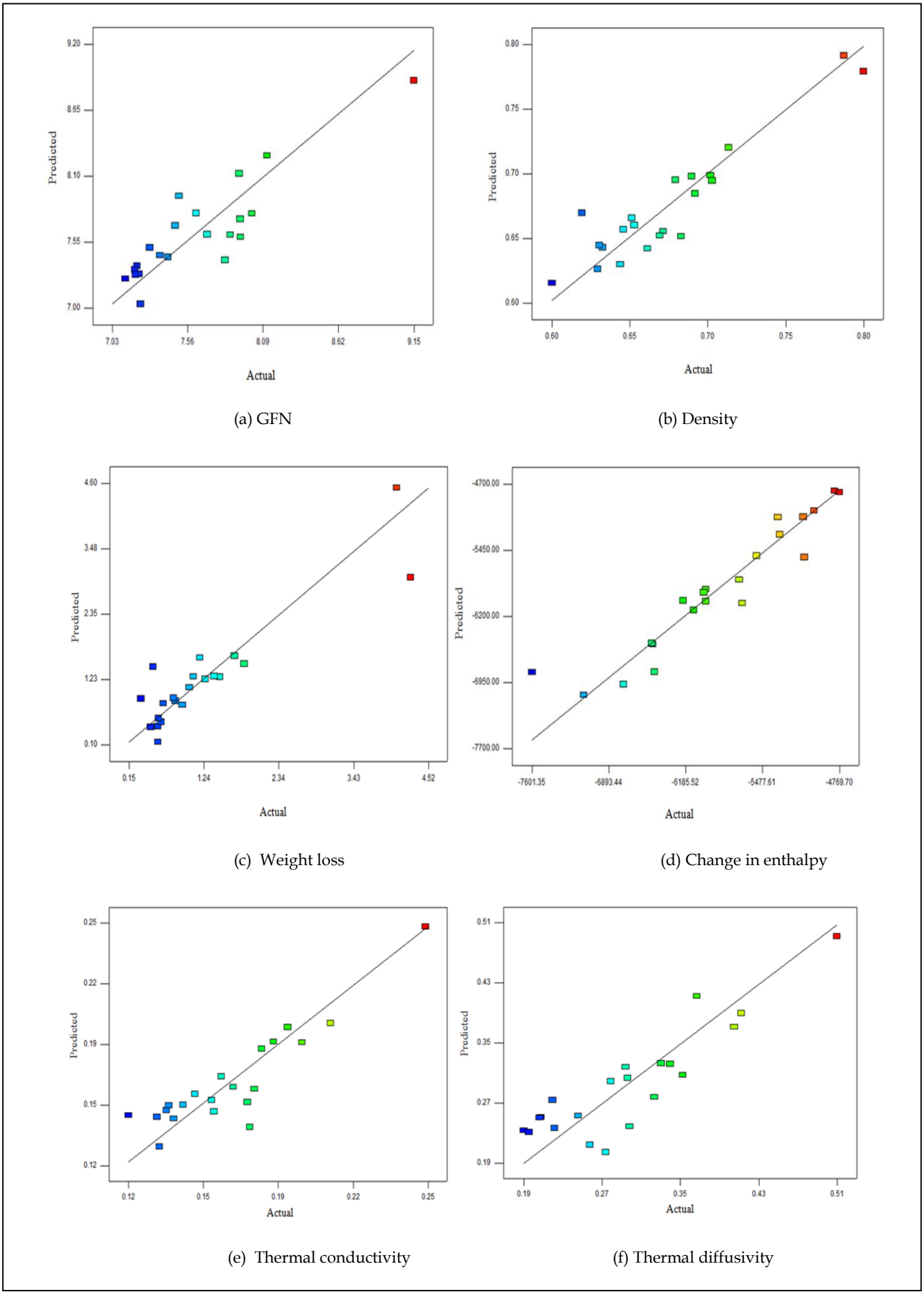

(a) GFN

(b) Density

(c) Weight loss

(d) Change in enthalpy

(e) Thermal conductivity

(f) Thermal diffusivity

Figure 5.1: Predicted versus actual plots for various properties; (a) Grain fineness number (GFN); (b) Density; (c) Weight loss; (d) Change in enthalpy; (e) Thermal conductivity; (f) Thermal diffusivity; (for basic flux system).

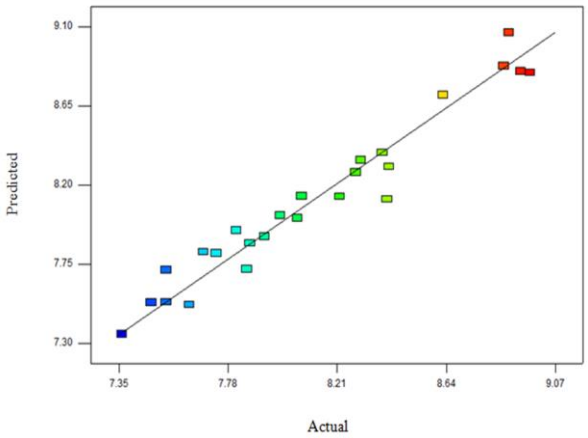

(a) GFN

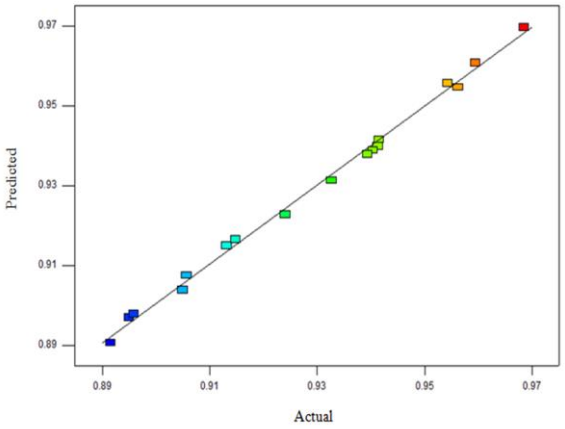

(b) Density

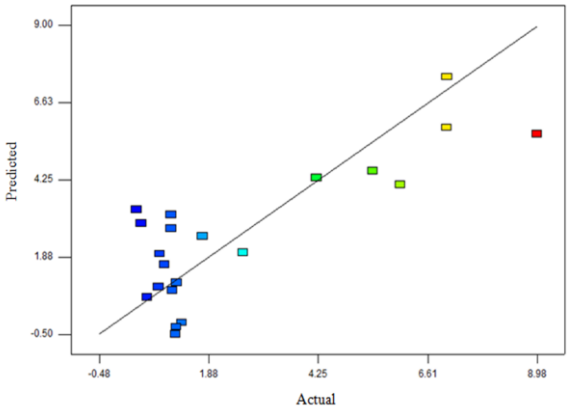

(c) Weight loss

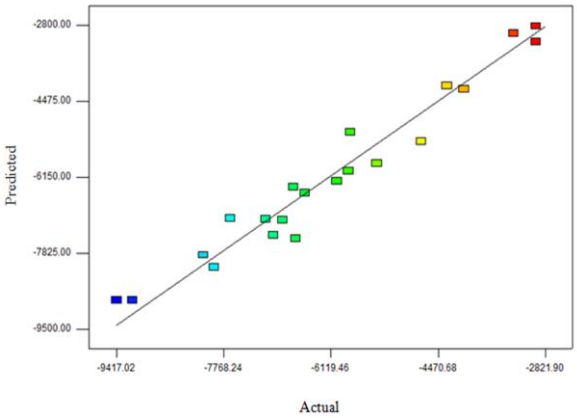

(d) Change in enthalpy

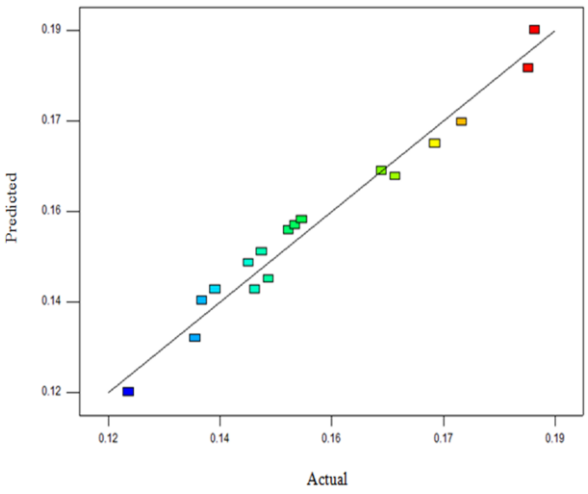

(e) Thermal conductivity

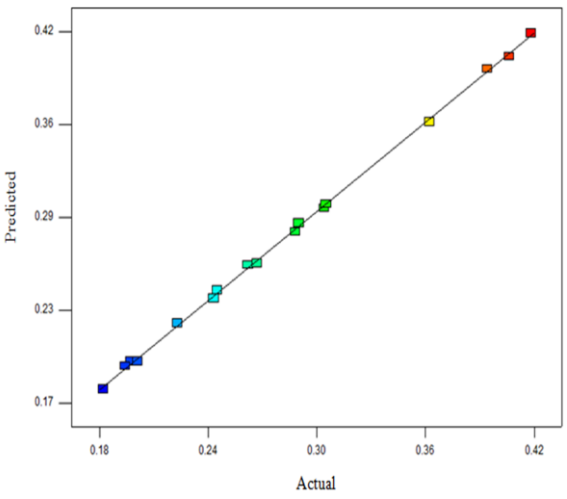

(f) Thermal diffusivity

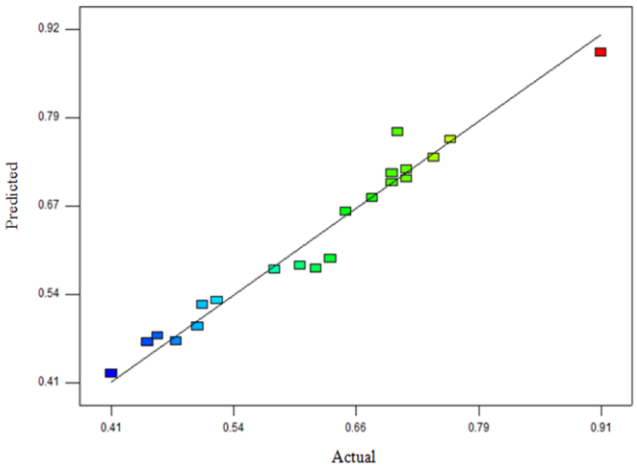

(g) Specific heat

Figure 5.2: Predicted versus actual plots for various properties; (a) Grain fineness number (GFN); (b) Density; (c) Weight loss; (d) Change in enthalpy; (e) Thermal conductivity; (f) Thermal diffusivity; (g) Specific heat (for rutile-basic flux system).

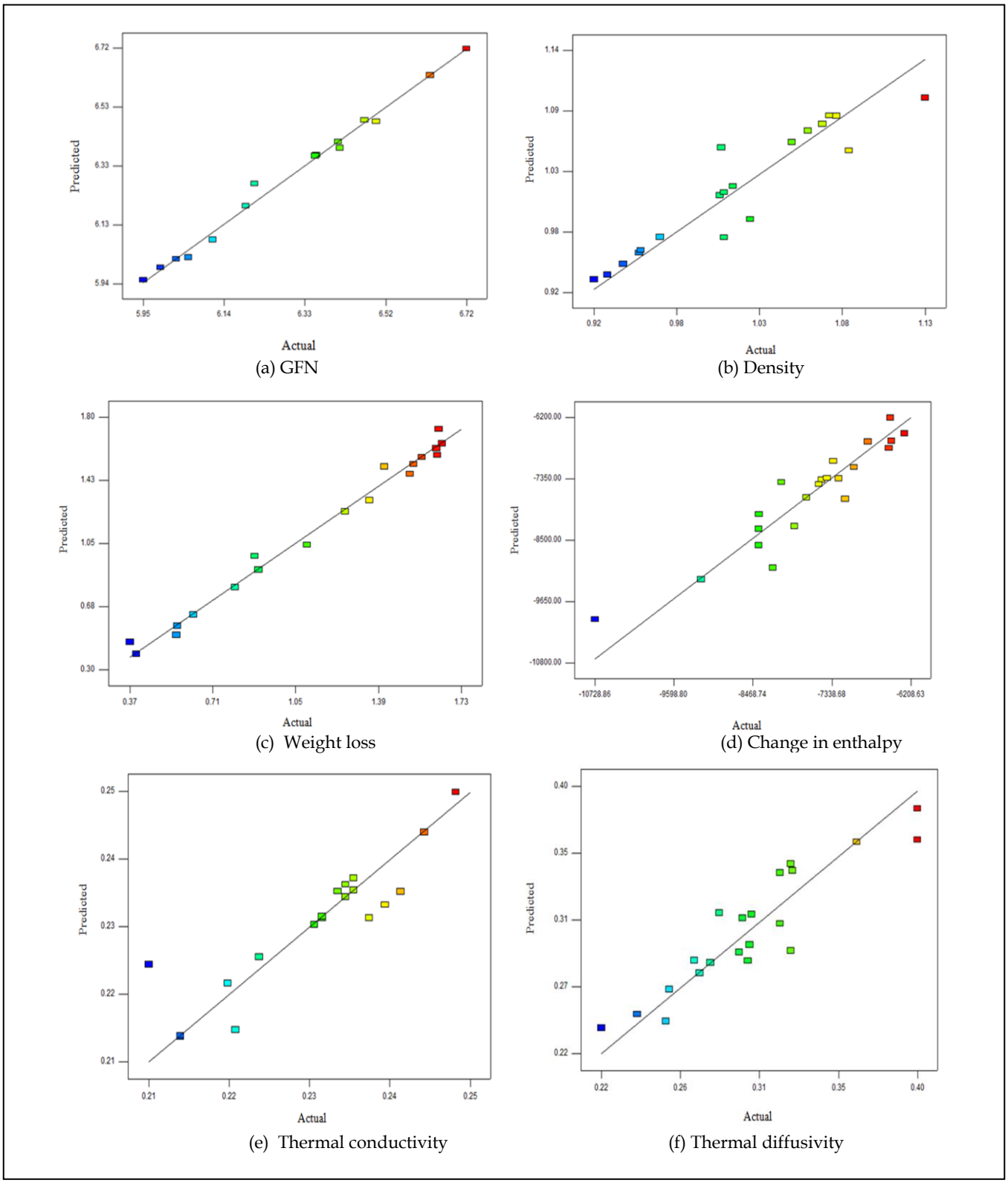

Figure 5.3: Predicted versus actual plots for various properties; (a) Grain fineness number (GFN); (b) Density; (c) Weight loss; (d) Change in enthalpy; (e) Thermal conductivity; (f) Thermal diffusivity; (for rutile-acidic flux system).

5.1.1.3 Discussion of regression analysis of SAW flux components (Individual, binary and ternary) on grain finesses number, density, weight change, change in enthalpy, thermal conductivity, thermal diffusivity and specific heat for three systems

From the regression analysis, it observed that individual flux constituents show antisynergistic effect on grain fineness number for basic, rutile-basic, and rutile-acidic flux systems (Table 5.3-5.5). For basic and rutile-basic flux systems, the binary interaction of flux constituents is more pronounced as compared to ternary constituents while for rutile-acidic flux system, both binary and ternary interactions, affect the grain fineness number. For the basic flux system, the binary constituents such as $CaO.SiO_2$, $SiO_2.CaF_2$ and $SiO_2.Al_2O_3$ shows synergistic effect and thus increase the grain fineness number while $CaO.CaF_2$, $CaO.Al_2O_3$ and $CaF_2.Al_2O_3$ show antisynergistic effect and thus decreases the grain fineness number. $TiO_2.SiO_2$ is the binary constituent, which reduces the grain finesses number in both rutile-basic and rutile-acidic flux systems. Other binary mixture constituents $TiO_2.CaO$, $SiO_2.CaO$, $SiO_2.Al_2O_3$, $TiO_2.MgO$, $TiO_2.Al_2O_3$, $SiO_2.Al_2O_3$ and $MgO.Al_2O_3$ decrease the grain fineness number in rutile-basic and rutile-acidic flux systems. Ternary mixture constituents $SiO_2.CaO.Al_2O_3$, $TiO_2.SiO_2.Al_2O_3$ and $SiO_2.MgO.Al_2O_3$ show synergistic effect on grain fineness number while $TiO_2.MgO.Al_2O_3$ and $TiO_2.Al_2O_3$. (TiO_2-Al_2O_3) show antisynergistic effect on grain fineness number in rutile-basic and rutile-acidic flux systems.

It is observed form regression analysis (Table 5.3-5.5) that individual flux constituents decrease the density for basic and rutile-basic flux systems while for rutile-acidic flux system they increase the density. Binary constituent $SiO_2.Al_2O_3$ increases the density for basic and rutile-acidic flux systems. Binary mixture $CaO.CaF_2$, $SiO_2.CaF_2$, $CaF_2.Al_2O_3$, $TiO_2.CaO$ and $MgO.Al_2O_3$ increases the density and show synergistic effect while $CaO.SiO_2$, $CaO.Al_2O_3$, $TiO_2.SiO_2$, $TiO_2.MgO$, $TiO_2.Al_2O_3$ and $SiO_2.MgO$ decreases density and shows antisynergistic effect for basic and rutile-acidic flux systems. Ternary mixture constituents $CaO.CaF_2.Al_2O_3$ and $SiO_2.MgO.Al_2O_3$ increase the density and show synergistic effect while $CaO.SiO_2.CaF_2$, $CaO.SiO_2.Al_2O_3$, $SiO_2.CaF_2.Al_2O_3$, $TiO_2.SiO_2.MgO$, $TiO_2.SiO_2.Al_2O_3$ and $TiO_2.MgO.Al_2O_3$ decrease the density for basic and rutile-acidic flux systems. Acidic fluxes increase the oxide inclusions content in the weld pool as compared to the basic fluxes during slag-metal reactions taking place in the submerged arc welding process. Increase in oxide content in weld pool increases the density due to which fluidity of molten metal decreases and thus affects the bead morphology and mechanical properties of the weld [Jindal et al., 2013, Kanjilal et al., 2005, M.L.E. Davis et al., 1977, J.H. Kim et al., 1990, Jindal et al., 2014].

It observed from the regression analysis that for the basic flux system, the individual flux constituents increase the weight loss while for rutile-basic and rutile-acidic flux systems, they decrease the weight loss. $SiO_2.Al_2O_3$ is the binary mixture constituent, which increases the weight loss in basic as well as in the rutile-basic flux system, while for the rutile-acidic system, it decreases. $CaO.SiO_2$ binary constituent increases the weight loss in the basic system, while for the rutile-basic flux system, it decreases the weight loss. Binary mixture constituent $CaO.Al_2O_3$ shows a negative effect on weight loss in the basic flux system, while for the rutile-basic flux system, it shows a synergistic effect. Binary mixture $TiO_2.Al_2O_3$ and $TiO_2.MgO$ shows a synergistic effect on weight loss for rutile-basic and rutile-acidic flux systems. $CaO.CaF_2$, $SiO_2.CaF_2$, $CaF_2.Al_2O_3$, $TiO_2.SiO_2$, $TiO_2.CaO$, $SiO_2.MgO$ and $MgO.Al_2O_3$ binary mixture constituents show antisynergistic effect on weight loss for basic, rutile-basic, and rutile-acidic flux systems. Ternary mixture constituent $TiO_2.SiO_2.Al_2O_3$ and $TiO_2.CaO.Al_2O_3$ increases the weight loss for the rutile-basic flux system while ternary constituent $SiO_2.MgO.Al_2O_3$ decreases the weight loss for the rutile-acidic flux system. Figure 5.4 shows some of the graphical plots of percentage weight change with temperature for three flux systems.

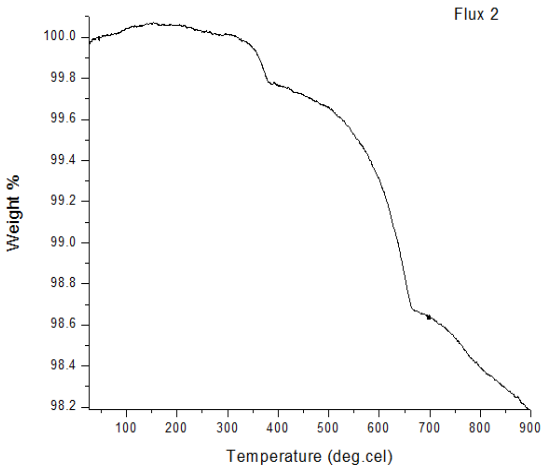
Flux 2
Weight %
Temperature (deg.cel)

(a)

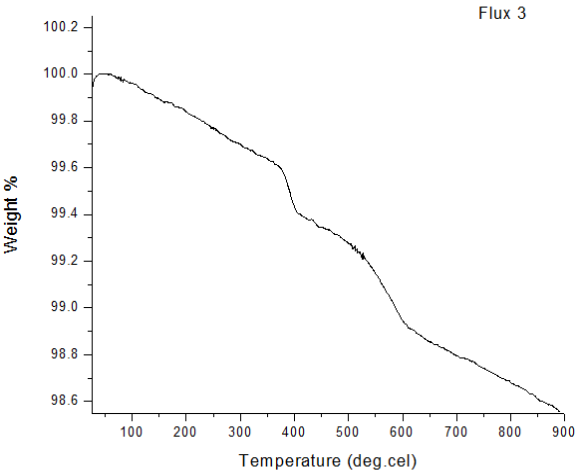
Flux 3
Weight %
Temperature (deg.cel)

(b)

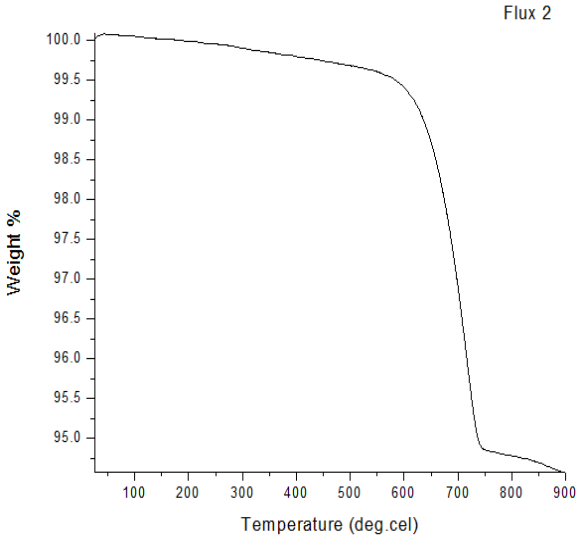
Flux 2
Weight %
Temperature (deg.cel)

(c)

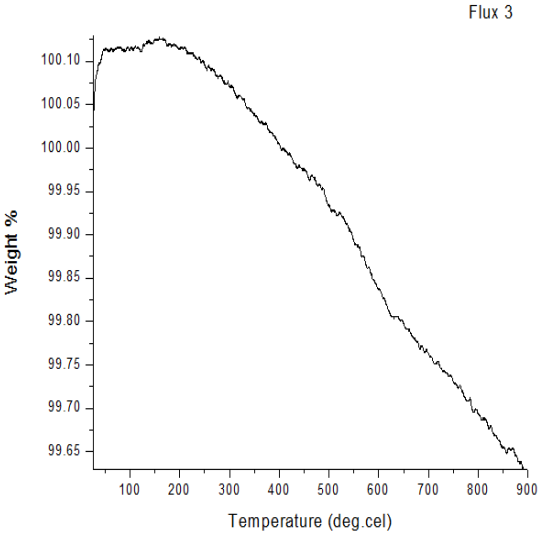
Flux 3
Weight %
Temperature (deg.cel)

(d)

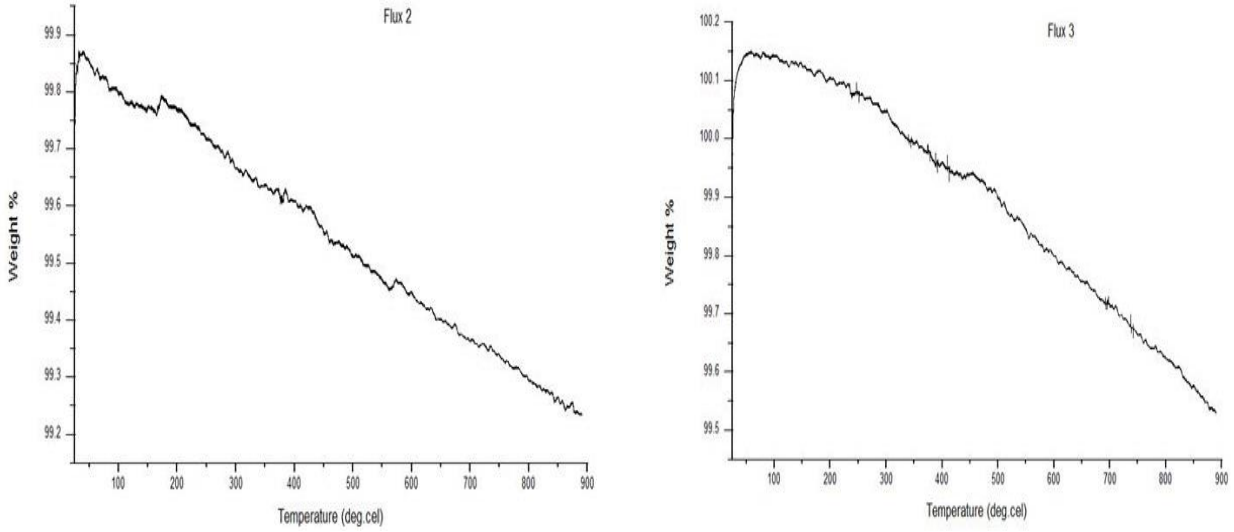

(e) (f)

Figure 5.4: Relation between percentage weight change and temperature for three flux systems; (a-b) graphical plots for basic flux system; (c-d) graphical plots for rutile-basic flux system; (e-f) graphical plots for rutile-acidic flux system

From regression analysis (Table 5.3-5.5) of change in enthalpy it observed that all individual flux constituents show a synergistic effect on change in enthalpy for the basic and rutile-basic flux system while for the rutile-acidic flux system it decreases the enthalpy. $SiO_2.CaF_2$ is the binary constituent which increases the enthalpy for basic system. $TiO_2.SiO_2$ and $TiO_2.Al_2O_3$ increases the enthalpy for rutile-basic system while causing a decrease in enthalpy for rutile-acidic system. $TiO_2.CaO$ shows synergistic effect while $TiO_2.MgO$, $SiO_2.MgO$ and $MgO.Al_2O_3$ show antisynergistic effects on change in enthalpy for rutile-basic and rutile-acidic flux system. $SiO_2.Al_2O_3$ is the only binary constituent, which decreases the enthalpy in all the three flux systems while binary mixture constituent $SiO_2.CaO$ and $CaO.Al_2O_3$ decrease the enthalpy in basic and rutile-basic flux systems. $TiO_2.SiO_2.Al_2O_3$ is the ternary mixture constituent which increases the enthalpy for rutile-basic and rutile-acidic flux systems. Ternary mixture constituent $CaO.SiO_2.Al_2O_3$, $TiO_2.SiO_2.CaO$ and $TiO_2.SiO_2.MgO$ increases the change in enthalpy for basic, rutile-basic and rutile-acidic flux systems while $CaO.SiO_2.CaF_2$, $CaO.CaF_2.Al_2O_3$, $SiO_2.Al_2O_3.(SiO_2\text{-}Al_2O_3)$, $TiO_2.CaO.Al_2O_3$, $SiO_2.CaO.Al_2O_3$, $TiO_2.MgO.Al_2O_3$ and $SiO_2.MgO.Al_2O_3$ ternary constituents decrease the enthalpy for three flux systems. Figure 5.5 shows some of the graphical plots of change in enthalpy with temperature for three flux systems.

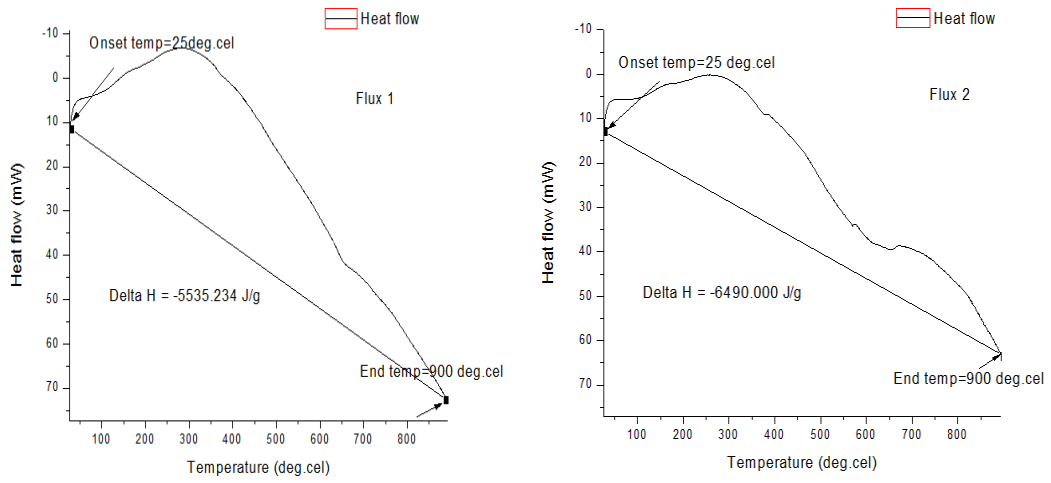

(a) (b)

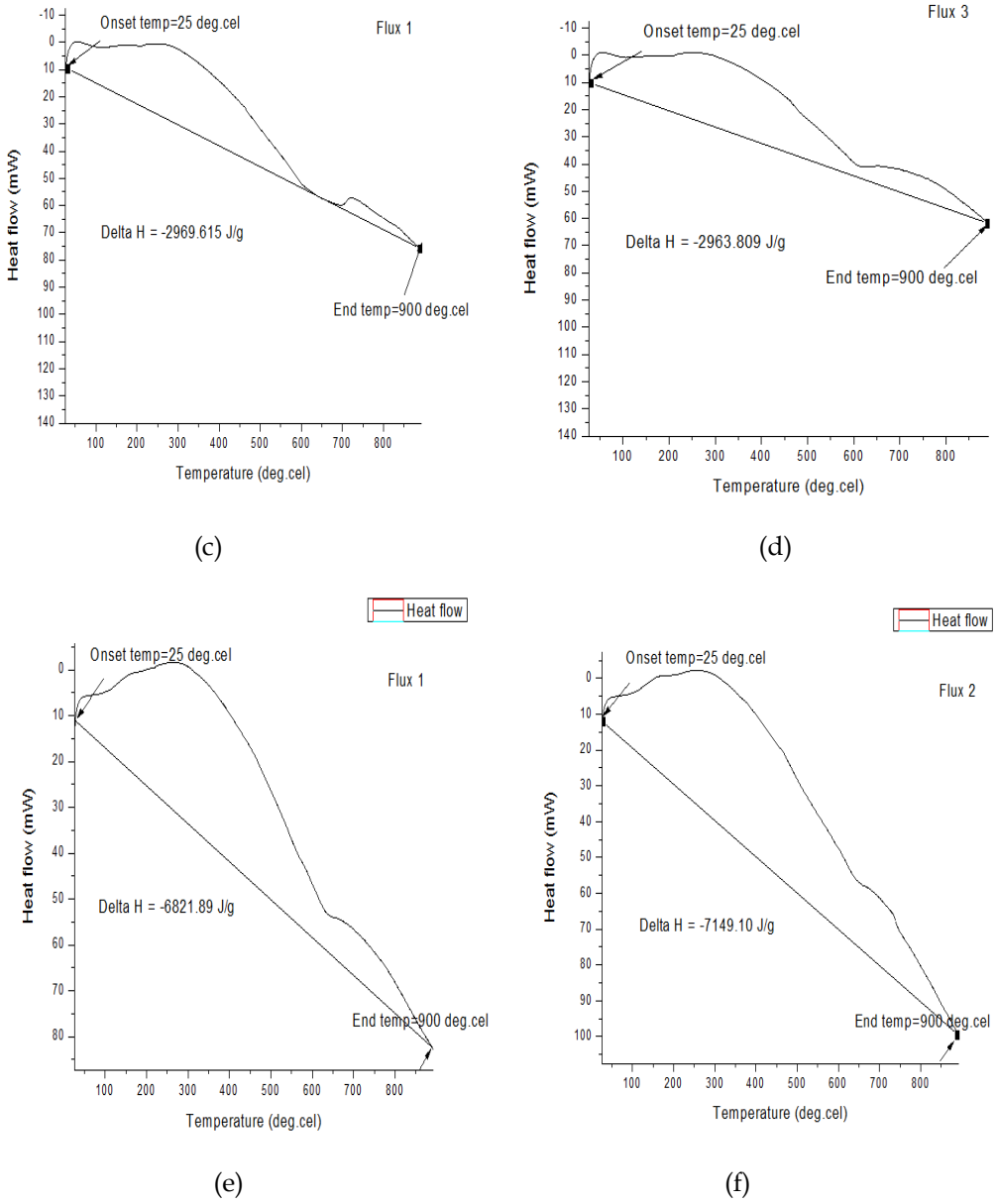

Figure 5.5: Plots between change in enthalpy vs. temperature for three flux systems; (a-b) plots for basic flux system; (c-d) plots for rutile-basic flux system; (e-f) plots for rutile-acidic flux system

From the regression analysis (Table 5.3-5.5) of thermal properties, it observed that individual flux constituents increase the thermal conductivity for the basic flux system while for rutile-basic and rutile-acidic flux system individual flux constituents decrease the thermal conductivity. Binary mixture constituent $SiO_2.Al_2O_3$ shows a synergistic effect while $CaO.SiO_2$ shows antisynergistic effect on thermal conductivity for basic and rutile-basic flux systems. $TiO_2.Al_2O_3$ binary constituent increases the thermal conductivity in the rutile-acidic flux system, while for the rutile-basic flux system, it decreases the thermal conductivity. Binary mixture constituent $CaO.CaF_2$, $CaO.Al_2O_3$, $SiO_2.CaF_2$ and $TiO_2.CaO$ reduces the thermal conductivity for the basic and rutile-basic flux system. All the ternary mixture constituents decrease the thermal conductivity in a basic and rutile-basic flux system. In the basic flux system, thermal diffusivity is increased by individual flux constituents, while for rutile-basic and rutile-acidic flux systems, it shows antisynergistic effect. Previous researchers studied that the presence of high covalently bonded ions (e.g., Si^{4+} and Al^{3+}) in the network chain increases the thermal conductivity. The presence of acidic oxides such as SiO_2, Al_2O_3 in the network chain increases the thermal conductivity because conductivity is affected due to the presence of cations. Alignment of

bridging and non-bridging oxygen ions (NBO/T) in the network chain widely affects the physical and thermal properties of slags. Polarization of slags in tetrahedron network structure increases due to the presence of a higher concentration of Si^{4+}, Ca^{2+}, and Al^{3+} ions [Mills, 2011, Mills, 2000, Kersten et al., 2011, Kaur et al., 2011].
Binary mixture components $SiO_2.Al_2O_3$ and $TiO_2.Al_2O_3$ increase the thermal diffusivity both in rutile-basic and rutile-acidic flux system while $CaO.SiO_2$ decreases the thermal diffusivity in the basic system, but for the rutile-basic flux system, it increased. Binary components $CaO.Al_2O_3$, $TiO_2.SiO_2$ and $MgO.Al_2O_3$ show a synergistic effect on thermal diffusivity for rutile-basic and rutile-acidic flux systems. In all the three flux systems, binary constituents $CaO.CaF_2$, $SiO_2.CaF_2$, $TiO_2.CaO$ and $SiO_2.MgO$ shows antisynergistic effect on thermal diffusivity. The ternary mixture component increases the thermal diffusivity for rutile-basic and rutile-acidic flux systems while the basic flux system is not affected by the ternary mixture constituents. All the individual flux constituents decrease the specific heat for basic, rutile-basic, and rutile-acidic flux systems. Binary mixture constituent $CaO.SiO_2$ increases specific heat for the basic system, while for the rutile-basic flux system, it decreases the specific heat. Binary constituent $SiO_2.Al_2O_3$ and $TiO_2.Al_2O_3$ decreases specific heat for the rutile-basic system, while for the rutile-acidic flux system, it shows a synergistic effect. $TiO_2.SiO_2$ binary constituent increases the specific heat for both rutile-basic and rutile-acidic flux systems while remaining all the binary mixture constituents decreases the specific heat for rutile-basic flux system. $CaO.CaF_2$ and $MgO.Al_2O_3$ increases the specific heat for basic and rutile-acidic flux systems. $TiO_2.SiO_2.CaO$ is the only ternary constituent which decreases the specific heat while all the remaining ternary mixture constituents increase the specific heat for basic, rutile-basic, and rutile-acidic flux systems.

5.1.1.4 Contour plots of physicochemical and thermophysical properties for three flux systems

For different proportions of flux constituents such as CaO, SiO_2, CaF_2, TiO_2, MgO, Al_2O_3, and keeping binder content constant, various contour plots of physicochemical and thermophysical properties shown in Figure (5.6-5.8). The contour surface plot (Hummel, 1984) represents the variation of different physicochemical and thermophysical responses with the variation of flux constituents. Each curve shows the constant value of responses on the contour surface. Figure (5.6-5.8) shows the contour plots of grain finesses number, density, weight change, change in enthalpy, thermal conductivity, thermal diffusivity, and specific heat for basic, rutile-basic and rutile-acidic flux systems.

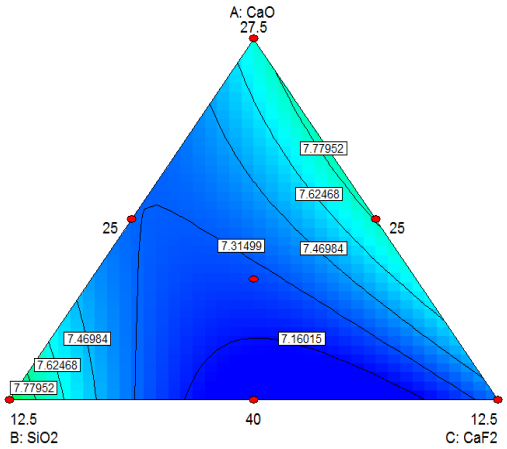

(a) Grain Finesses Number

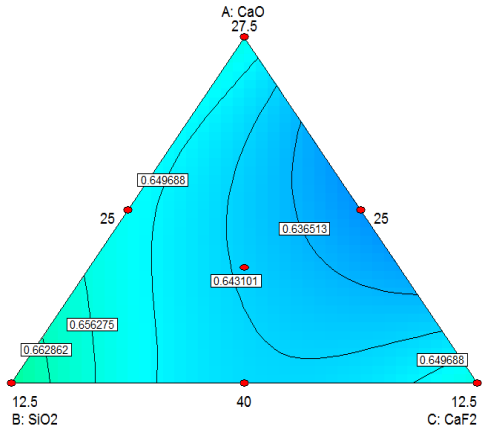

(b) Density

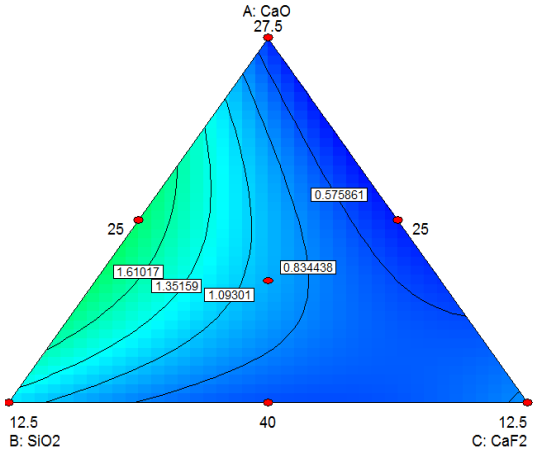

(c) Weight loss

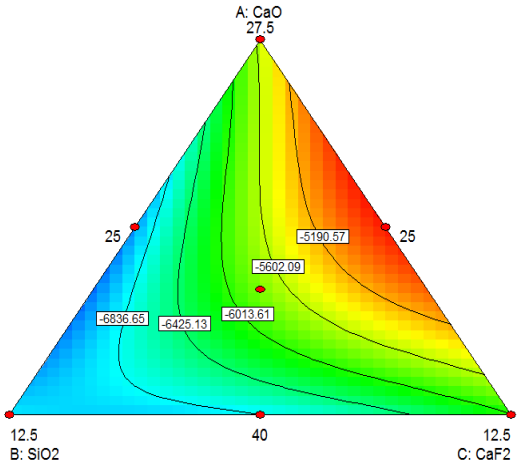

(d) Change in enthalpy

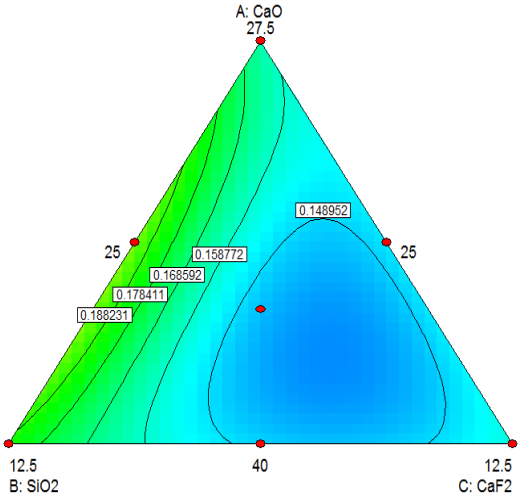

(e) Thermal conductivity

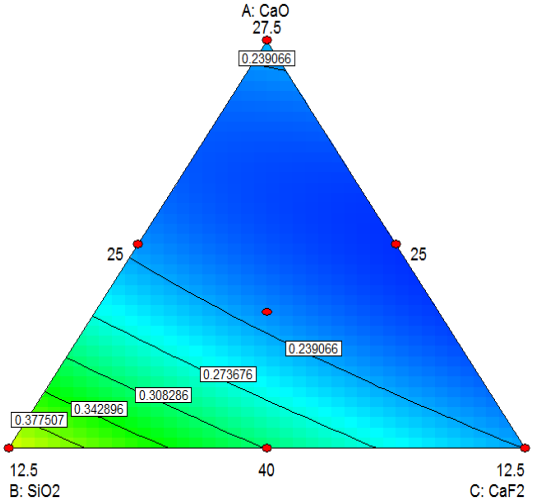

(f) Thermal diffusivity

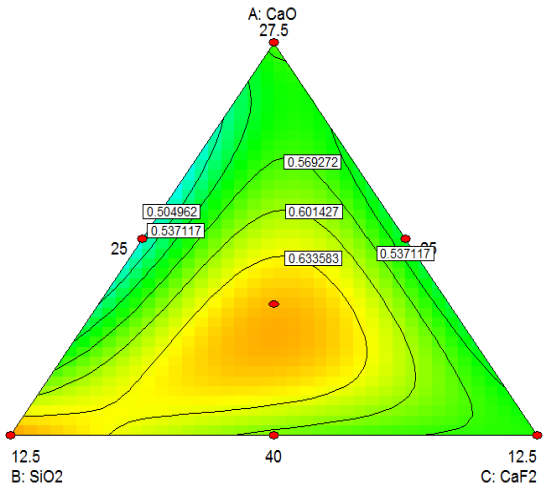

(g) Specific heat

Figure 5.6: Contour plot of physicochemical & thermophysical properties for basic flux system

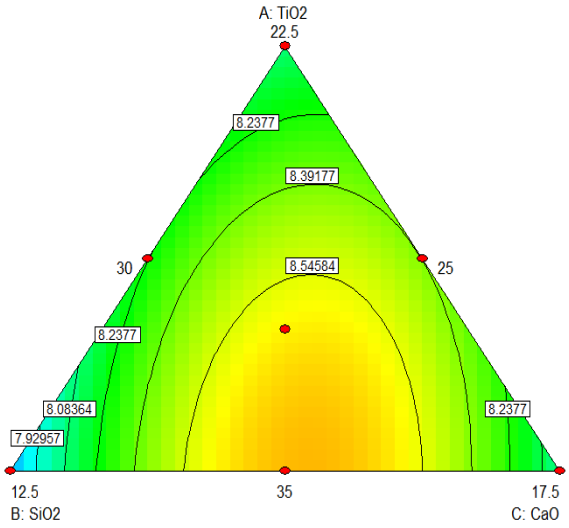

(a) Grain Finesses Number

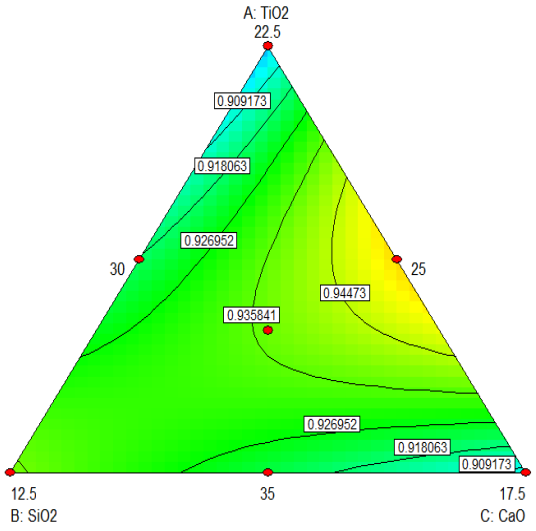

(b) Density

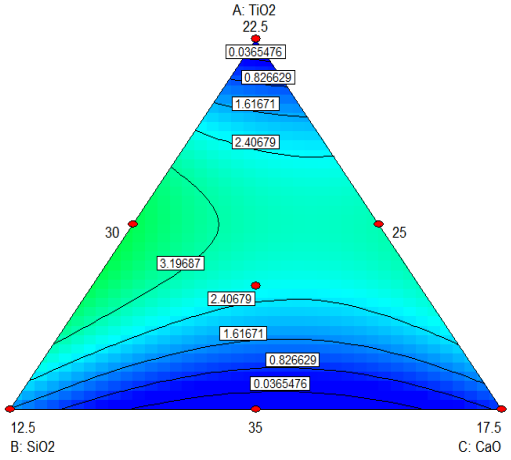

(c) Weight loss

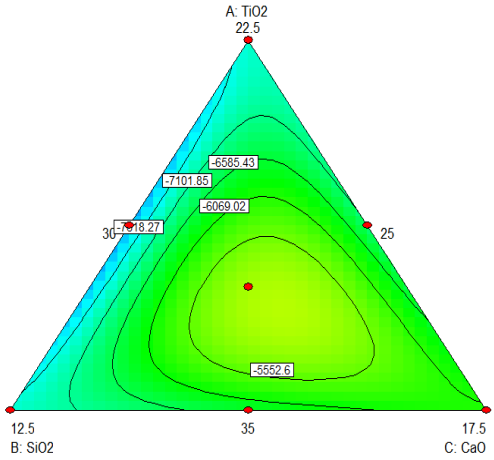

(d) Change in enthalpy

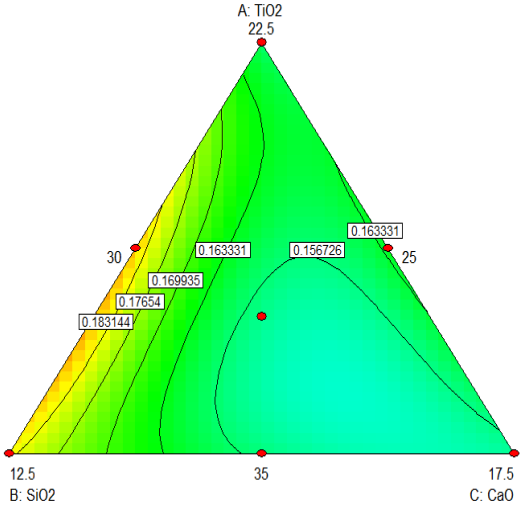

(e) Thermal Conductivity

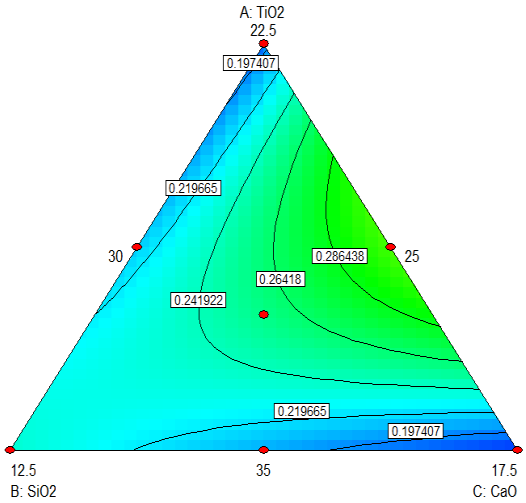

(f) Thermal diffusivity

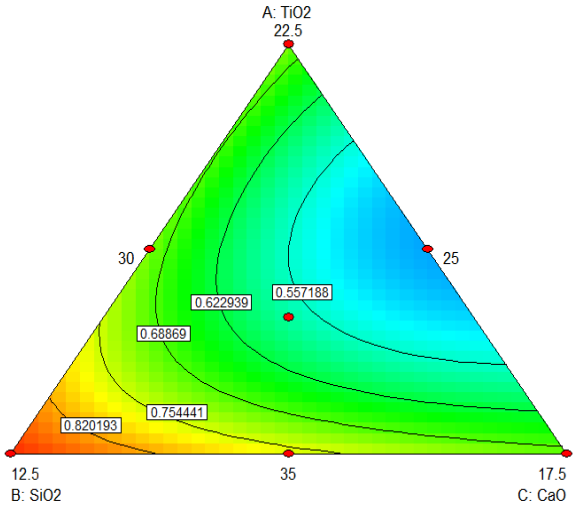

(g) Specific heat

Figure 5.7: Contour plot of physicochemical & thermophysical properties for rutile-basic flux system

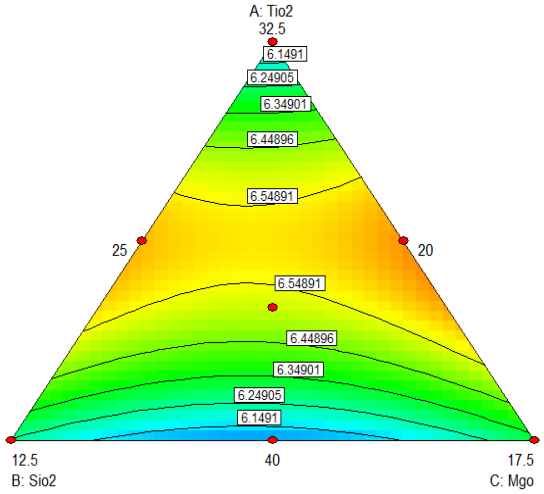

(a) Grain Finesses Number

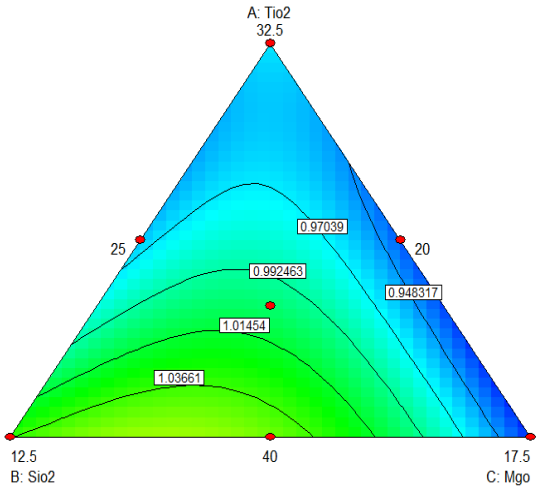

(b) Density

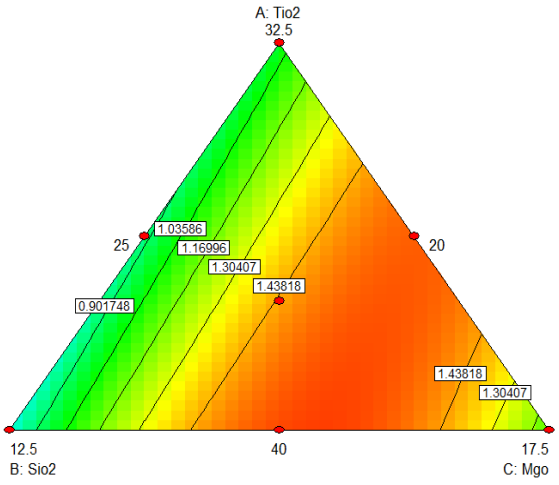

(c) Weight loss

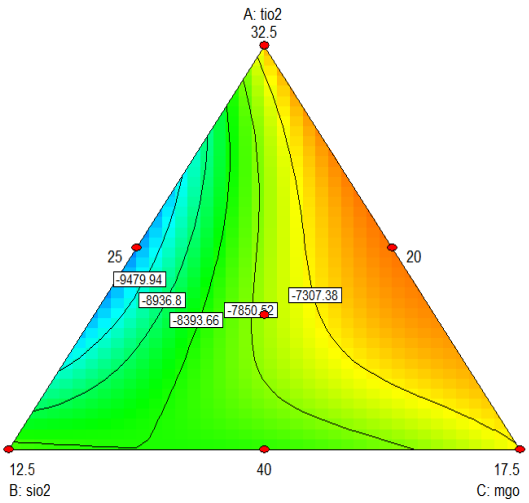

(d) Change in enthalpy

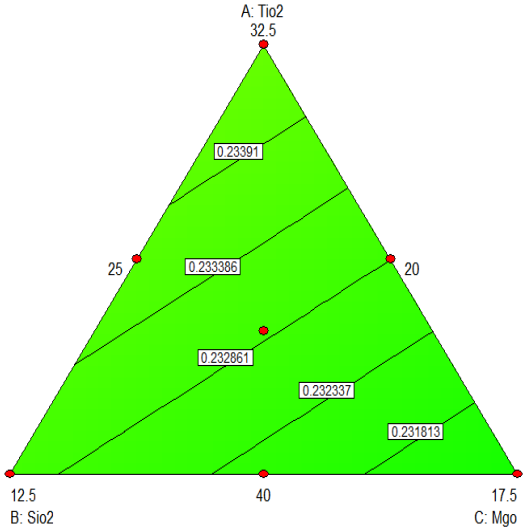

(e) Thermal conductivity

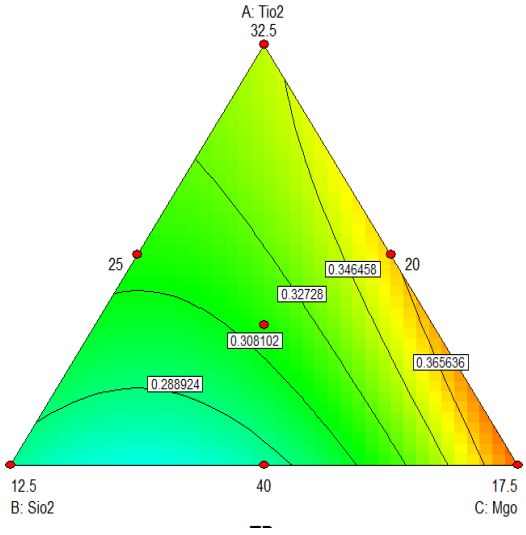

(f) Thermal diffusivity

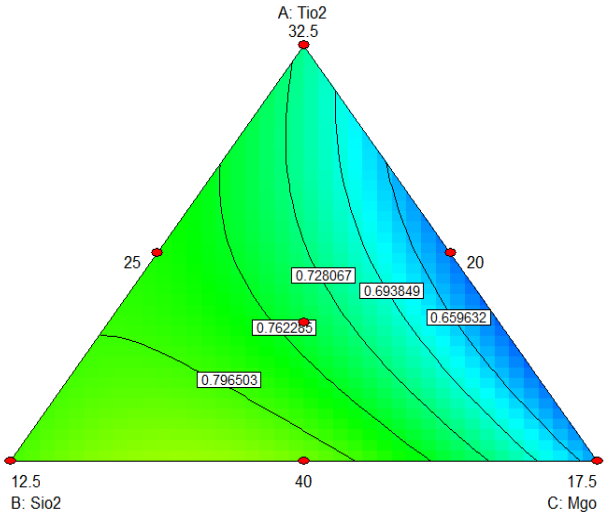

(g) Specific heat

Figure 5.8: Contour plot of physicochemical & thermophysical properties for rutile-acidic flux system

5.1.1.5 Optimization of physicochemical and thermophysical properties

To optimize various physicochemical and thermophysical properties a complex desirability optimization method, was suggested by [Derringer et al., 1980]. In this method predicted results are converted into desired responses using an unbiased function D(x) called desirability function and all the cumulative mean of individual responses taken for desirability value [Harington, 1965]. Equation 5.1 and 5.2 represent the complex desirability function (Castello et. al., 1996).

$$D = [d_1^{w1}.\ d_2^{w2}.\ldots\ldots d_n^{wn}]^{1/(w_1+w_2+\ldots..\ w_n)} \quad (5.1)$$

$$D = [\prod^{i\to n} d_i\ ]^{1/\sum i\to n\ w_i} \quad (5.2)$$

Where d_i is the desirability of particular response, n is the number of responses and w_i are the weights satisfying $0 < w_i < 1$ and $(w_1 + w_2 + w_3 +.....+ w_n) = 1$. At different levels of desirability, three optimum solutions with equal weightage given for different properties; is shown in Table (5.6-5.8) for basic, rutile-basic, and rutile-acidic flux systems (three flux systems).

Table 5.6: Optimized flux mixtures of different physicochemical and thermophysical properties for basic flux system

S.No	CaO	SiO_2	CaF_2	Al_2O_3	GFN	D	WL	ΔH	TC	TD	SH	Desirability
1	40.0	22.31	15.92	6.76	7.123	0.656	1.009	-6170	0.183	0.311	0.562	0.955
2	40.0	18.81	16.71	9.46	7.123	0.625	1.258	-6373	0.153	0.263	0.586	0.952
3	40.0	18.74	16.25	10.00	7.194	0.622	1.273	-6451	0.147	0.239	0.618	0.949

Table 5.7: Optimized flux mixtures of different physicochemical and thermophysical properties for rutile-basic flux system

S.No	TiO_2	SiO_2	CaO	Al_2O_3	GFN	D	WL	ΔH	TC	TD	SH	Desirability
1	35.0	25.0	15.00	10.00	7.816	0.890	1.253	-6932	0.158	0.255	0.650	0.710
2	35.0	16.84	27.15	6.00	8.270	0.926	0.312	-6370	0.174	0.260	0.645	0.620
3	25.51	25.0	28.0	6.41	7.907	0.928	2.691	-7967	0.166	0.267	0.648	0.610

Table 5.8: Optimized flux mixtures of different physicochemical and thermophysical properties for rutile-acidic flux system

S.No	TiO_2	SiO_2	MgO	Al_2O_3	GFN	D	WL	ΔH	TC	TD	SH	Desirability
1	35.58	16.40	23.01	10.0	6.374	0.966	0.372	-7538	0.235	0.301	0.775	0.630
2	35.34	16.57	23.08	10.0	6.371	0.967	0.377	-7546	0.235	0.301	0.775	0.629
3	35.18	16.72	23.09	10.0	6.360	0.967	0.372	-7556	0.235	0.301	0.775	0.628

Table 5.9: Percentage error of different physicochemical and thermophysical properties for basic flux system

Flux mixture				Predicted values							Actual values							Error (%)						
CaO	SiO_2	CaF_2	Al_2O_3	GFN	D	WL	ΔH	TC	TD	SH	GFN	D	WL	ΔH	TC	TD	SH	GFN	D	WL	ΔH	TC	TD	SH
40	18.7	18.7	7.5	6.40	0.61	0.63	6836	0.14	0.3	0.5	7.23	0.6	1.38	6001	0.13	0.24	0.56	1.4	3.1	54	13	1.4	25	4.2
33.7	18.7	25	7.5	7.32	0.65	1.82	7100	0.19	0.2	0.4	7.19	0.6	1.02	5005	0.15	0.32	0.47	1.8	2.5	77	41	3.8	29	0.6
32.5	25	17.5	10	7.78	0.79	0.31	5003	0.15	0.2	0.4	8.01	0.7	1.47	7601	0.16	0.29	0.56	2.8	0.5	78	34	6.6	13	1.7

Table 5.10: Percentage error of different physicochemical and thermophysical properties for rutile-basic flux system

Flux mixture				*Predicted values*							*Actual values*							*Error (%)*						
TiO_2	SiO_2	*CaO*	Al_2O_3	*GFN*	*D*	*WL*	*ΔH*	*TC*	*TD*	*SH*	*GFN*	*D*	*WL*	*ΔH*	*TC*	*TD*	*SH*	*GFN*	*D*	*WL*	*ΔH*	*TC*	*TD*	*SH*
35	25	20	5	8.02	0.89	4.39	4298	0.14	0.28	0.64	8.40	0.97	6.01	4336	0.14	0.28	0.7	4.5	7.9	27	0.6	4.0	1.0	1.5
28.7	18.7	30	7.5	8.23	0.93	3.69	8134	0.18	0.21	0.71	7.86	0.95	2.61	7922	0.2	0.27	0.6	4.6	1.3	41	2.6	8.8	24	2.2
35	25	17.5	7.5	7.97	0.82	1.53	6009	0.14	0.16	0.68	7.73	0.90	1.17	6133	0.13	0.19	0.7	3.1	1.1	30	2.7	5.8	13	3.5

Table 5.11: Percentage error of different physicochemical and thermophysical properties for rutile-acidic flux system

Flux mixture				*Predicted values*							*Actual values*							*Error (%)*						
TiO_2	SiO_2	*MgO*	Al_2O_3	*GFN*	*D*	*WL*	*ΔH*	*TC*	*TD*	*SH*	*GFN*	*D*	*WL*	*ΔH*	*TC*	*TD*	*SH*	*GFN*	*D*	*WL*	*ΔH*	*TC*	*TD*	*SH*
40	12.5	25	7.5	6.08	1.03	0.77	8244	0.23	0.27	0.78	6.05	0.96	0.80	7873	0.22	0.27	0.81	0.4	7.2	3.4	4.7	4.9	2.5	4.0
35	20	20	10	6.50	1.02	1.63	7456	0.21	0.24	0.58	6.35	1.08	1.62	7528	0.22	0.25	0.61	2.3	5.0	0.3	0.9	1.8	4.0	5.0
40	15	25	5	6.68	0.99	0.61	9238	0.23	0.27	0.80	6.02	1.00	0.56	8381	0.21	0.25	0.83	5.0	1.0	9.0	1.0	1.4	5.4	3.2

The confirmatory experiments were performed by randomly selecting flux mixture components to validate the regression models. Three flux mixtures randomly selected from basic, rutile-basic, and rutile-acidic flux systems, and it is observed that the error percentage for most of the properties is almost 5% (Table 5.9-5.11). Error percentage for weight loss, change in enthalpy, and thermal diffusivity is more than 5% for a basic flux system (Table 5.9). Table 5.10 shows that the error percentage for weight loss, thermal conductivity, and thermal diffusivity is more than 5% for the rutile-basic flux system.

5.1.1.6 Discussion of contact angle & surface tension properties

To determine the wetting and surface tension properties of SAW fluxes (for three flux systems) different pallets placed on the X70 substrate. Diffeent pallets placed in the muffle furnace which is maintained at different target temperatures. In this section wetting as well as surface tension behaviour of rutile-acidic fluxes was studied at 1700 K. Similar results were observed for basic & rutile-basic flux systems.

5.1.1.6.1 Influence of TiO_2/SiO_2, TiO_2/MgO & TiO_2/Al_2O_3 flux ratios on the measured contact angle

The influence of flux compositional ratios on the measured contact angle shown in fig. 5.9 (a-c). With an increase in the TiO_2/SiO_2 ratio, the measured contact angle value increases while a higher value of contact angle observed in the compositional range varies from 1.5 to 2.7, after which it starts decreasing. Measured contact angle value increased with an increase in the TiO_2/MgO & TiO_2/Al_2O_3 flux ratio. Available literature suggests that lower contact angle between fluxes and heating substrate gives good wetting properties. Optimum wettability of the welding flux reduces the chances of entrapment of unwanted gaseous inclusions (e.g., H_2, N_2 & O_2 gases) in the weld zone and provides coverage to weld region by protecting the molten weld metal from different welding defects [Kim et al., 2015]. Flux number 3, 9, 10, 16, 17 & 18 gives the optimum value of measured contact angle due to lesser spreading area over the heating substrate. Flux 7 gives a very lower value of contact angle ($\theta = 0^o$) and due to the higher value of spreading area over the heating substrate. Due to the acidic nature of Al_2O_3 & SiO_2, both try to increase the interfacial tensions at the interface due to its capability of decreasing free oxygen (O^{2-}) ions, if any present in the network structure. Free oxygen ions readily combine with the Si^{4+} or Al^{3+} cations present in the network structure and thus increases the surface properties [Jung et al., 2010 & 2012]. The variation of contact angle with the spreading area of different flux pallets shown in fig.5.10. From fig.5.10 it observed that at lower contact angle ($\theta = 0^o$), maximum spreading area (1300.12 mm^2) was observed while as the contact angle increases, the spreading area decreases.

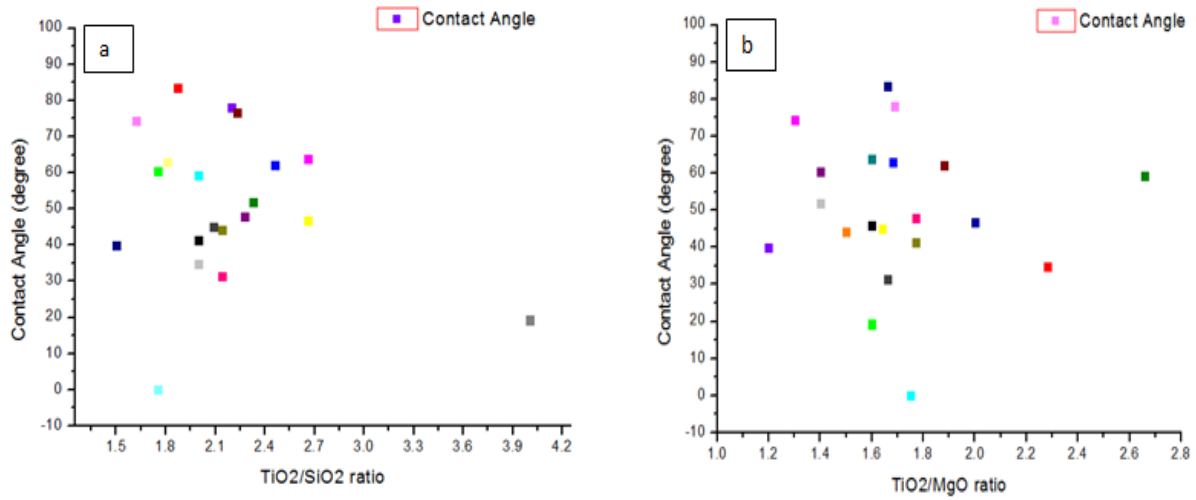

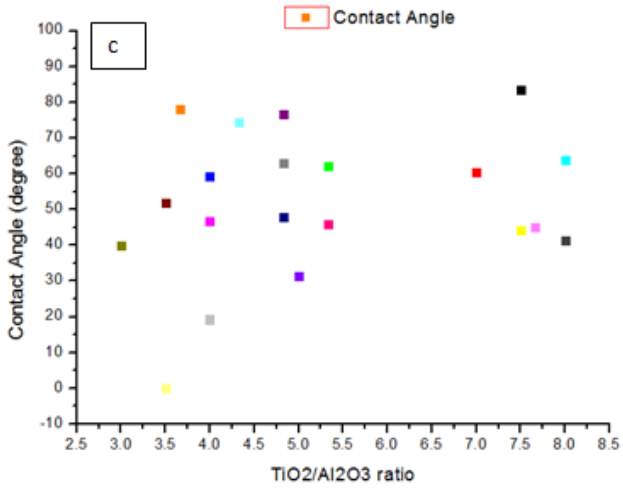

Figure 5.9 (a-c): Influence of flux compositional ratios on contact angle (Rutile-acidic system)

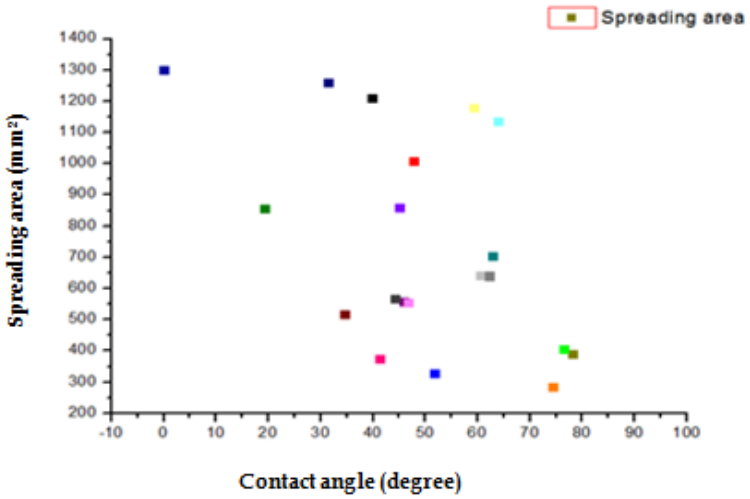

Figure 5.10: Contact angle vs. spreading area variation (Rutile-acidic system)

5.1.1.6.2 Influence of TiO_2/SiO_2, TiO_2/MgO & TiO_2/Al_2O_3 flux ratios on the surface tension properties

Figure 5.11 (a-c) shows the effect of TiO_2/SiO_2, TiO_2/MgO, and TiO_2/Al_2O_3 flux ratio on the surface tension. From fig.5.11a, it is clear that with an increase in the TiO2/SiO2 ratio from 1.5 to 2.0, the calculated surface tension value decreases while, after that, it increases with an increase in TiO_2/SiO_2 ratio. It means that surface tension of flux components is having a lesser affect up to 1.5 to 2.0 compositional flux ratios,, while after that, it significantly increase the surface tension. Kim et al. investigated that an increase in CaO/SiO_2 ratio increases the surface tension value for the $CaO\text{-}SiO_2\text{-}14.9MgO\text{-}8.1Al_2O_3$ slag system due to the difference in surface tension factors of corresponding constituents [Wang et al., 2005, Benesch et al., 1976]. Fig. 5.11 (b-c), it is observed that with an increase in TiO_2/MgO & TiO_2/Al_2O_3 ratio, the calculated surface tension value decreases. It means that surface tension factor of flux constituents having a lesser effect on surface tension at both of these compositional ratios. It observed that if oxides exhibit acidic tendencies of network formation, then surface tension factor generally decreased while it increased if basic oxides present in the structure during network formation.

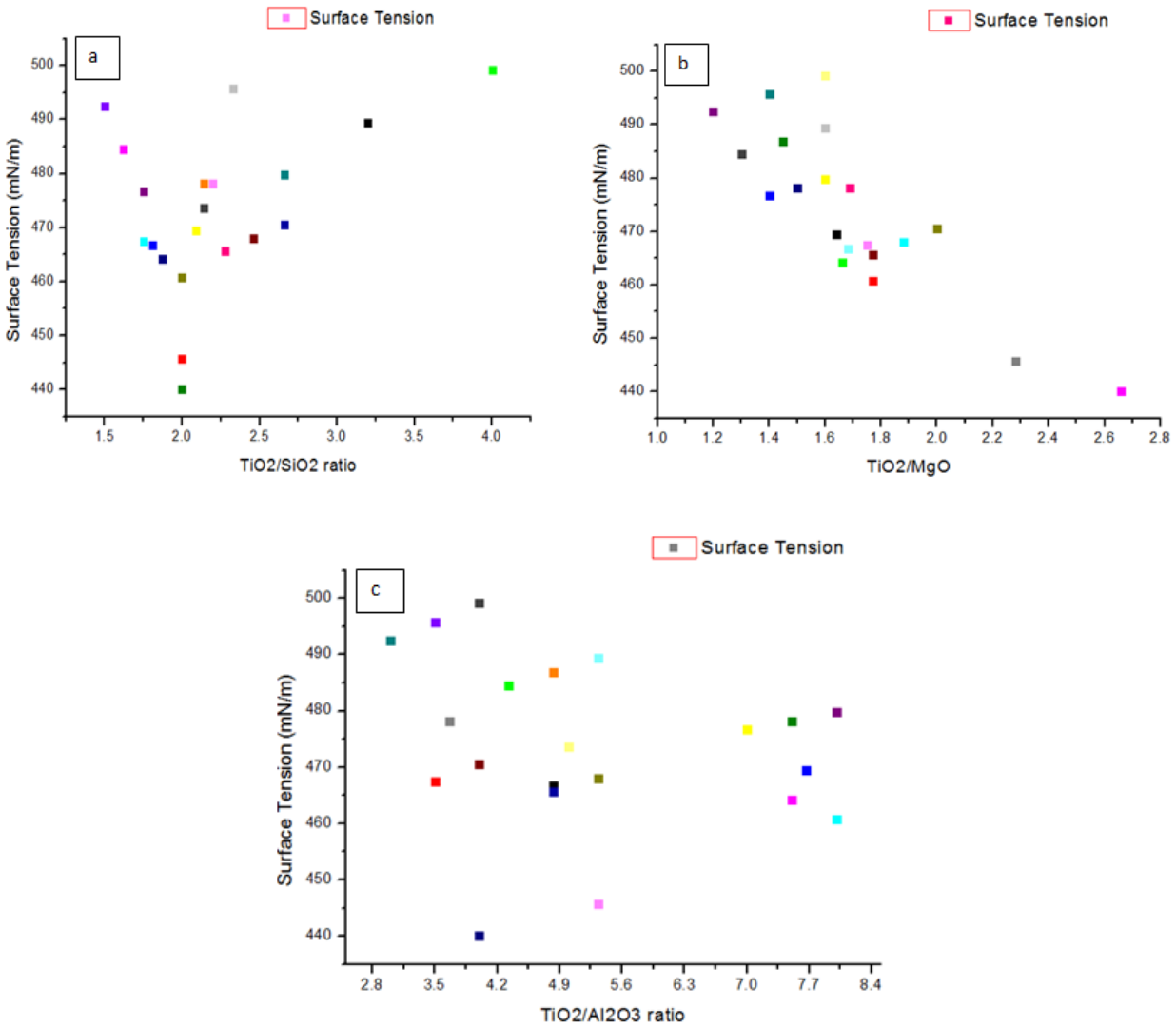

Figure 5.11 (a-c): Influence of flux compositional ratios on surface tension (Rutile-acidic system)

5.1.1.6.3 Influence of TiO_2/SiO_2, TiO_2/MgO & TiO_2/Al_2O_3 flux ratios on the work of adhesion

The relation between liquid phase and gaseous phase can be indirectly related with important interfacial parameter known as work of adhesion (W_a). Previous literature study reveals that there is inverse relationship between contact angle and work of adhesion [Li et al., 1992]. The amount of energy per unit area required for removing the contacting material from the heating plate or substrate is known as work of adhesion. Work of adhesion can be calculated using Dupre-Young equation [Li et al., 1989]. The results of work of adhesion (W_a) are shown in fig. 5.12 (a-c) based on the contact angle as well as surface tension calculations. It is clear from fig. 5.12 (a) that with increase of TiO_2/SiO_2 ratio the calculated work of adhesion value is increased while maximum value of work of adhesion is obtained in the 1.5 to 1.8 or 2.4 to 2.6 compositional range. From fig. 5.12 (b) it is clear that with increase of TiO_2/MgO ratio the work of adhesion value firstly increased up to 1.2 to 2.0 flux ratio but after that it little bit decreased. Similar trend was observed for fig. 5.12 (c) as observed in fig. 5.12 (b). Previous study reveals that if between two dissimilar surfaces the adhesion energy increases then the contact angle between the two surfaces is subsequently reduced, which results in higher wettability as well as high spreading area. Higher flowability of molten flux on the substrate takes place due to high wettability as spreading area is more and there is less chances of removal of flux from the substrate due to high resistance between molten flux and substrate [Li et al., 1989]. Flux 7 shows high wettability & spreading area due lower value of contact angle as compared to the other fluxes.

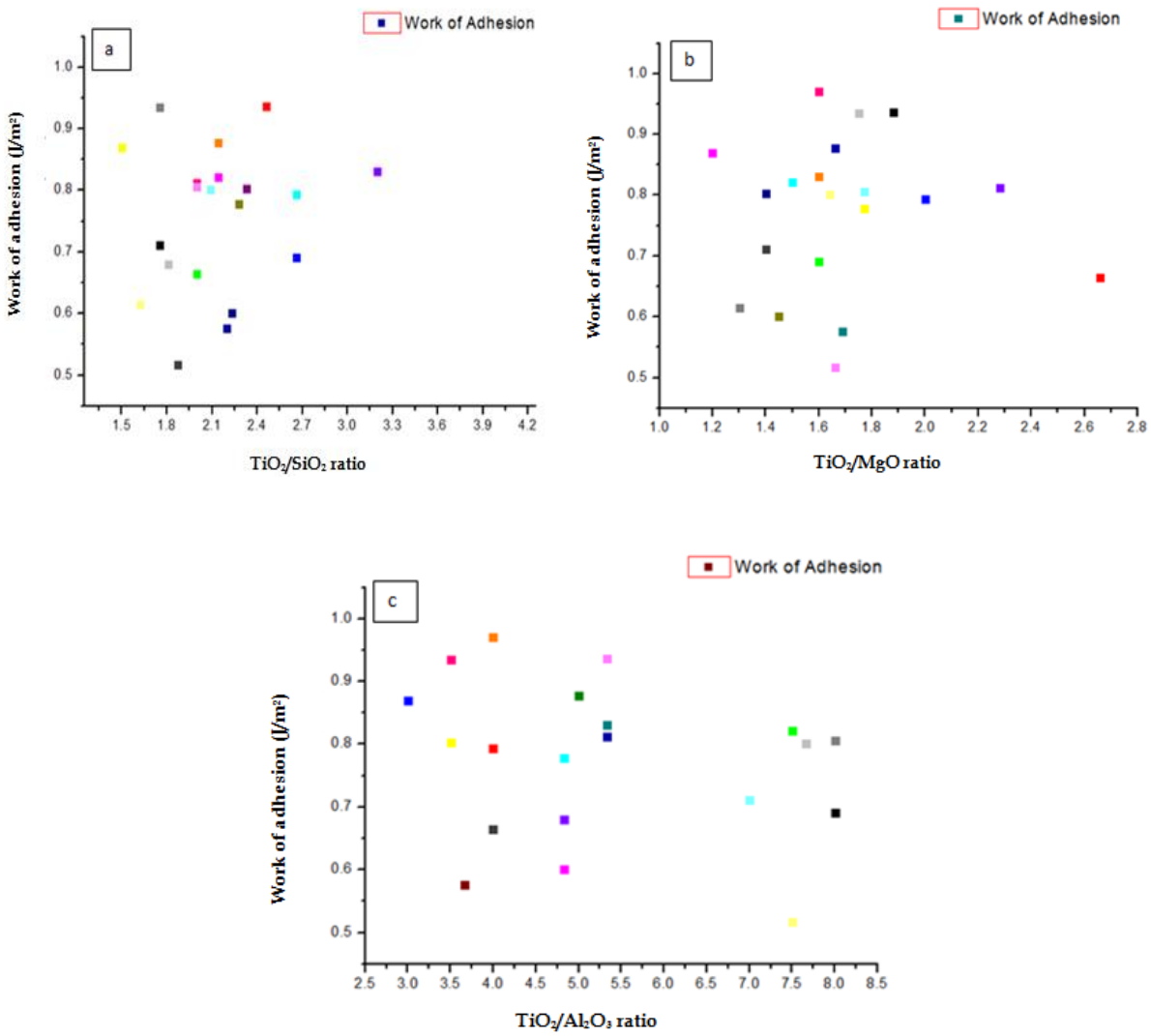

Figure 5.12 (a-c): Work of adhesion behaviour at different flux ratios (Rutile-acidic system)

5.1.1.7 Phase analysis of flux constituents for three flux systems

X-ray diffraction analysis of basic, rutile-basic, and rutile-acidic flux systems was performed using 2θ diffraction mode in the range of 20° to 80°. Various crystalline phases such as CaO, SiO_2, CaF_2, $CaAlF(SiO_4)$, TiO_2, Ti_4O_7, Ti_8O_{15}, $CaCO_3$, $CaTiSiO_5$, Al_2O_3, $K_2MgSi_5O_{12}$, and Mg_2SiO_4 formed in basic, rutile-basic and rutile-acidic flux systems which are in close agreement with the previous literature (Baune, et al., 2000, Chang et al., 2008, Jindal et al., 2013). Calcium carbonates, calcium silicate, titanium oxide, and potassium magnesium silicate compounds observed in the basic, rutile-basic, and rutile-acidic flux systems. Silicates and potassium silicates formed due to the oxidation of different elements such as Ca, Mg, Al, K, and Si present in the binder as well as in the three flux systems. Depending upon the flux composition, the intensity of peaks varies in three different flux systems. Figure 5.13 shows the X-ray diffraction pattern for basic, rutile-basic, and rutile-acidic flux systems.

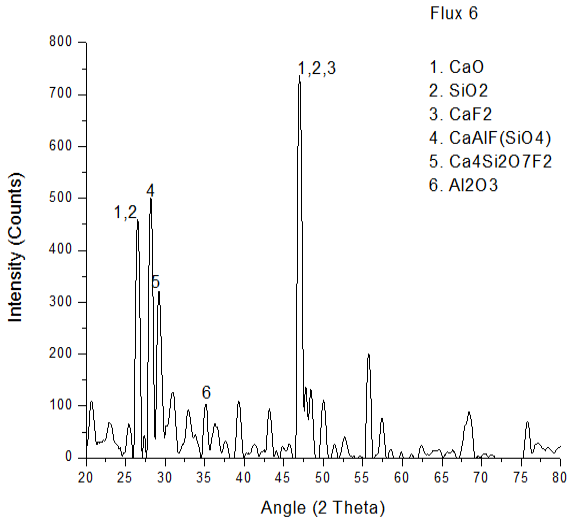
Flux 6
1. CaO
2. SiO2
3. CaF2
4. CaAlF(SiO4)
5. Ca4Si2O7F2
6. Al2O3
Intensity (Counts)
Angle (2 Theta)
1,2
4
5
6
1,2,3

(a)

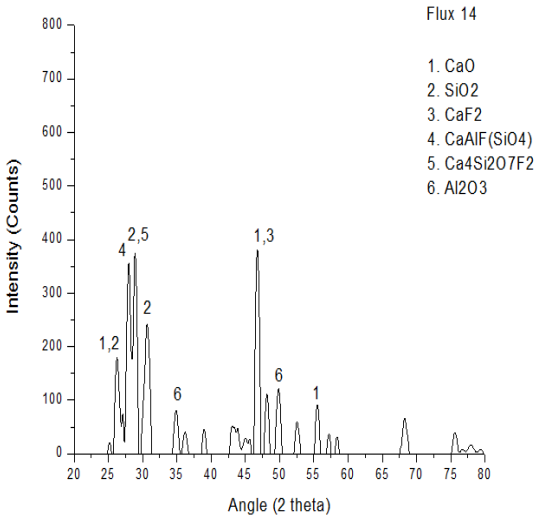
Flux 14
1. CaO
2. SiO2
3. CaF2
4. CaAlF(SiO4)
5. Ca4Si2O7F2
6. Al2O3
Intensity (Counts)
Angle (2 theta)
1,2
4
2,5
2
6
1,3
6
1

(b)

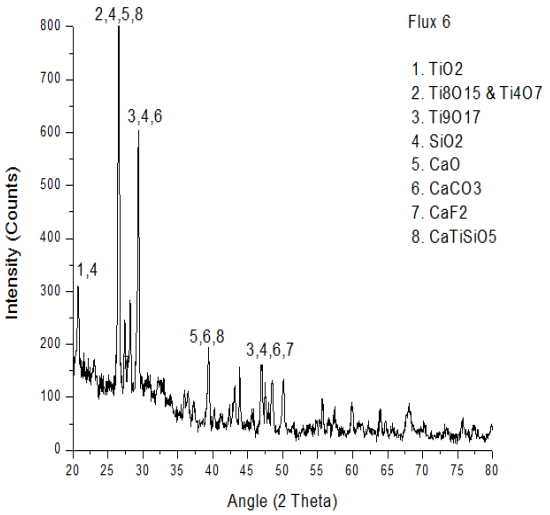
Flux 6
1. TiO2
2. Ti8O15 & Ti4O7
3. Ti9O17
4. SiO2
5. CaO
6. CaCO3
7. CaF2
8. CaTiSiO5
Intensity (Counts)
Angle (2 Theta)
2,4,5,8
3,4,6
1,4
5,6,8
3,4,6,7

(c)

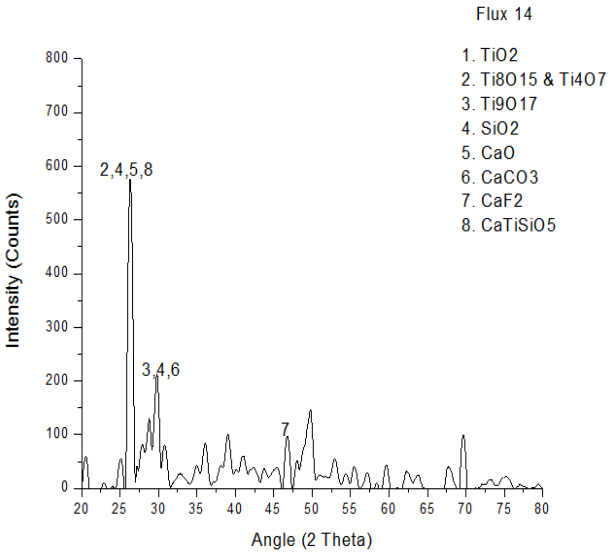
Flux 14
1. TiO2
2. Ti8O15 & Ti4O7
3. Ti9O17
4. SiO2
5. CaO
6. CaCO3
7. CaF2
8. CaTiSiO5
Intensity (Counts)
Angle (2 Theta)
2,4,5,8
3,4,6
7

(d)

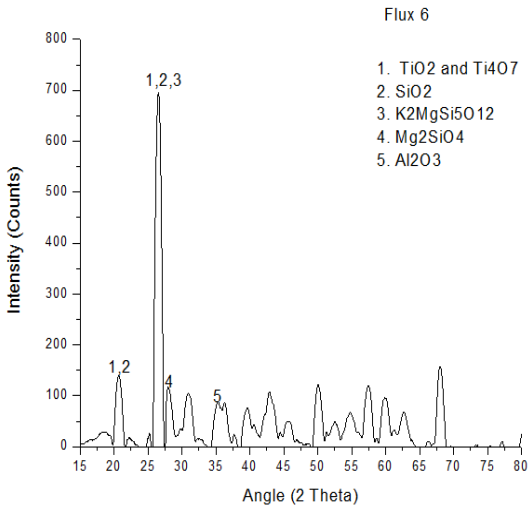
Flux 6
1. TiO2 and Ti4O7
2. SiO2
3. K2MgSi5O12
4. Mg2SiO4
5. Al2O3
Intensity (Counts)
Angle (2 Theta)
1,2,3
1,2
4
5

(e)

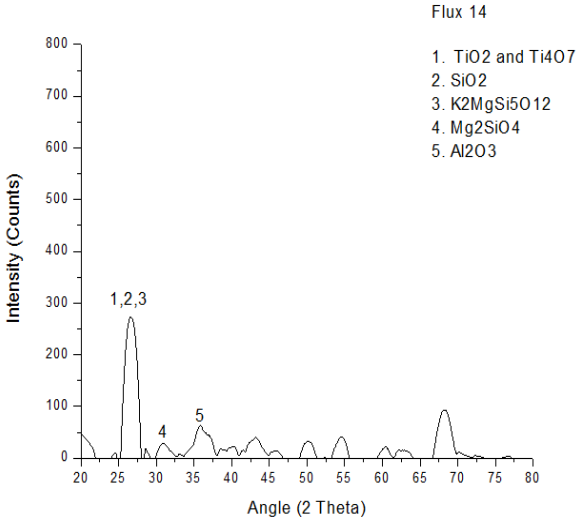
Flux 14
1. TiO2 and Ti4O7
2. SiO2
3. K2MgSi5O12
4. Mg2SiO4
5. Al2O3
Intensity (Counts)
Angle (2 Theta)
1,2,3
4
5

(f)

Figure 5.13: X-ray diffraction pattern for (a-b) basic flux system; (c-d) rutile-basic flux system; (e-f) rutile-acidic flux system.

5.1.1.8 Structural analysis of flux constituents for three flux systems

Different types of symmetric and asymmetric bonds were observed during Fourier transform infrared spectroscopy (FTIR) of basic, rutile-basic, and rutile-acidic flux components. Symmetric Si-O-Si, asymmetric Si-O-O, symmetric Al-O-Al, asymmetric Al-O-Al, O-H vibration, B-O vibration modes were observed in basic, rutile-basic and rutile-acidic flux systems which are in close agreement with the previous literature. TiO_2 used as an impurity in mould fluxes, but it can be used as a replacement for CaF_2 in F-free (fluorine) powders. The presence of TiO_2 in the flux would give TiO^{4+} ions, which combine with Si^{4+} ions in the network. It is reported that the addition of TiO_2 in the flux reduces the slag viscosity. In network structure TiO^{4+} ions may act as network former/breaker, may form clusters with Si-O-Si & Ti-O-Ti ions because it has tendency for formation of bonds with their own or other functioned groups [G. Kaur et al., 2011, M. Garai et al., 2014 & 2015, T. Sowmya et al., 2004]. Depending upon the flux composition intensity of peaks varies in three flux systems. Figure 5.14 shows the FTIR plots for basic, rutile-basic, and rutile-acidic flux systems.

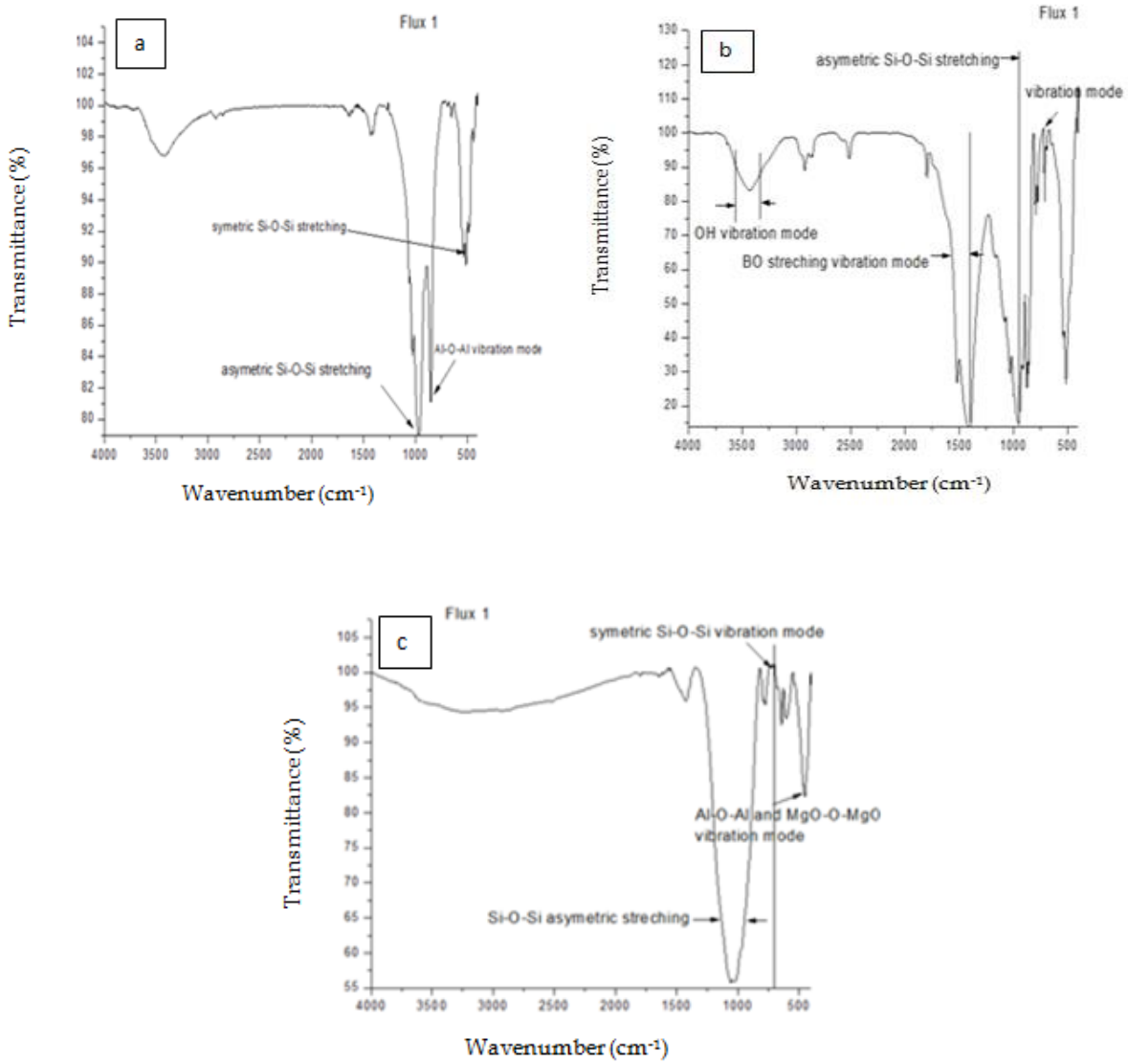

Figure 5.14: FTIR plots for three flux systems; (a) flux 1 (F1) basic flux system; (b) flux 1 (F1) rutile-basic flux system; (c) flux 1 (F1) rutile-acidic flux system

5.2 MULTI-PASS BEAD ON PLATE EXPERIMENTATION FOR THREE FLUX SYSTEMS

Multi-pass bead on plate weld deposits experimentation performed (for three flux systems) on submerged arc welding machine available at Jindal SAW Limited, Mundra. API X70 grade steel having dimensions 290 x 290 x 22 mm was used for a multi-pass bead on plate weld deposits experimentation (Shown in Section 4 Experimentation, Figure 4.9).

5.2.1 Bead profile analysis

After multi-pass bead on plate experimentation, bead width, bead height, and penetration analyzed for basic, rutile-basic, and rutile-acidic flux systems. For analyzing the bead width, height, and penetration, the weld bead deposits lightly etched with nital solution, and then using stereo microscope full weld bead cross-section was checked at 4X magnification. Table 5.12 shows the bead width, bead height, and penetration values for some of the fluxes from three flux systems. Depth of penetration has a higher value for rutile-basic and rutile-acidic fluxes as compared to the basic fluxes due to the presence of titanium and silica constituents in rutile-basic and rutile-acidic fluxes. Figure 5.15 represents the graphical plots showing full weld bead cross-section of F5B, F14B, F1RB, F3RB, F4RA, and F6RA fluxes.

Table 5.12: Bead width, height and penetration analysis for three flux systems

S.No	*Basic Flux system*			*S.No*	*Rutile-basic system*			*S.No*	*Rutile-acidic system*		
Flux	W	H	P	Flux	W	H	P	Flux	W	H	P
F5B	2.8mm	2.0mm	1.5mm	F1RB	2.8mm	1.7mm	2.2mm	F4RA	3.1mm	1.5mm	1.9mm
F14B	3.0mm	1.2mm	1.5mm	F3RB	3.3mm	1.6mm	2.1mm	F6RA	1.8mm	1.4mm	2.1mm

W: bead width; H: bead height; P: penetration

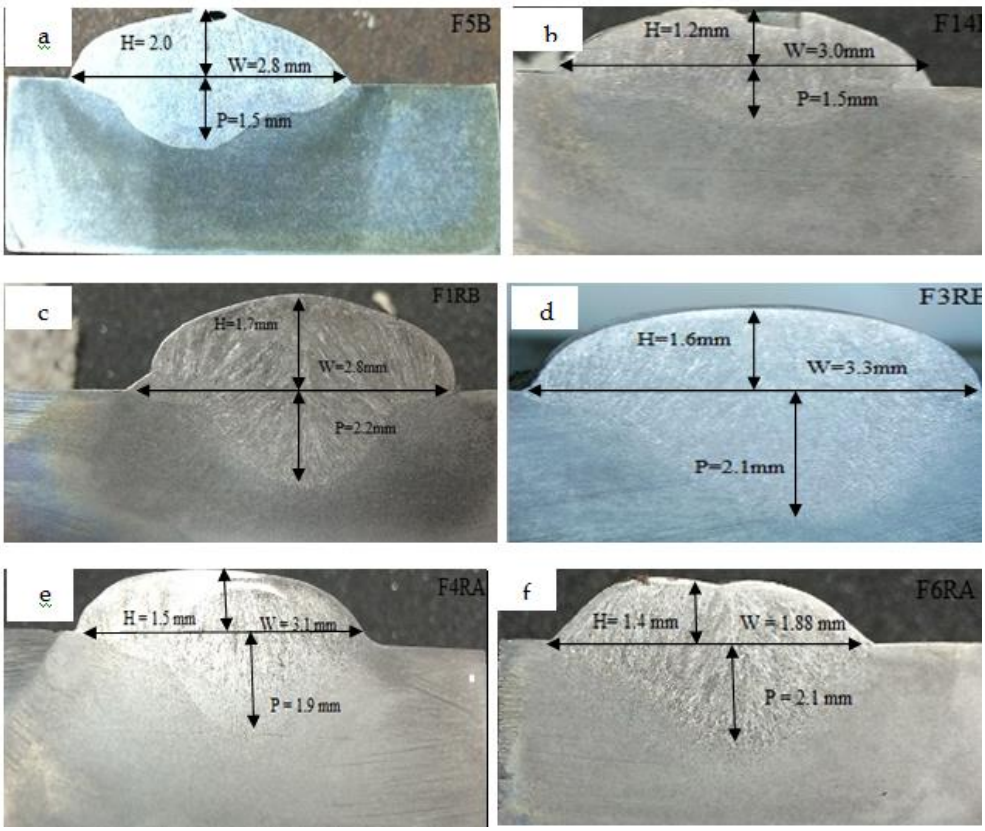

Figure 5.15: Weld bead depth of penetration, bead width and bead height analysis; (a-b) for flux 4 and 14 of basic flux system; (c-d) for flux 1 and 3 of rutile-basic flux system; (e-f) for flux 4 and 6 of rutile-acidic flux system.

5.2.2 Optimization of grain size, bead chemistry and microhardness during multi-pass weld deposits for three flux systems

Regression models of multi-pass bead on plate weld deposit properties such as bead chemistry, grain size, and microhardness developed for basic, rutile-basic, and rutile-acidic flux systems. The adequacy of developed regression models checked using analysis of variance (ANOVA).

5.2.2.1 Analysis of grain size, bead chemistry and microhardness for SAW multi-pass weld deposits

Experimental properties such as bead chemistry, average grain size, and microhardness analyzed in terms of individual, binary, and ternary flux components for basic, rutile-basic, and rutile-acidic flux systems. Table 5.13-5.15 shows the results of bead chemistry, average grain size, and microhardness properties for three flux systems.

5.2.2.1.1 Regression model of grain size, bead chemistry and microhardness for three flux system

Linear, quadratic, reduced quadratic, cubic, special cubic and reduced special cubic regression models of bead chemistry, grain size and microhardness were developed in terms of individual, binary and ternary flux components for three flux systems. Equations A21-A31, A32-A41 and A42-A51 show the regression model equations for basic, rutile-basic and rutile-acidic flux systems. All regression equations (A24-A51) are shown in Appendix 1.

Table 5.13: Bead chemistry, average grain size and microhardness value for basic flux system

Flux	*C*	*Si*	*P*	*S*	*Cu*	*Ti*	*Mn*	*Ni*	*Cr*	*Mo*	*V*	*Nb*	*B*	*ASTM GS*	*MH (HV)*	*CE*
F1	0.0515	0.2570	0.0221	0.0015	0.0422	0.0124	0.9876	0.0110	0.0633	0.3391	0.0056	0.0091	0.0010	8.8	206	0.30
F2	0.0561	0.3425	0.0168	0.0020	0.0363	0.0131	0.9994	0.0098	0.0646	0.2893	0.0043	0.0116	0.0013	8.9	209	0.29
F3	0.0442	0.3877	0.0209	0.0030	0.0392	0.0130	0.7543	0.0100	0.0604	0.3071	0.0039	0.0082	0.0012	7.9	192	0.24
F4	0.0425	0.5439	0.0203	0.0037	0.0355	0.0127	0.5788	0.0096	0.0581	0.2821	0.0029	0.0090	0.0013	8.5	209	0.21
F5	0.0542	0.4240	0.0184	0.0026	0.0369	0.0152	0.8769	0.0095	0.0627	0.2952	0.0041	0.0109	0.0014	8.8	207	0.27
F6	0.0513	0.3735	0.0195	0.0056	0.0356	0.0134	0.7271	0.0101	0.0626	0.2876	0.0037	0.0095	0.0014	7.6	199	0.24
F7	0.0470	0.3935	0.0174	0.0050	0.0362	0.0127	0.7337	0.0108	0.0627	0.2842	0.0037	0.0102	0.0013	9.0	207	0.24
F8	0.0443	0.4654	0.0249	0.0065	0.0418	0.0128	0.7447	0.0099	0.0647	0.3025	0.0042	0.0101	0.0013	8.7	203	0.24
F9	0.0483	0.3975	0.0237	0.0082	0.0376	0.0136	0.7449	0.0099	0.0667	0.2892	0.0042	0.0120	0.0015	7.9	190	0.24
F10	0.0475	0.3692	0.0202	0.0045	0.0402	0.0128	0.7596	0.0105	0.0653	0.2970	0.0042	0.0102	0.0012	8.1	189	0.25
F11	0.0422	0.5871	0.0215	0.0044	0.0396	0.0134	0.5813	0.0103	0.0599	0.3151	0.0032	0.0098	0.0015	9.3	218	0.21
F12	0.0566	0.2797	0.0196	0.0020	0.0376	0.0161	1.0671	0.0099	0.0730	0.2762	0.0048	0.0151	0.0012	8.9	206	0.30
F13	0.0483	0.5519	0.0208	0.0062	0.0376	0.0164	0.6837	0.0103	0.0653	0.2842	0.0040	0.0129	0.0017	9.3	217	0.23
F14	0.0592	0.4519	0.0224	0.0059	0.0379	0.0180	0.7608	0.0103	0.0644	0.3183	0.0045	0.0113	0.0016	9.0	206	0.26
F15	0.0562	0.3462	0.0206	0.0034	0.0398	0.0176	0.9887	0.0106	0.0676	0.3082	0.0050	0.0120	0.0013	8.6	207	0.30
F16	0.0501	0.4239	0.0219	0.0043	0.0386	0.0162	0.8652	0.0107	0.0695	0.2966	0.0051	0.0130	0.0014	8.1	207	0.27
F17	0.0489	0.5227	0.0221	0.0045	0.0373	0.0121	0.7110	0.0107	0.0672	0.2923	0.0041	0.0116	0.0013	7.7	204	0.24
F18	0.0458	0.5686	0.0213	0.0057	0.0390	0.0123	0.5816	0.0109	0.0618	0.3127	0.0032	0.0085	0.0013	9.1	216	0.22
F19	0.0459	0.4622	0.0230	0.0031	0.0368	0.0099	0.8116	0.0106	0.0699	0.2764	0.0039	0.0133	0.0008	9.1	214	0.25
F20	0.0471	0.5480	0.0187	0.0059	0.0358	0.0145	0.6590	0.0104	0.0701	0.2610	0.0040	0.0146	0.0013	8.5	198	0.22
F21	0.0516	0.4653	0.0186	0.0047	0.0335	0.0167	0.8487	0.0090	0.0718	0.2725	0.0040	0.0141	0.0015	9.0	223	0.28

Table 5.14: Bead chemistry, average grain size and microhardness value for rutile-basic flux system

Flux	*C*	*Si*	*P*	*S*	*Cu*	*Ti*	*Mn*	*Ni*	*Cr*	*Mo*	*V*	*Nb*	*B*	*ASTM GS*	*MH (HV)*	*CE*
F1	0.0559	0.3654	0.0244	0.0039	0.0290	0.0248	0.8518	0.0073	0.0646	0.3029	0.0131	0.0217	0.0018	7.2	204	0.26
F2	0.0503	0.3432	0.0146	0.0021	0.0314	0.0212	0.5634	0.0079	0.0630	0.2809	0.0118	0.0181	0.0014	8.8	217	0.21
F3	0.0456	0.5022	0.0152	0.0024	0.0314	0.0248	0.6178	0.0081	0.0664	0.2657	0.0103	0.0200	0.0016	8.4	204	0.21
F4	0.0403	0.5979	0.0149	0.0023	0.0376	0.0234	0.3955	0.0085	0.0494	0.3448	0.0139	0.0178	0.0015	8.5	205	0.19
F5	0.0454	0.4404	0.0145	0.0017	0.0321	0.0170	0.4966	0.0080	0.0617	0.2985	0.0130	0.0182	0.0014	7.2	206	0.20
F6	0.0501	0.3631	0.0157	0.0021	0.0340	0.0215	0.4526	0.0087	0.0571	0.3094	0.0141	0.0160	0.0014	7.0	203	0.20
F7	0.0499	0.2899	0.0166	0.0020	0.0304	0.0209	0.5461	0.0079	0.0678	0.2816	0.0139	0.0174	0.0012	8.6	201	0.21
F8	0.0498	0.3029	0.0176	0.0051	0.0353	0.0257	0.5220	0.0083	0.0575	0.2840	0.0088	0.0124	0.0014	8.9	200	0.21
F9	0.0496	0.3289	0.0185	0.0039	0.0346	0.0207	0.5012	0.0090	0.0639	0.3041	0.0170	0.0165	0.0012	8.8	188	0.21
F10	0.0451	0.4752	0.0175	0.0029	0.0356	0.0174	0.4584	0.0084	0.0594	0.3113	0.0142	0.0181	0.0011	8.7	195	0.20
F11	0.0483	0.4269	0.0159	0.0023	0.0362	0.0203	0.4262	0.0089	0.0556	0.3387	0.0150	0.0170	0.0013	7.3	202	0.20
F12	0.0519	0.3656	0.0166	0.0024	0.0360	0.0230	0.4873	0.0089	0.0603	0.3065	0.0147	0.0177	0.0014	8.5	203	0.21
F13	0.0530	0.3247	0.0248	0.0041	0.0345	0.0180	0.4476	0.0086	0.0678	0.3033	0.0182	0.0208	0.0012	8.0	216	0.20
F14	0.0572	0.3077	0.0217	0.0035	0.0270	0.0221	0.6346	0.0076	0.0771	0.2510	0.0159	0.0261	0.0012	9.0	227	0.24
F15	0.0521	0.4296	0.0263	0.0045	0.0348	0.0175	0.3889	0.0074	0.0621	0.3117	0.0159	0.0202	0.0011	5.8	201	0.19
F16	0.0514	0.4273	0.0261	0.0051	0.0348	0.0192	0.3463	0.0073	0.0577	0.3210	0.0162	0.0211	0.0011	8.7	207	0.19
F17	0.0549	0.3348	0.0273	0.0049	0.0347	0.0173	0.3637	0.0071	0.0628	0.3132	0.0179	0.0210	0.0010	8.9	210	0.19
F18	0.0468	0.5528	0.0242	0.0057	0.0378	0.0214	0.3589	0.0079	0.0540	0.3469	0.0143	0.0219	0.0014	8.4	214	0.19
F19	0.0543	0.3818	0.0233	0.0047	0.0331	0.0239	0.4695	0.0072	0.0627	0.3028	0.0145	0.0227	0.0013	7.3	209	0.21
F20	0.0527	0.5249	0.0252	0.0047	0.0327	0.0204	0.4078	0.0075	0.0604	0.3186	0.0139	0.0221	0.0013	7.5	212	0.20
F21	0.0522	0.5377	0.0215	0.0050	0.0292	0.0232	0.4671	0.0075	0.0615	0.2683	0.0123	0.0245	0.0014	8.5	211	0.20

Table 5.15: Bead chemistry, average grain size and microhardness value for rutile-acidic flux system

Flux	*C*	*Si*	*P*	*S*	*Cu*	*Ti*	*Mn*	*Ni*	*Cr*	*Mo*	*V*	*Nb*	*B*	*ASTM GS*	*MH (HV)*	*CE*
F1	0.0497	0.7669	0.0118	0.0032	0.0357	0.0243	0.3719	0.0131	0.0495	0.3302	0.0115	0.0187	0.0024	8.9	228	0.19
F2	0.0499	0.6577	0.0133	0.0029	0.0327	0.0190	0.3949	0.0123	0.0541	0.2856	0.0132	0.0241	0.0019	8.8	242	0.18
F3	0.0450	0.7290	0.0127	0.0032	0.0030	0.0183	0.3964	0.0125	0.0541	0.2835	0.0118	0.0218	0.0019	9.4	205	0.19
F4	0.0497	0.7006	0.0123	0.0030	0.0304	0.0207	0.4627	0.0118	0.0580	0.2729	0.0111	0.0229	0.0021	7.8	209	0.19
F5	0.0511	0.6978	0.0127	0.0032	0.0316	0.0179	0.4569	0.0129	0.0573	0.2802	0.0106	0.0216	0.0019	9.2	167	0.19
F6	0.0547	0.7961	0.0112	0.0030	0.0291	0.0194	0.4570	0.0114	0.0585	0.2703	0.0097	0.0221	0.0024	9.6	228	0.20
F7	0.0555	0.6420	0.0125	0.0035	0.0230	0.0154	0.6372	0.0106	0.0707	0.1960	0.0091	0.0279	0.0016	8.3	217	0.21
F8	0.0531	0.6210	0.0119	0.0030	0.0213	0.0151	0.3536	0.0105	0.0710	0.1982	0.0081	0.0274	0.0015	8.9	232	0.20
F9	0.0541	0.6854	0.0132	0.0029	0.0280	0.0143	0.5640	0.0115	0.0648	0.2428	0.0090	0.0234	0.0017	9.3	172	0.21
F10	0.0551	0.7366	0.0132	0.0036	0.0330	0.0149	0.3918	0.0118	0.0528	0.2898	0.0115	0.0206	0.0021	7.9	223	0.19
F11	0.0536	0.7313	0.0120	0.0033	0.0316	0.0194	0.4096	0.0118	0.0542	0.2801	0.0113	0.0211	0.0021	10.4	213	0.19
F12	0.0501	0.6050	0.0159	0.0028	0.0364	0.0170	0.3679	0.0133	0.0515	0.3218	0.0135	0.0208	0.0017	8.4	208	0.19
F13	0.0518	0.7121	0.0131	0.0033	0.0377	0.0117	0.3088	0.0132	0.0476	0.3134	0.0126	0.0188	0.0016	7.4	253	0.23
F14	0.0521	0.7331	0.0121	0.0040	0.0368	0.0114	0.4023	0.0130	0.0472	0.2913	0.0118	0.0187	0.0012	7.6	233	0.19
F15	0.0471	0.6972	0.0153	0.0050	0.0359	0.0191	0.3751	0.0101	0.0510	0.3060	0.0091	0.0216	0.0024	8.6	228	0.18
F16	0.0447	0.6474	0.0164	0.0055	0.0338	0.0222	0.3968	0.0104	0.0538	0.3013	0.0103	0.0238	0.0025	8.9	232	0.18
F17	0.0492	0.6139	0.0147	0.0039	0.0272	0.0142	0.5796	0.0107	0.0686	0.2297	0.0082	0.0272	0.0016	8.9	220	0.20
F18	0.0555	0.7178	0.0151	0.0044	0.0333	0.0135	0.4696	0.0112	0.0601	0.2780	0.0091	0.0223	0.0019	9.8	218	0.20
F19	0.0557	0.6988	0.0120	0.0041	0.0322	0.0132	0.3966	0.0111	0.0623	0.2777	0.0089	0.0222	0.0018	9.1	233	0.20
F20	0.0535	0.6827	0.0153	0.0051	0.0328	0.0212	0.4225	0.0113	0.0559	0.2897	0.0105	0.0234	0.0021	9.5	224	0.19
F21	0.0539	0.6583	0.0146	0.0045	0.0303	0.0179	0.4882	0.0113	0.0620	0.2581	0.0095	0.0240	0.0019	8.6	222	0.20

5.2.2.1.2 Analysis of variance for grain size, bead chemistry and microhardness for three flux system

For three flux systems, there were many insignificant terms in the models which observed during regression analysis of different properties such as bead chemistry, grain size, and microhardness. Backward elimination procedure used in equations A24-A51 to improve the properties of each model. Backward elimination is a model reduction method used to eliminate the insignificant terms present in the existing models. Table 5.16-5.18 shows the ANOVA results after backward elimination for three flux systems.

Table 5.16: ANOVA results for chemical composition, grain size and microhardness for multi-pass bead on plate for basic flux system

S.No	Source	SS	DF	MS	F value	P value	R^2 value	Status
C	Model	2.606E-004	5	5.213E-005	3.73	0.0215	0.65	Significant
	Linear	1.171E-004	3	3.903E-005	2.79	0.0764		Not Significant
	$CaO.CaF_2$	8.723E-005	1	8.723E-005	6.24	0.0246		Not Significant
	$CaF_2.Al_2O_3$	6.077E-005	1	6.077E-005	4.35	0.0546		Not Significant
	Residual	2.097E-004	15	1.398E-005				
	Total	4.703E-004	20					
Si	Model	0.12	8	0.015	3.16	0.0359	0.67	Significant
	Linear	0.052	3	0.017	3.64	0.0448		Significant
	$CaO.Al_2O_3$	0.025	1	0.025	5.35	0.0392		Significant
	$SiO_2.CaF_2$	0.035	1	0.035	7.48	0.0181		Significant
	$SiO_2.Al_2O_3$	0.035	1	0.035	7.41	0.0185		Significant
	$CaF_2.Al_2O_3$	0.031	1	0.031	6.64	0.0243		Significant
	$SiO_2.CaF_2.Al_2O_3$	0.035	1	0.035	7.33	0.0190		Significant
	Residual	0.057	12	4.719E-003				
Mn	Model	0.25	7	0.036	3.28	0.0309	0.63	Significant

	Linear	0.058	3	0.019	1.75	0.2070		Not Significant
	$SiO_2.CaF_2$	0.069	1	0.069	6.29	0.0262		Significant
	$CaO.SiO_2.CaF_2$	0.046	1	0.046	4.19	0.0615		Not Significant
	$CaO.CaF_2.Al_2O_3$	0.036	1	0.036	3.25	0.0947		Not Significant
	$SiO_2.CaF_2.Al_2O_3$	0.11		0.11	9.96	0.0076		Not Significant
	Residual	0.14	13	0.011				
	Total	0.40	20					
	Total	9.195E-005	20					
Mo	Model	4.232E-003	7	6.045E-004	3.50	0.0245	0.65	Significant
	Linear	1.072E-003	3	3.575E-004	2.07	0.1535		Not Significant
	$SiO_2.CaF_2$	5.459E-004	1	5.459E-004	3.16	0.0987		Not Significant
	$SiO_2.Al_2O_3$	1.413E-003	1	1.413E-003	8.19	0.0134		Significant
	$CaF_2.Al_2O_3$	1.033E-004	1	1.033E-004	0.60	0.4528		Not Significant
	$SiO_2.CaF_2.Al_2O_3$	3.957E-004		3.957E-004	2.29	0.1539		Not Significant
	Residual	2.243E-003	13	1.725E-004				
	Total	6.475E-003	20					

Ti	Model	6.965E-005	10	6.965E-006	3.85	0.0222	0.79	Significant
	Linear	1.770E-005	3	5.899E-006	3.26	0.0677		Not Significant
	$CaO.SiO_2$	8.594E-006	1	8.594E-006	4.75	0.0542		Not Significant
	$CaO.CaF_2$	1.417E-005	1	1.417E-005	7.84	0.0188		Significant
	$CaO.Al_2O_3$	8.339E-006		8.339E-006	4.61	0.0573		Not Significant
	$SiO_2.CaF_2$	3.793E-006	1	3.793E-006	2.10	0.1781		Not Significant
	$CaF_2.Al_2O_3$	9.771E-006		9.771E-006	5.41	0.0424		Significant
	$CaO.SiO_2.Al_2O_3$	1.623E-005	1	1.623E-005	8.98	0.0134		Significant
	$CaO.CaF_2.Al_2O_3$	1.341E-005		1.341E-005	7.42	0.0214		Significant
	Residual	1.808E-005	10	1.808E-006				
	Total	8.773E-005	20					
Cr	Model	2.423E-004	10	2.423E-005	3.20	0.0402	0.76	Significant
	Linear	4.046E-005	3	1.349E-005	1.78	0.2141		Not Significant
	$CaO.CaF_2$	2.163E-006	1	2.163E-006	0.29	0.6046		Not Significant

	$CaO.Al_2O_3$	4.564E-006	1	4.564E-006	0.60	0.4554		Not Significant
	$SiO_2.CaF_2$	1.036E-006	1	1.036E-006	0.14	0.7191		Not Significant
	$SiO_2.Al_2O_3$	2.110E-005	1	2.110E-005	2.79	0.1260		Not Significant
	$CaF_2.Al_2O_3$	1.389E-007	1	1.389E-007	0.018	0.8950		Not Significant
	$CaO.CaF_2.Al_2O_3$	7.386E-005	1	7.386E-005	9.76	0.0108		Significant
	$SiO_2.CaF_2.Al_2O_3$	1.096E-005	1	1.096E-005	1.45	0.2566		Not Significant
	Residual	7.570E-005	10	7.570E-006				
	Total	3.180E-004	20					
GS	Model	4.19	9	0.47	3.79	0.0207	0.75	Significant
	Linear	0.27	3	0.090	0.73	0.5541		Not Significant
	$CaO.SiO_2$	0.39	1	0.39	3.19	0.1017		Not Significant
	$CaO.CaF_2$	1.04	1	1.04	8.44	0.0143		Significant
	$CaO.Al_2O_3$	1.71		1.71	13.92	0.0033		Significant
	$SiO_2.CaF_2$	5.992E-003	1	5.992E-003	0.049	0.8292		Not Significant
	$SiO_2.Al_2O_3$	2.16	1	2.16	17.60	0.0015		Significant
	$CaF_2.Al_2O_3$	1.30		1.30	10.61	0.0076		Significant
	Residual	1.35	11	0.12				
	Total	5.54	20					

MH	Model	1223.54	9	135.95	3.90	0.0187	0.76	Significant
	Linear	65.51	3	21.84	0.63	0.6127		Not Significant
	$CaO.SiO_2$	2.36	1	2.36	0.068	0.7995		Not Significant
	$CaO.CaF_2$	127.89	1	127.89	3.67	0.0818		Not Significant
	$CaO.Al_2O_3$	664.89	1	664.89	19.08	0.0011		Significant
	$SiO_2.CaF_2$	18.61	1	18.61	0.53	0.4803		Not Significant
	$SiO_2.Al_2O_3$	894.86	1	894.86	25.67	0.0004		Significant
	$CaF_2.Al_2O_3$	547.13	1	547.13	15.70	0.0022		Significant
	Residual	383.41	11	34.86				
	Total	1606.95	20					

Table 5.17: ANOVA results for chemical composition, grain size and microhardness properties of multi-pass bead on plate for rutile-basic flux system

S.No	*Source*	*SS*	*DF*	*MS*	*F value*	*P value*	R^2 *value*	*Status*
C	Model	1.583E-004	3	5.275E-005	5.22	0.0098	0.71	Significant
	Linear	1.583E-004	3	5.275E-005	5.22	0.0098		Significant
	Residual	1.719E-004	17	1.011E-005				
	Total	3.301E-004	20	4.47				
Si	Model	0.12	6	0.019	4.11	0.0138	0.63	Significant
	Linear		3	0.022	4.62	0.0190		Significant
	$TiO_2.SiO_2$	0.065	1	0.018	3.89	0.0687		Not Significant
	$TiO_2.Al_2O_3$		1	0.028	6.02	0.0278		Significant
	$CaO.Al_2O_3$	0.018	1	0.020	4.34	0.0561		Not Significant
	Residual		14	4.667E-003				
P	Model	3.095E-004	9	3.439E-005	3.31	0.0326	0.73	Significant
	Linear	8.981E-005	3	2.994E-005	2.88	0.0840		Not Significant
	$TiO_2.SiO_2$	3.561E-	1	3.561E-	3.43	0.0910		Not

		005		005				Significant
	TiO_2.CaO	1.585E-004	1	1.585E-004	15.27	0.0024		Significant
	TiO_2.Al_2O_3	1.933E-007	1	1.933E-007	0.019	0.8939		Not Significant
	SiO_2.CaO	1.603E-005	1	1.603E-005	1.54	0.2399		Not Significant
	SiO_2. Al_2O_3	1.015E-006	1	1.015E-006	0.098	0.7604		Not Significant
	CaO.Al_2O_3	9.294E-007		9.294E-007	0.090	0.7703		Not Significant
	Residual	1.142E-004	11	1.038E-005				
	Total	4.237E-004	20					
S	Model	1.978E-005	5	3.956E-006	3.61	0.0241	0.74	Significant
	Linear	2.562E-006	3	8.542E-007	0.78	0.5232		Not Significant
	TiO_2.SiO_2	6.417E-006	1	6.417E-006	5.86	0.0286		Significant
	TiO_2.CaO	1.003E-005	1	1.003E-005	9.16	0.0085		Significant
	Residual	1.642E-005	15	1.095E-006				

	Total	3.620E-005	20					
Mn	Model	0.15	5	0.031	4.05	0.0158	0.60	Significant
	Linear	0.043	3	0.014	1.90	0.1726		Not Significant
	SiO_2.CaO	0.089	1	0.089	11.83	0.0037		Significant
	CaO.Al_2O_3	0.023	1	0.023	3.09	0.0993		Not Significant
	Residual	0.11	15	7.557E-003				
	Total	0.27	20					
Mo	Model	7.277E-003	5	1.455E-003	3.06	0.0422	0.70	Significant
	Linear	2.498E-003	3	8.328E-004	1.75	0.1994		Not Significant
	SiO_2.CaO	1.681E-003	1	1.681E-003	3.54	0.0796		Not Significant
	CaO.Al_2O_3	2.952E-003	1	2.952E-003	6.21	0.0249		Significant
	Residual	7.130E-003	15	4.753E-004				
	Total	0.014	20					
Cr	Model	3.510E-004	3	1.170E-004	4.26	0.0205	0.75	Significant
	Linear	3.510E-004	3	1.170E-004	4.26	0.0205		Significant
	Residual	4.671E-	17	2.748E-				

		004		005				
	Total	8.181E-004	20					
Ti	Model	1.565E-004	4	3.913E-005	3.71	0.0255	0.70	Significant
	Linear	9.817E-005	3	3.272E-005	3.10	0.0564		Not Significant
	TiO_2.CaO	5.835E-005	1	5.835E-005	5.53	0.0319		Significant
	Residual	1.689E-004	16	1.055E-005				
	Total	3.254E-004	20					
GS	Model	14.89	8	1.86	3.85	0.0180	0.71	Significant
	Linear	3.10	3	1.03	2.14	0.1487		Not Significant
	TiO_2.SiO_2	1.29	1	1.29	2.67	0.1279		Not Significant
	TiO_2.CaO	5.383E-003	1	5.383E-003	0.011	0.9177		Not Significant
	SiO_2.CaO	4.12	1	4.12	8.52	0.0129		Significant
	CaO.Al_2O_3	2.04	1	2.04	4.22	0.0625		Not Significant
	TiO_2.SiO_2.CaO	2.80	1	2.80	5.80	0.0331		Significant
	Residual	5.80	12	0.48				
	Total	20.69	20					
MH	Model	901.67	5	180.33	5.62	0.0041	0.67	Significant

	Linear	336.34	3	112.11	3.49	0.0422		Significant
	$TiO_2.Al_2O_3$	297.03	1	297.03	9.25	0.0082		Significant
	$SiO_2.Al_2O_3$	512.78	1	512.78	15.98	0.0012		Significant
	Residual	481.48	15	32.10				
	Total	1383.14	20	180.33				

Table 5.18: ANOVA results for chemical composition, grain size and microhardness properties of multi-pass bead on plate for rutile-acidic flux system

S.No	*Source*	*SS*	*DF*	*MS*	*F value*	*P value*	*R^2 value*	*Status*
C	Model	9.598E-005	6	1.600E-005	2.88	0.0484	0.75	Significant
	Linear	4.771E-005	3	1.590E-005	2.86	0.0747		Not Significant
	TiO_2. Al_2O_3	1.821E-005	1	1.821E-005	3.28	0.0918		Not Significant
	SiO_2.Al_2O_3	4.224E-005	1	4.224E-005	7.60	0.0155		Significant
	MgO. Al_2O_3	3.445E-005	1	3.445E-005	6.20	0.0260		Significant
	Residual	7.784E-005	14	5.560E-006				
Si	Model	0.026	5	5.119E-003	3.15	0.0383	0.81	Significant
	Linear	7.380E-003	3	2.460E-003	1.52	0.2510		Not Significant
	TiO_2. SiO_2	0.013	1	0.013	8.13	0.0121		Significant
	TiO_2.Al_2O_3	5.800E-003	1	5.800E-003	3.58	0.0781		Not Significant
	Residual	0.024	15	1.622E-003				
	Total	0.050	20					
P	Model	2.802E-005	6	4.670E-006	3.46	0.0261	0.60	Significant

	Linear	1.611E-005	3	5.370E-006	3.98	0.0305		Significant
	TiO_2. Al_2O_3	1.058E-005	1	1.058E-005	7.83	0.0142		Significant
	SiO_2.Al_2O_3	1.030E-005	1	1.030E-005	7.63	0.0153		Significant
	MgO. Al_2O_3	6.683E-006	1	6.683E-006	4.95	0.0431		Significant
	Residual	1.891E-005	14	1.351E-006				
	Total	4.693E-005	20					
S	Model	6.484E-006	3	2.161E-006	5.65	0.0071	0.70	Significant
	Linear	6.484E-006	3	2.161E-006	5.65	0.0071		Significant
	Residual	6.502E-006	17	3.824E-007				
	Cor Total	1.299E-005	20					
Mn	Model	0.084	7	0.012	3.48	0.0250	0.65	Significant
	Linear	0.023	3	7.527E-003	2.19	0.1383		Not Significant
	TiO_2.SiO_2	0.046	1	0.046	13.42	0.0029		Significant
	TiO_2. Al_2O_3	9.237E-005	1	9.237E-005	0.027	0.8724		Not Significant

	$SiO_2.Al_2O_3$	0.011	1	0.011	3.08	0.1030		Not Significant
	$TiO_2.SiO_2.Al_2O_3$	0.020	1	0.020	5.75	0.0323		Significant
	Residual	0.045	13	3.440E-003				
	Total	0.13	20					
Mo	Model	0.018	9	1.977E-003	3.09	0.0414	0.71	Significant
	Linear	2.765E-003	3	9.216E-003	1.44	0.2842		Not Significant
	$TiO_2.SiO_2$	1.811E-003	1	1.811E-003	2.83	0.1208		Not Significant
	$TiO_2.MgO$	1.447E-003	1	1.447E-003	2.26	0.1609		Not Significant
	$TiO_2.Al_2O_3$	1.684E-005	1	1.684E-003	0.026	0.8741		Not Significant
	$SiO_2.MgO$	1.520E-003	1	1.520E-003	2.37	0.1516		Not Significant
	$SiO_2.Al_2O_3$	1.043E-003	1	1.043E-003	1.63	0.2282		Not Significant
	$MgO.Al_2O_3$	4.206E-003	1	4.206E-003	6.57	0.0264		Significant

	Residual	7.044E-003	11	6.404E-004				
	Total	0.025	20					
Cr	Model	7.980E-004	11	7.255E-005	3.19	0.0462	0.79	Significant
	Linear	7.934E-005	3	2.645E-005	1.16	0.3765		Not Significant
	$TiO_2.SiO_2$	1.771E-004	1	1.771E-004	7.78	0.0210		Significant
	$TiO_2.MgO$	6.157E-006	1	6.157E-006	0.27	0.6154		Significant
	$TiO_2.Al_2O_3$	1.189E-005	1	1.189E-005	0.52	0.4881		Not Significant
	$SiO_2.MgO$	9.460E-005	1	9.460E-005	4.16	0.0719		Not Significant
	$SiO_2.Al_2O_3$	4.721E-005	1	4.721E-005	2.08	0.1835		Not Significant
	$MgO.Al_2O_3$	1.388E-004	1	1.388E-004	6.10	0.0355		Significant
	$TiO_2.SiO_2.MgO$	1.314E-004	1	1.314E-004	5.78	0.0397		Significant
	$TiO_2.SiO_2.Al_2O_3$	1.599E-004	1	1.599E-004	7.03	0.0264		Significant
	Residual	2.047E-004	9	2.275E-005				
	Total	1.003E-003	20					
Ti	Model	1.674E-004	7	2.391E-005	3.96	0.0160	0.65	Significant

	Linear	1.102E-005	3	3.674E-006	0.61	0.6233		Not Significant
	TiO_2.MgO	3.573E-005	1	3.573E-005	5.88	0.0360		Significant
	SiO_2.MgO	2.522E-005	1	2.522E-005	4.15	0.0624		Not Significant
	TiO_2.SiO_2.MgO	4.765E-005	1	4.765E-005	7.85	0.0150		Significant
	TiO_2.SiO_2.Al_2O_3	2.909E-005	1	2.909E-005	4.79	0.0475		Significant
	Residual	7.894E-005	13	6.072E-006				
	Total	2.463E-004	20					
GS	Model	9.84	9	1.09	3.83	0.0199	0.75	Significant
	Linear	3.21	3	1.07	3.75	0.0447		Significant
	TiO_2.SiO_2	3.92	1	3.92	13.75	0.0035		Significant
	TiO_2.MgO	1.35	1	1.35	4.72	0.0526		Not Significant
	TiO_2. Al_2O_3	0.69	1	0.69	2.40	0.1493		Not Significant
	SiO_2.MgO	0.11	1	0.11	0.38	0.5495		Not Significant
	SiO_2.Al_2O_3	0.91	1	0.91	3.18	0.1020		Not Significant
	MgO. Al_2O_3	0.33	1	0.33	1.16	0.3049		Not Significant
	Residual	3.14	11	0.29				

	Total	12.98	20					
MH	Model	3299.17	3	1099.72	3.91	0.0271	0.81	Significant
	Linear	3299.17	3	1099.72	3.91	0.0271		Significant
	Residual	4777.78	17	281.05				
	Total	8076.95	20					

DF: degree of freedom

P values (Table 5.16-5.18) less than 0.005 for all the properties indicate that the models are significant, and there are very lesser chances of error due to noise. The difference between predicted and experimental results is not high due to moderate R^2 value for all properties. Figure 5.16, 5.17, and 5.18 (for three flux systems) show the variation of predicted values with actual responses for bead chemistry, grain size, and microhardness values.

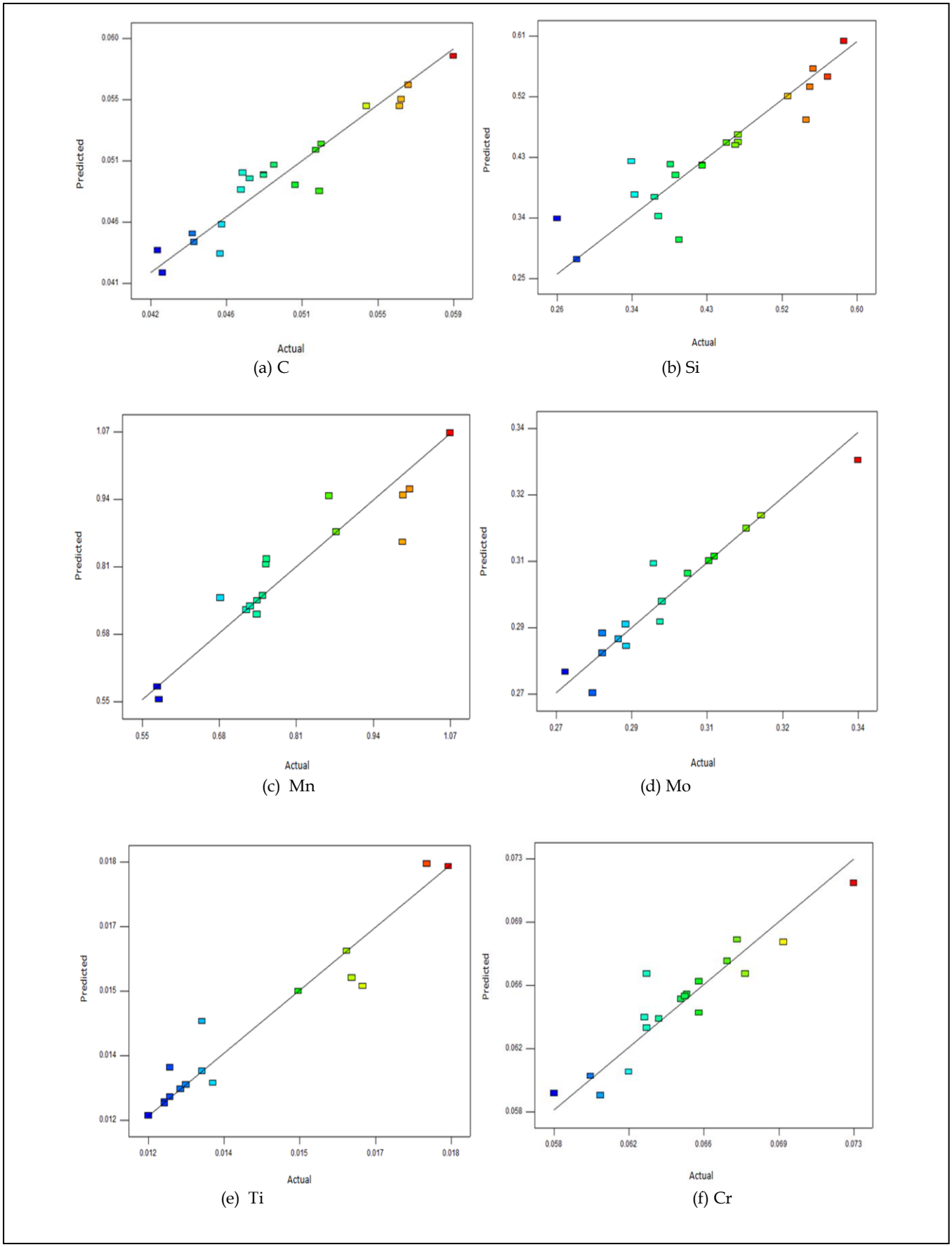

Figure 5.16: Predicted versus actual plots for various properties of multi-pass bead on plate; (a-f) bead chemical composition constituents; (for basic flux system)

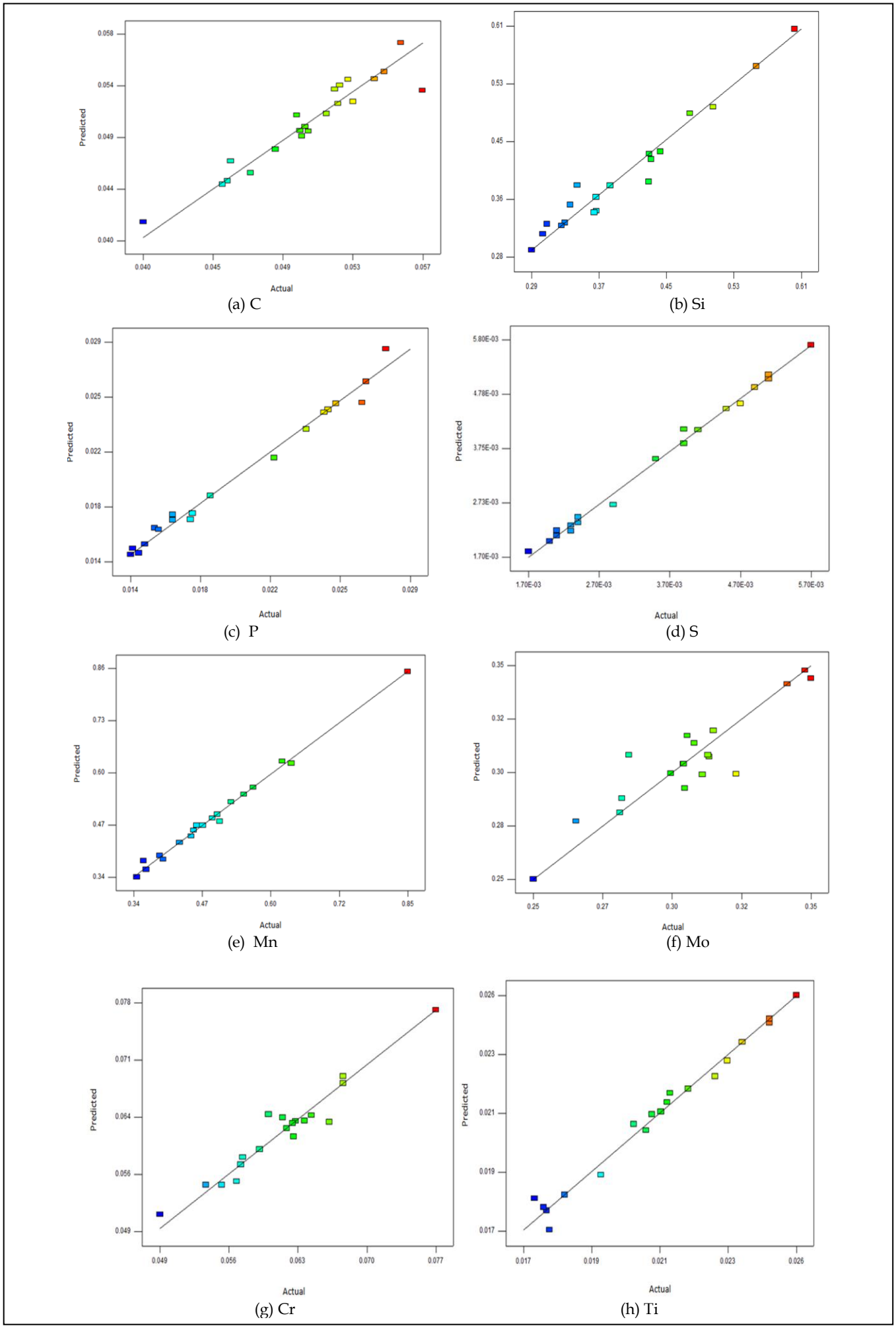

Figure 5.17: Predicted versus actual plots for various properties of multi-pass bead on plate; (a-h) bead chemical composition constituents; (for rutile-basic flux system)

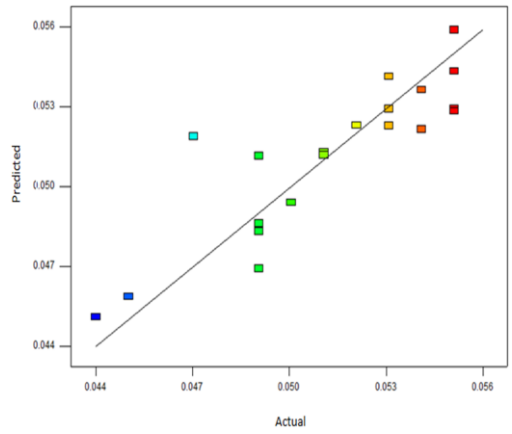

(a) C

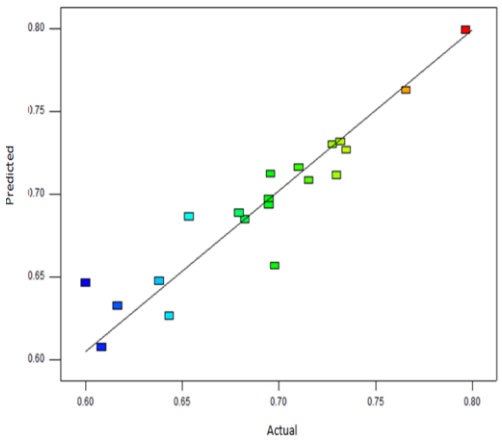

(b) Si

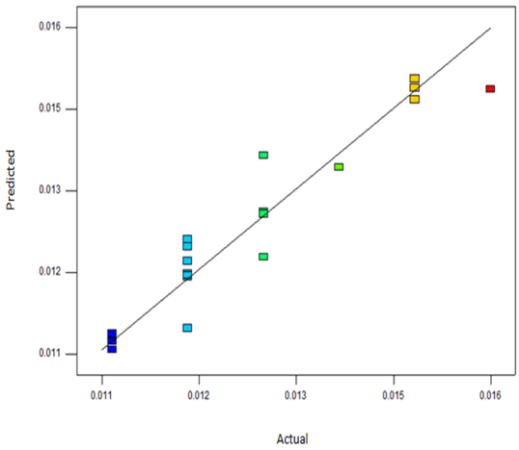

(c) P

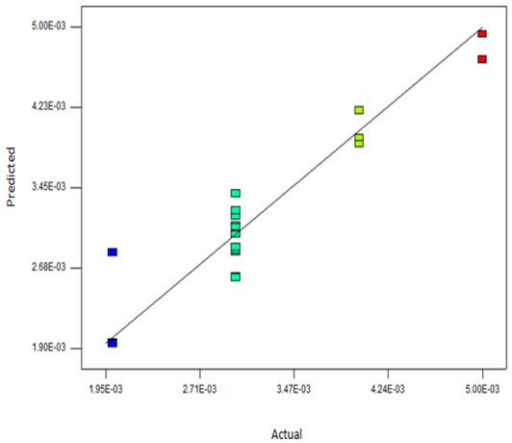

(d) S

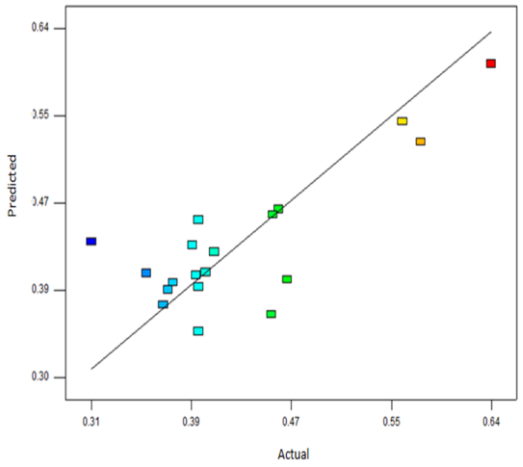

(e) Mn

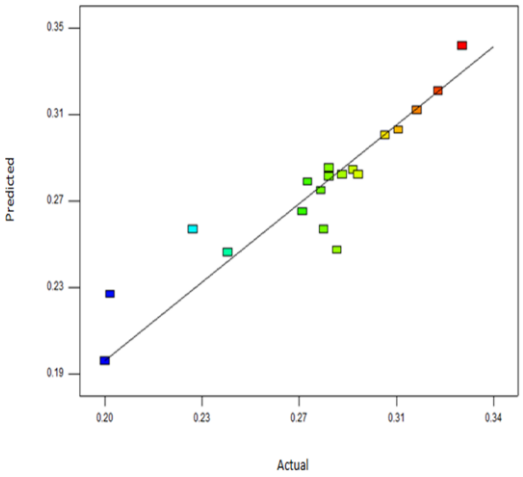

(f) Mo

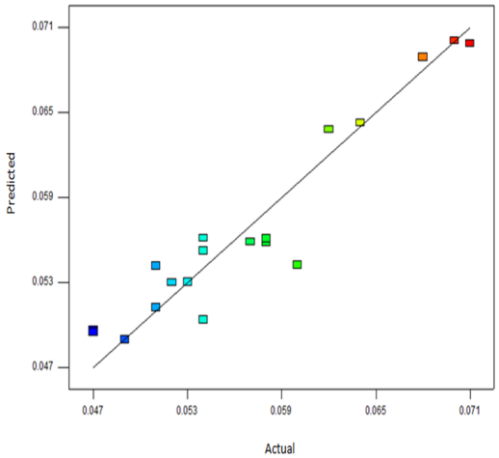

(g) Cr

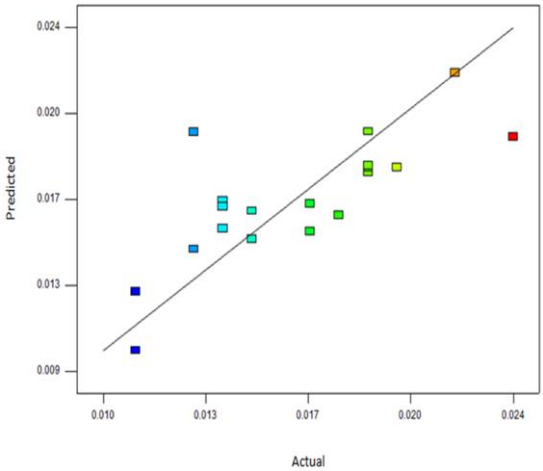

(h) Ti

Figure 5.18: Predicted versus actual plots for various properties of multi-pass bead on plate; (a-h) bead chemical composition constituents; (for rutile-acidic flux system).

5.2.2.1.3 Discussion of regression analysis of flux components on grain size, bead chemistry and microhardness for three flux systems

It observed from the regression analysis that individual flux constituents (linear mixture constituents) show antisynegistic effect on carbon content for basic flux system while for rutile-basic and rutile-acidic flux systems it show synergistic effect (Table 5.16-5.18). For the basic flux system, all the binary mixture constituents decrease the carbon content in the multi-pass bead on plate weld deposit experimentation while for rutile-basic flux system binary and ternary mixture constituents do not affect carbon. Binary mixture constituents $TiO_2.Al_2O_3$ and $SiO_2.Al_2O_3$ decreases the carbon content and shows antisynergistic effect while $MgO.Al_2O_3$ increases the carbon content and shows synergistic effect. Transfer of carbon from weld to slag is affected by the presence of oxygen in the weld metal. It observed in the literature that as the oxygen content increases, there is a transfer of carbon from weld to slag. The oxygen amount in the weld metal is more dependent on the basicity of the flux. Basic fluxes significantly reduce the carbon content in the weld as compared to the acidic fluxes [Jindal et al., 2013, Bhandari et al., 2016, Jindal et al., 2013, North et al., 1979, KooK et al., 2009, Tuliani et al., 1969, Fleck et al., 1986]. From regression analysis (Table 5.19-5.21), it noticed that all the individual flux constituents significantly increase the silicon content and show synergistic effect for basic and rutile-basic flux system while for rutile-acidic flux system it shows antisynergistic effect. $CaO.Al_2O_3$ is the only binary mixture constituent, which increases the weld bead silicon content for the basic flux system, while for the rutile-basic flux system, it decreases. Binary mixture constituent $SiO_2.CaF_2$, $SiO_2.Al_2O_3$ and $CaF_2.Al_2O_3$ increases the weld silicon content and shows a positive effect on the basic flux system. $SiO_2.CaF_2.Al_2O_3$ is the ternary mixture constituent, which significantly increases the weld bead silicon content for the basic flux system. Binary mixture constituent $TiO_2.SiO_2$ decreases the weld bead silicon content for the rutile-basic system, while for the rutile-acidic flux system, it increases the silicon content. $TiO_2.Al_2O_3$ increases the weld bead silicon content for the rutile-basic flux system, while for the rutile-acidic flux system, it decreases. Previous literature suggests that presence of SiO_2 and TiO_2 in the weld metal improves the slag detachability, bead appearance and joint strength [Chai & Eagar et al., 1980, North et al., 1979, Kanjilal et al., 2007, Burck et al., 1990, Jindal et al., 2103, Bhandari et al, 2016]. Regression analysis (Table 5.19-5.21) of manganese shows that all the individual flux constituents decrease the weld bead manganese content for basic, rutile-basic and rutile-acidic flux systems. $SiO_2.CaF_2$ is the only binary constituent that increases the manganese content for the basic flux system. $SiO_2.CaO$ increases the weld bead manganese content while $CaO.Al_2O_3$ decreases the manganese content for the rutile-basic flux system. $TiO_2.SiO_2$ shows a positive effect on weld bead manganese content while $TiO_2.Al_2O_3$ and $SiO_2.Al_2O_3$ shows a negative effect on manganese content for the rutile-acidic flux system. All the ternary mixture constituents of basic flux system decreases the weld bead manganese content while $TiO_2.SiO_2.Al_2O_3$ is the ternary constituent which increases the manganese content for the rutile-acidic flux system. Regression analysis (Table 5.17-5.18) of phosphorous and sulfur shows that all the individual flux components show antisynergistic effect on weld bead phosphorous and sulphur content for the rutile-basic flux system while they show significant synergistic effect for the rutile-acidic flux system. $TiO_2.CaO$ is the only binary constituent which significantly increases the weld bead phosphorous and sulphur content for rutile-basic flux system. $TiO_2.SiO_2$ significantly decreases the weld bead phosphorous content while it increased the weld bead sulphur content for the rutile-basic flux system. Binary mixture constituent $TiO_2.Al_2O_3$, $SiO_2.Al_2O_3$ and $MgO.Al_2O_3$ increases the weld bead phosphorous content for the rutile-acidic flux system. All the ternary mixture constituents decrease the weld bead phosphorous content for basic flux system. It is reported that lime fluxes significantly reduces the level of sulfur in weld metal. Because calcium oxide (present in lime) reacts with sulfur of weld metal which forms calcium sulphide and

releases oxygen, (equation 5.3) thus reduces the level of sulfur in the weld metal [Chai & Eagar et al., 1980, Davis et al., 1991, North et al., 1979, J.H. Palm, 1979].

$$CaO + S \rightarrow CaS + \tfrac{1}{2} O_2 \quad (5.3)$$

From regression analysis (Table 5.16-5.18), it is observed that all the individual flux constituents decrease the weld bead chromium content for the basic and rutile-acidic flux systems while for the rutile-basic system they tend to increase the chromium content. For a basic flux system, all the binary mixture constituents significantly decrease the chromium content and thus show antisynergistic effect. Ternary mixture constituent $CaO.CaF_2.Al_2O_3$ increases the weld bead chromium content while $SiO_2.CaF_2.Al_2O_3$ decreases the chromium content. For rutile-acidic flux system, binary mixture constituents $TiO_2.SiO_2$ and $MgO.Al_2O_3$ shows a positive effect and thus increases the weld bead chromium content while remaining binary constituent significantly decrease the weld bead chromium content. All ternary mixture constituents significantly increase the chromium content and thus show synergistic effect on chromium.

Regression analysis of molybdenum shows (Table 5.16-5.18) that the individual constituents decrease the weld bead molybdenum content for basic, rutile-basic and rutile-acidic flux systems. Binary mixture constituent $SiO_2.CaF_2$ and $CaF_2.Al_2O_3$ shows antisynergistic effect while $CaF_2.Al_2O_3$ increases the molybdenum content and thus shows synergistic effect for the basic flux system. A ternary mixture of the basic flux system decreases the molybdenum content. Binary component $CaO.Al_2O_3$ shows a positive effect on weld bead molybdenum content while $SiO_2.Al_2O_3$ shows a negative effect and thus reduces the molybdenum content. $MgO.Al_2O_3$ is the only binary component of the rutile-acidic flux system, which increases the weld bead molybdenum content while all other binary constituents significantly decrease the molybdenum content.

It observed from the regression analysis (Table 5.16-5.18) of titanium that all the individual (linear mixture components) flux constituents significantly decrease the weld bead titanium content for three flux systems. Binary mixture constituents $CaO.CaF_2$, $CaF_2.Al_2O_3$, $TiO_2.CaO$ and $TiO_2.MgO$ significantly increases the titanium content and thus show synergistic effect for basic, rutile-basic, and rutile-acidic flux systems while all remaining binary constituents decrease the weld bead titanium content for basic and rutile-acidic flux system. Previous literature suggests that slag detachability and bead morphology improved due to the presence of acidic constituent in the fluxes such as TiO_2 and SiO_2. Too high and too low value of acidic constituents has adverse effect on the slag detachability as well as bead appearance [Paniagua et al., 2003, Yan et al., 2006, North et al., 1978, Chai & Eagar et al., 1980, Tsuboi et al., 1983].

It observed from the regression analysis (Table 5.16-5.18) that linear mixture constituent decreases the weld bead grain size for basic and rutile-basic flux systems while there is an increase in grain size for rutile-acidic flux system. $TiO_2.SiO_2$ is the only binary mixture constituent that shows antisynergistic effect on grain size, while for the rutile-acidic flux system, it shows synergistic effect. Binary mixture constituent $CaO.Al_2O_3$ increases the grain size for the basic flux system while it decreases the grain size for the rutile-basic flux system. Binary mixture constituent $SiO_2.Al_2O_3$ significantly increases the grain size for the basic system while it decreases the grain size for the rutile-acidic flux system. $CaO.SiO_2$ binary mixture constituent shows a negative effect on weld bead grain size for the basic system while it shows a positive effect for the rutile-basic flux system. For a basic flux system, other binary constituents $CaO.CaF_2$ and $CaF_2.Al_2O_3$ significantly increase the grain size and thus show synergistic effect while $SiO_2.CaF_2$ shows antisynergistic effect. Binary constituent $TiO_2.SiO_2$ shows a negative effect on grain size for the rutile-basic flux system while it shows a positive effect on grain size for the rutile-acidic flux system. Binary mixture constituent $TiO_2.CaO$, $TiO_2.MgO$, $TiO_2.Al_2O_3$ and $MgO.Al_2O_3$ significantly decrease the grain size for rutile-basic and rutile-acidic flux system. $TiO_2.SiO_2.CaO$ is the only ternary mixture component that significantly increases the

grain size for the rutile-basic flux system. Fine-grain matrix exhibits acicular ferrite, less grain boundary ferrite, and ferrite side plate microstructure, which is beneficial to toughness. Larger grain size results in the coarse microstructure, which shows the brittle behavior of metal and poor mechanical properties. The addition of alloying elements in the parent metal refines the microstructure and mechanical properties [Pandey et al., 1994; Olson et al., 1979; Sharma et al., 2018].

From regression analysis (Table 5.16-5.18) of microhardness, it observed that all individual flux constituents decrease the weld bead microhardness for the basic flux system while it increases the microhardness for rutile-basic and rutile-acidic flux system and shows a synergistic effect. $SiO_2.Al_2O_3$ is the only binary mixture constituent, which significantly increases the weld bead microhardness for basic as well as rutile-basic flux system. Binary mixture constituents $CaO.Al_2O_3$, $CaF_2.Al_2O_3$ and $TiO_2.Al_2O_3$ show a significant synergistic effect on weld bead microhardness for basic and rutile-basic flux system while $CaO.SiO_2$, $CaO.CaF_2$ and $SiO_2.CaF_2$ shows antisynergistic effect on microhardness. Literature suggests that the microhardness value of the weld joint can be related to the equivalent carbon content. Higher the value of carbon equivalent (up to optimum level i.e., CE=0.3-0.4) higher will be the microhardness value but too high value of microhardness (if C.E > 0.45) is not desirous because it results in susceptibility of cold cracking due to the formation of martensite phase in the weld or heat affected zone [Lancaster et al., 1980, Kohno et al., 1982]. It observed from Table 5.16-5.18 that there is an almost similar increase in the microhardness value for all the specimens for basic, rutile-basic, and rutile-acidic flux systems.

5.2.2.1.4 Contour plots of grain size, bead chemistry and microhardness for three flux systems

Different proportions of flux constituents such as CaO, SiO_2, CaF_2, TiO_2, MgO, Al_2O_3, and keeping binder content constant, various contour plots of bead properties were drawn. Contour plots of bead chemical composition constituents, grain size, and microhardness properties are shown in Figure (5.19-5.21) for three flux systems. Contour surface plot (Hummel, 1984) represents the variation of weld bead chemical components, grain size, and microhardness responses with the variation of flux components. Each curve shows the constant value of responses on the contour surface.

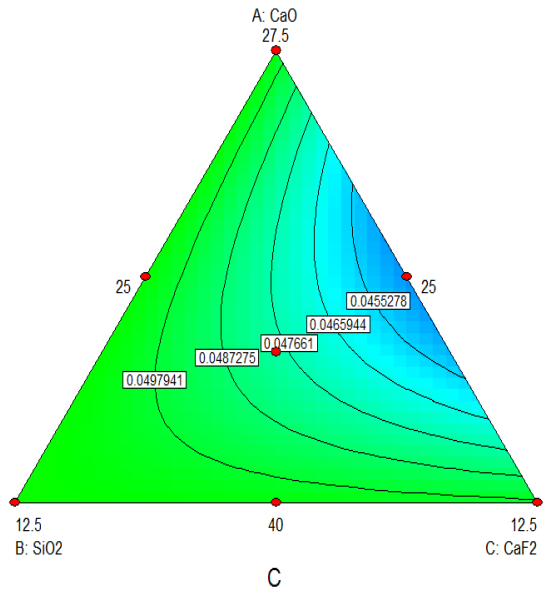

(a)

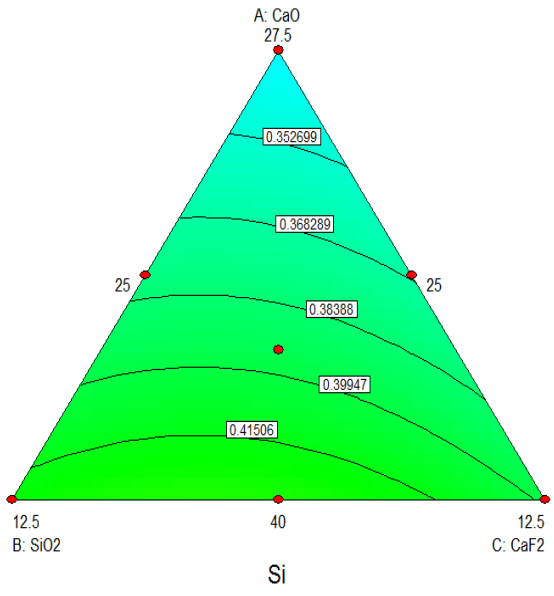

(b)

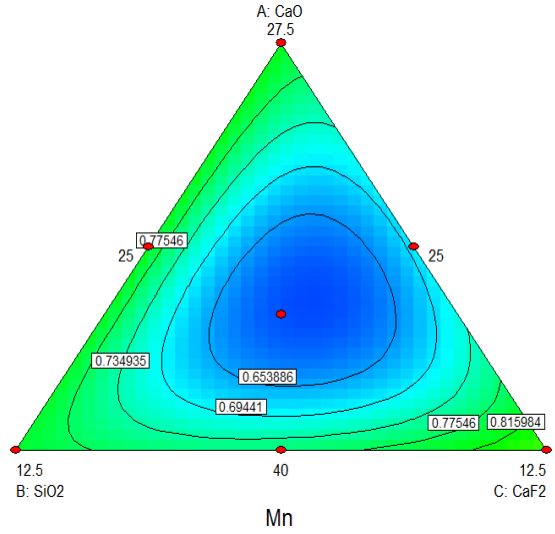

(c)

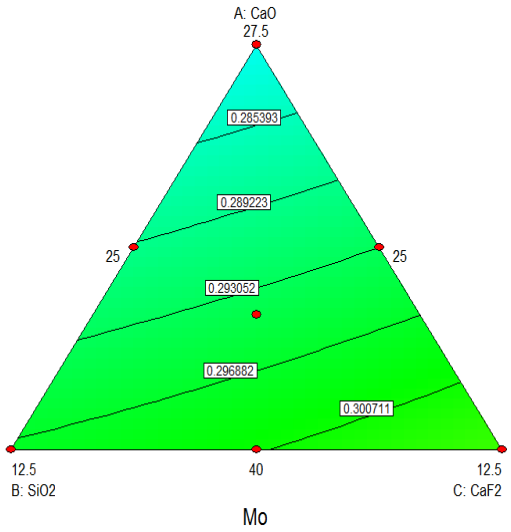

(d)

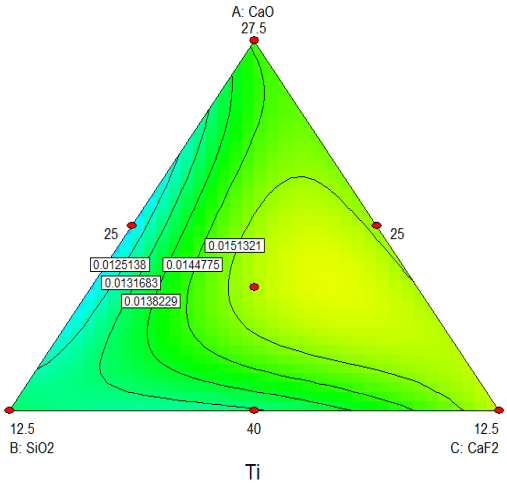

(e)

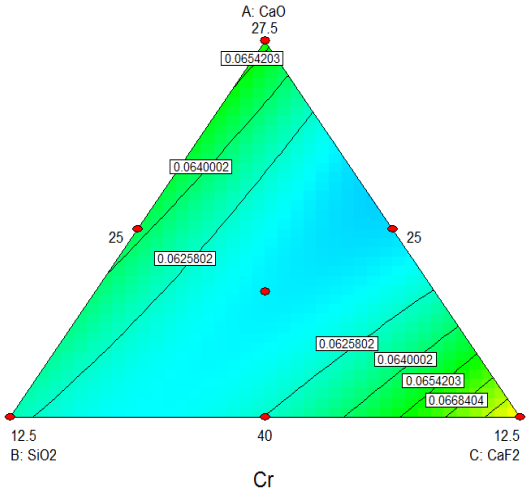

(f)

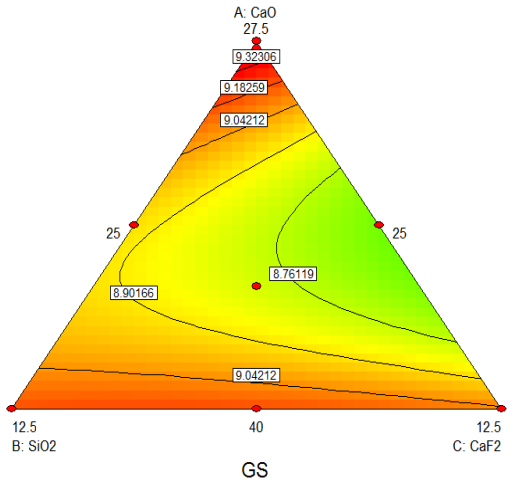

(g)

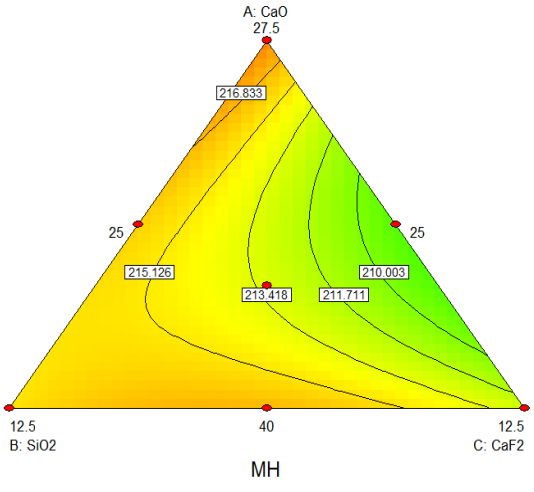

(h)

Figure 5.19: Contour plot of multi-pass bead on plate weld deposit properties for basic flux system; (a-f) chemical constituents; (g) grain size; (h) microhardness

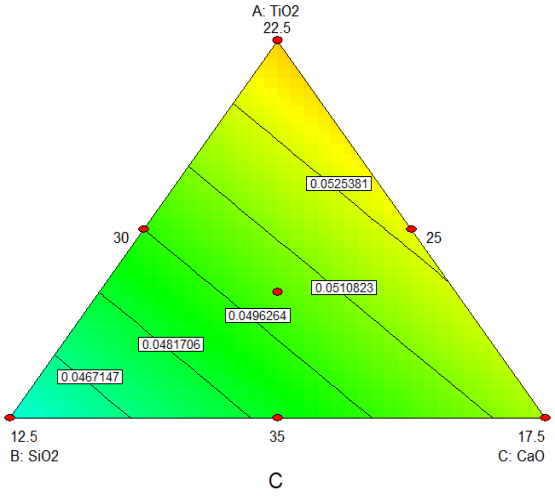

C

(a)

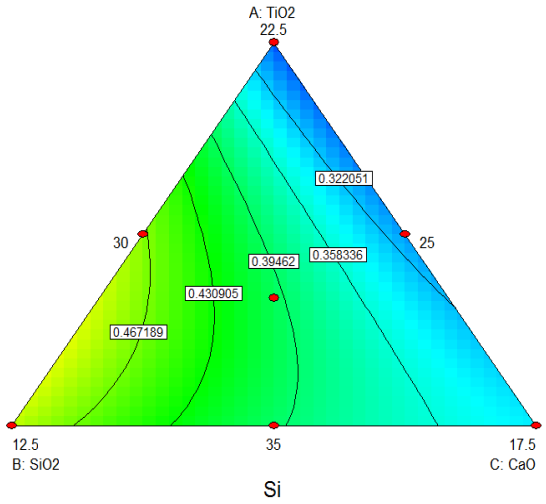

Si

(b)

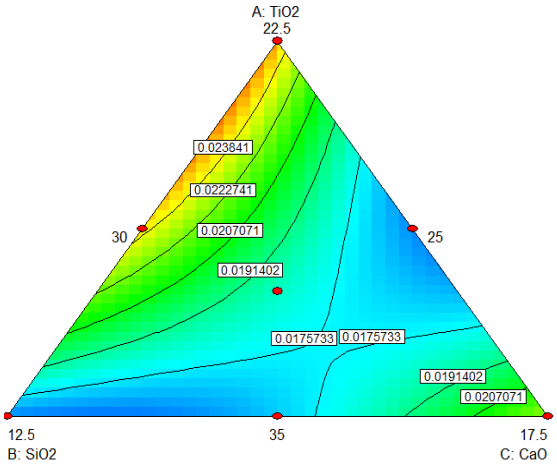

P

(c)

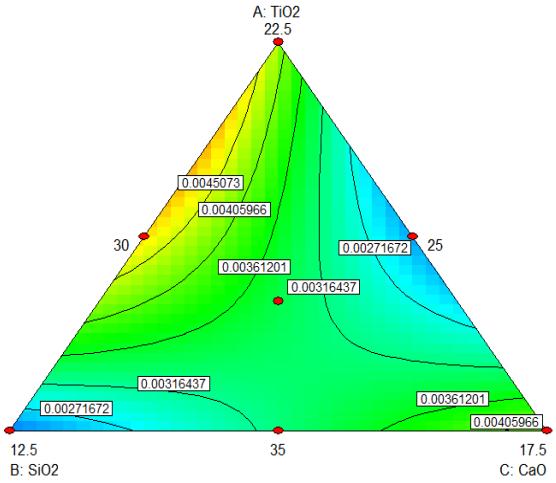

S

(d)

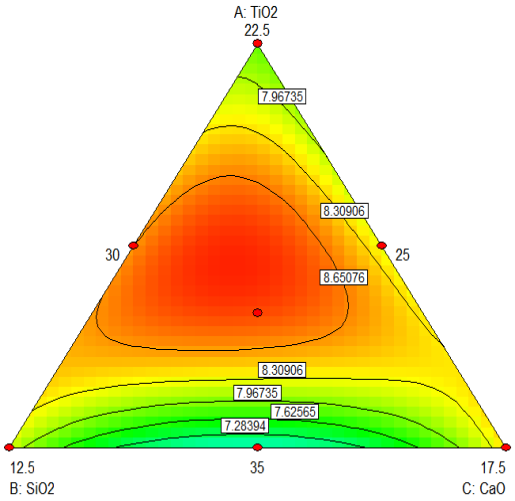

Mn

(e)

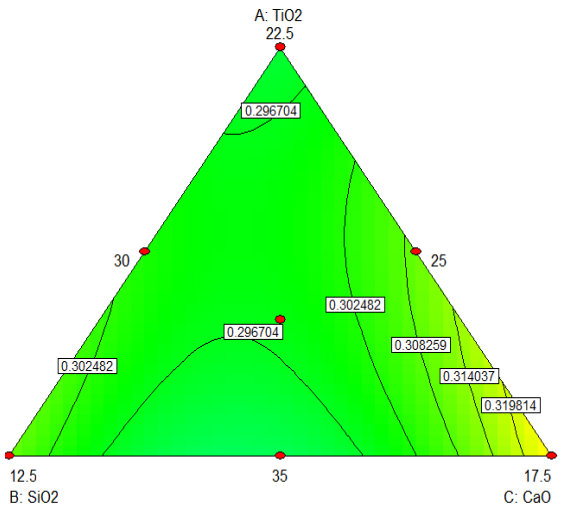

Mo

(f)

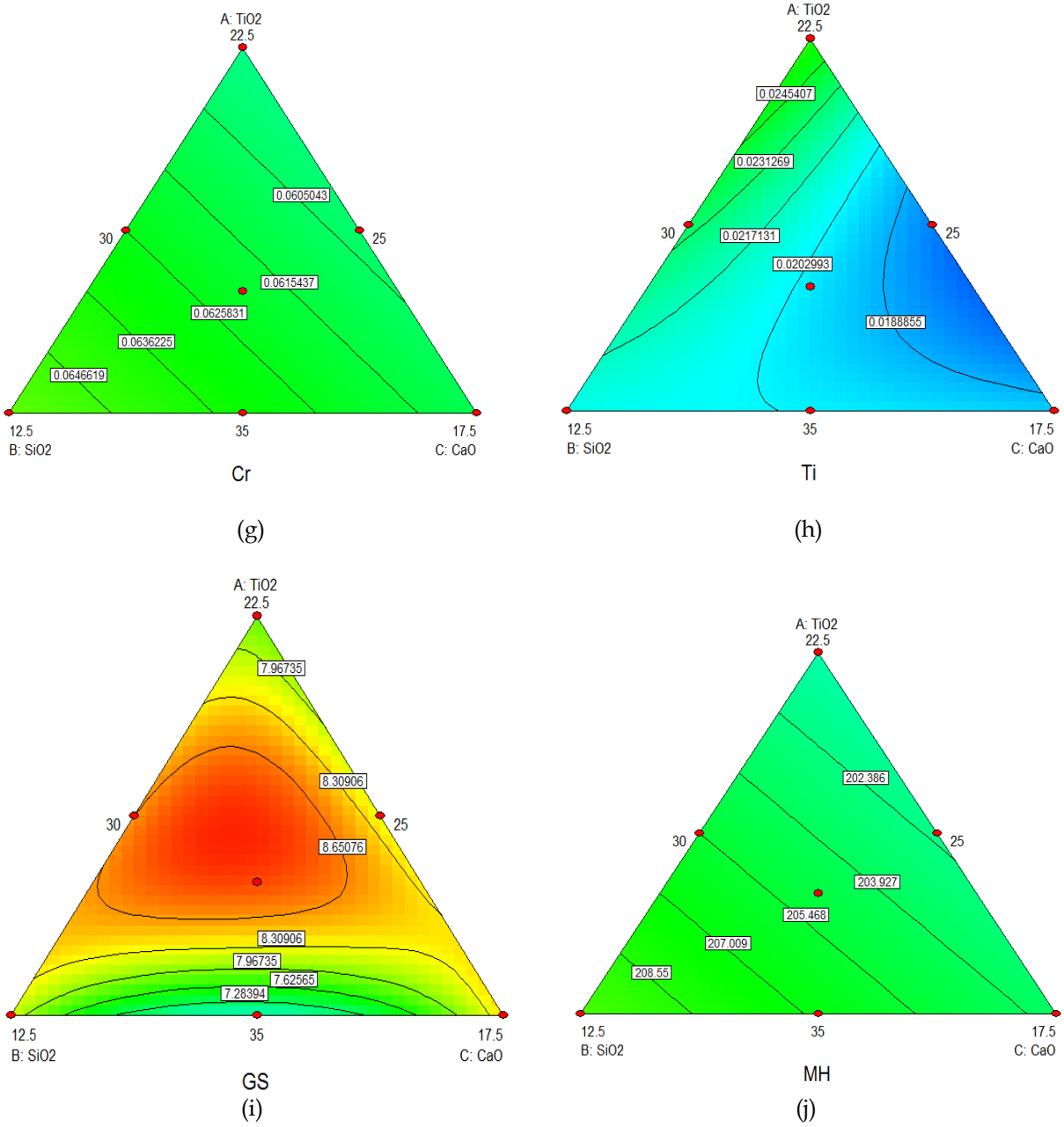

Figure 5.20: Contour plot of multi-pass bead on plate weld deposit properties for rutile-basic flux system; (a-h) weld bead chemical constituents; (i) weld bead grain size; (j) weld bead microhardness

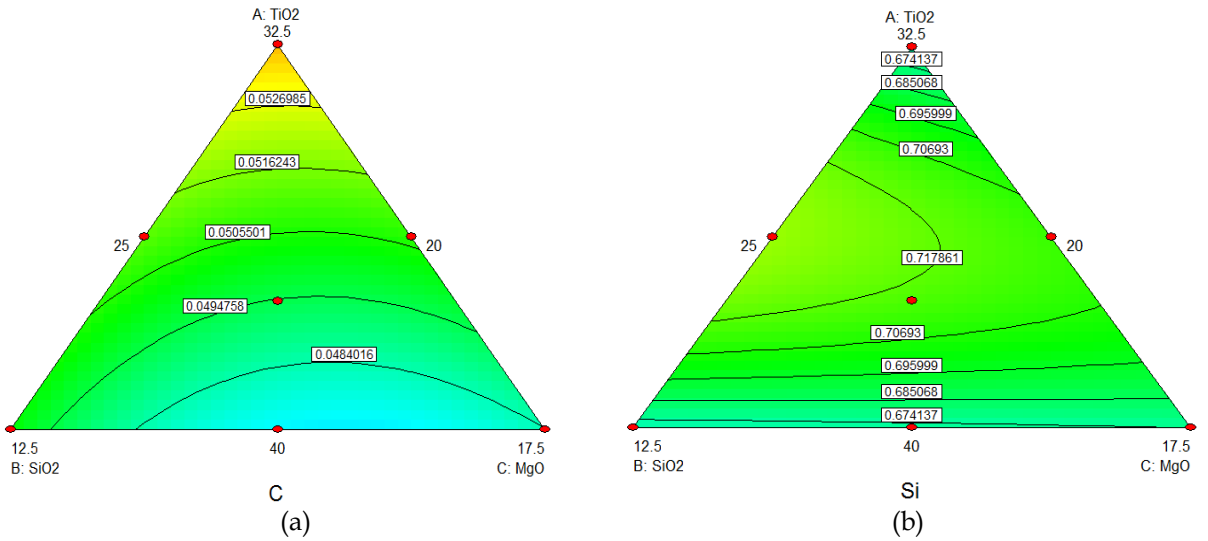

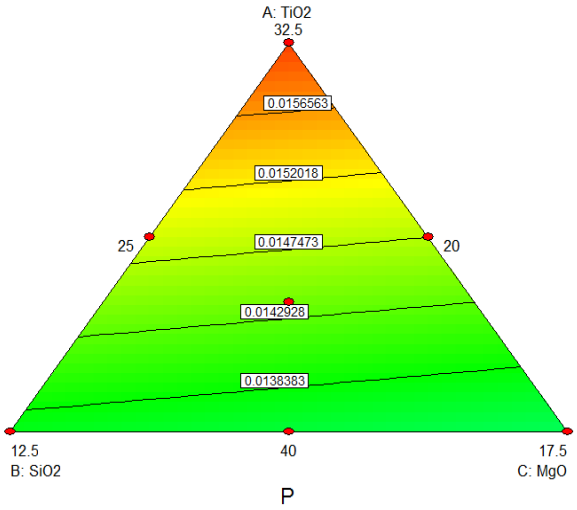
A: TiO2
32.5
0.0156563
0.0152018
0.0147473
0.0142928
0.0138383
25
20
12.5
B: SiO2
40
17.5
C: MgO
P

(c)

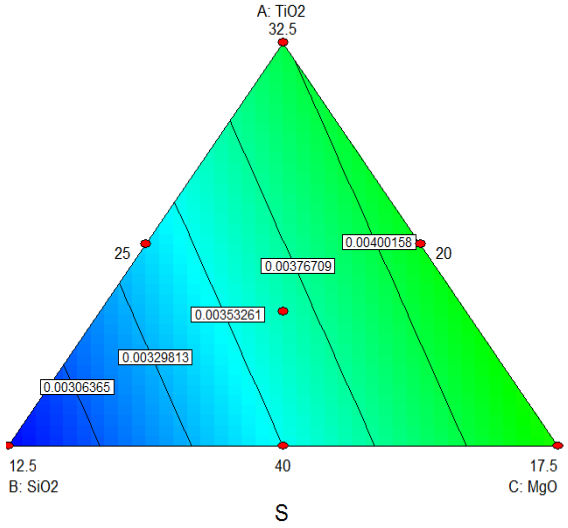
A: TiO2
32.5
0.00400158
0.00376709
0.00353261
0.00329813
0.00306365
25
20
12.5
B: SiO2
40
17.5
C: MgO
S

(d)

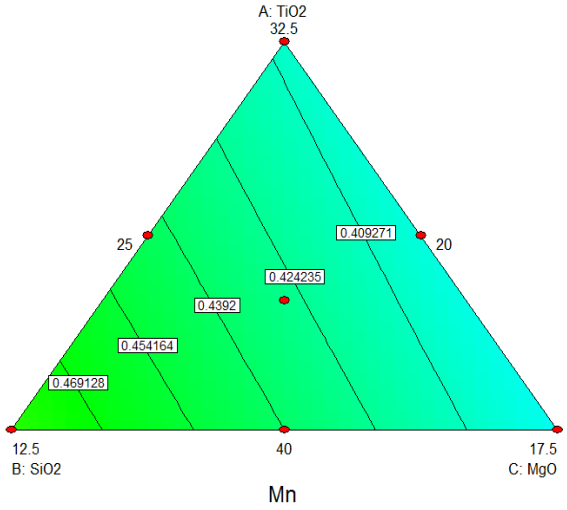
A: TiO2
32.5
0.409271
0.424235
0.4392
0.454164
0.469128
25
20
12.5
B: SiO2
40
17.5
C: MgO
Mn

(e)

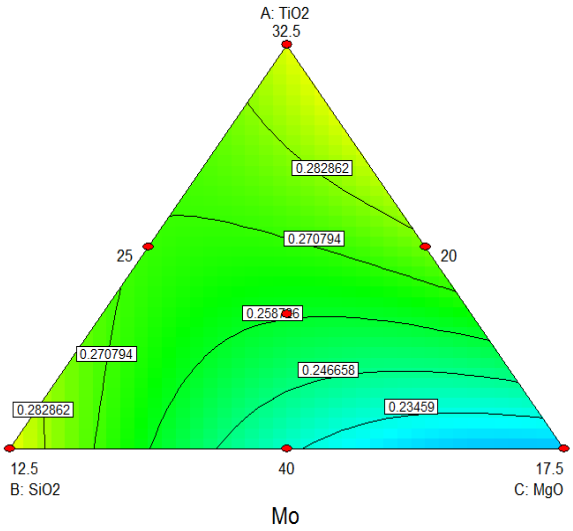
A: TiO2
32.5
0.282862
0.270794
0.270794
0.246658
0.23459
0.282862
25
20
12.5
B: SiO2
40
17.5
C: MgO
Mo

(f)

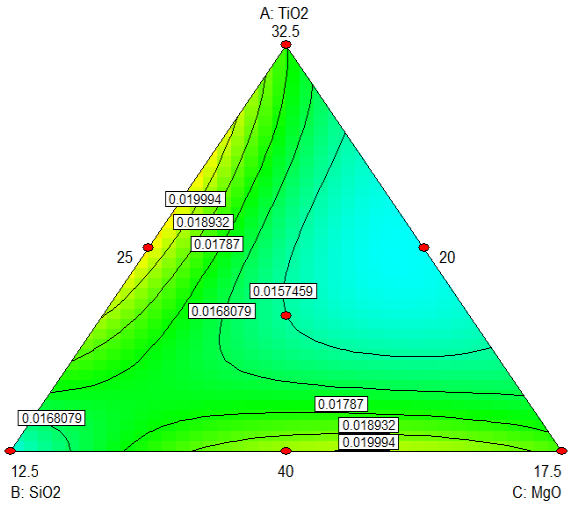
A: TiO2
32.5
0.019994
0.018932
0.01787
0.0157459
0.0168079
0.0168079
0.01787
0.018932
0.019994
25
20
12.5
B: SiO2
40
17.5
C: MgO
Ti

(g)

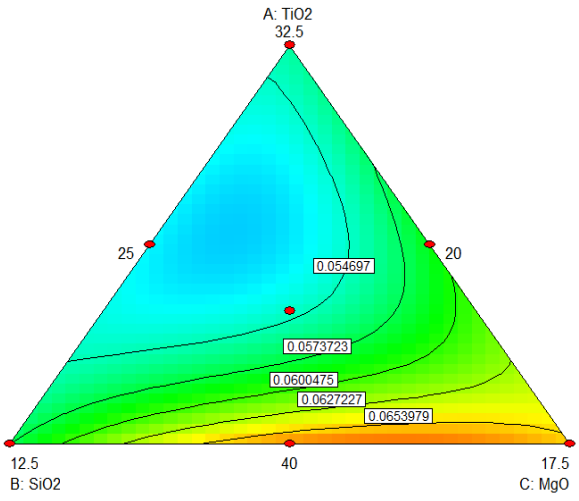
A: TiO2
32.5
0.054697
0.0573723
0.0600475
0.0627227
0.0653979
25
20
12.5
B: SiO2
40
17.5
C: MgO
Cr

(h)

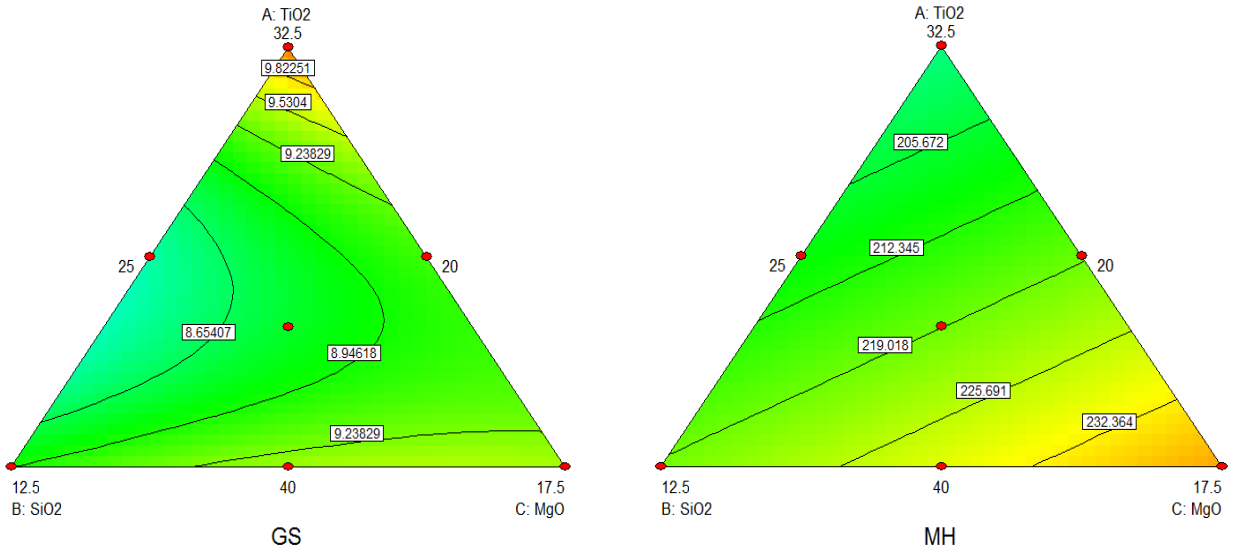

Figure 5.21: Contour plot of multi-pass bead on plate weld deposit properties for rutile-acidic flux system; (a-h) weld bead chemical constituents; (i) weld bead grain size; (j) weld bead microhardness

5.2.2.1.5 Optimization of grain size, bead chemistry and microhardness for three flux systems

To optimize bead chemistry, grain size, and microhardness properties, a complex desirability optimization method was used, which was suggested by [Derringer et al., 1980]. In this method, predicted results are converted into desired responses using an unbiased function D(x) called desirability function and all the cumulative mean of individual responses taken for desirability value [Harington, 1965]. For basic, rutile-basic, and rutile-acidic flux systems, Table (5.19-5.21) shows the optimized solution of different properties.

Table 5.19: Optimized flux mixtures of bead chemical composition, grain size and microhardness properties for basic flux system

S.No	*CaO*	SiO_2	CaF_2	Al_2O_3	*C*	*Si*	*Mn*	*Mo*	*Ti*	*Cr*	*GS*	*MH*	Desirability
1.	40	10.0	25	10.0	0.052	0.533	0.881	0.292	0.014	0.065	9.10	222	0.64
2.	35	19.9	25	5.0	0.049	0.482	0.791	0.292	0.014	0.065	9.10	222	0.55
3.	40	11.5	25	8.4	0.050	0.422	0.830	0.301	0.013	0.067	8.59	223	0.54

Table 5.20: Optimized flux mixtures of bead chemical composition, grain size and microhardness properties for rutile-basic flux system

S.No	TiO_2	SiO_2	*CaO*	Al_2O_3	*C*	*Si*	*P*	*S*	*Mn*	*Mo*	*Ti*	*Cr*	*GS*	*MH*	*Desirability*
1.	35	10.0	30.0	10.0	0.044	0.440	0.014	0.002	0.520	0.297	0.019	0.064	7.74	204	0.60
2.	35	15.1	28.4	6.40	0.046	0.491	0.016	0.002	0.448	0.322	0.020	0.055	9.00	202	0.54
3.	31.9	21.7	26.3	5.0	0.050	0.420	0.018	0.003	0.513	0.303	0.023	0.060	7.30	205	0.50

Table 5.21: Optimized flux mixtures of bead chemical composition, grain size and microhardness properties for rutile-acidic flux system

S.No	TiO_2	SiO_2	MgO	Al_2O_3	C	Si	P	S	Mn	Mo	Ti	Cr	GS	MH	Desirability
1.	38.1	11.8	25.0	10.0	0.051	0.722	0.012	0.003	0.487	0.285	0.017	0.061	9.02	231	0.60
2.	37.9	12.0	25.0	10.0	0.050	0.721	0.012	0.003	0.493	0.283	0.016	0.062	9.02	231	0.59
3.	36.5	13.4	25.0	10.0	0.050	0.716	0.013	0.003	0.535	0.262	0.015	0.068	9.04	231	0.58

Table 5.22: Percentage error of weld bead chemical composition, grain size and microhardness properties for basic flux system

Flux Mixture				*Predicted Values*								*Actual values*								*Error*							
CaO	*SiO_2*	*CaF_2*	*Al_2O_3*	*C*	*Si*	*Mn*	*Mo*	*Ti*	*Cr*	*GS*	*MH*	*C*	*Si*	*Mn*	*Mo*	*Ti*	*Cr*	*GS*	*MH*	C	Si	Mn	Mo	Ti	Cr	GS	MH
40	18 .7	18.7	7.5	0.041	0.372	0.733	0.289	0.012	0.059	7.2	189	0.044	0.387	0.754	0.307	0.013	0.060	7.9	192	7.2	4.0	2.7	5.8	2.3	1.9	8.8	1.5
33.7	18.7	25.0	7.5	0.039	0.455	0.727	0.270	0.012	0.063	8.3	201	0.044	0.465	0.744	0.302	0.012	0.064	8.7	203	11.7	2.1	2.3	10.0	2.3	2.4	4.5	0.4
32.5	25.0	17.5	10.0	0.042	0.538	0.647	0.250	0.015	0.062	8.8	204	0.048	0.551	0.683	0.284	0.016	0.065	9.3	207	13.1	2.5	5.6	12.0	3.6	4.2	5.3	1.4

Table 5.23: Percentage error of weld bead chemical composition, grain size and microhardness properties for rutile-basic flux system

Flux Mixture				*Predicted Values*										*Actual values*										Error									
TiO_2	*SiO_2*	*CaO*	*Al_2O_3*	*C*	*Si*	*P*	*S*	*Mn*	*Mo*	*Ti*	*Cr*	*GS*	*MH*	*C*	*Si*	*P*	*S*	*Mn*	*Mo*	*Ti*	*Cr*	*GS*	*MH*	C	Si	P	S	Mn	Mo	Ti	Cr	GS	MH
20	25	30	10	0.054	0.363	0.026	0.005	0.377	0.319	0.026	0.063	7.5	206	0.055	0.365	0.024	0.003	0.851	0.302	0.064	0.024	7.2	204	2.3	0.6	6.5	33.3	55.0	5.5	2.1	4.8	4.0	0.9
25	25	30	5	0.053	0.286	0.021	0.004	0.447	0.267	0.025	0.055	7.9	199	0.049	0.302	0.017	0.005	0.522	0.284	0.057	0.025	8.9	200	6.1	5.5	18.1	22.0	14.2	5.8	3.6	0.3	11	0.2
35	20	25	5	0.048	0.457	0.022	0.003	0.408	0.332	0.021	0.058	8.0	212	0.046	0.552	0.024	0.005	0.358	0.346	0.054	0.021	8.4	214	3.7	17.2	7.0	24.0	13.8	4.2	8.5	0.4	4.8	0.9

Table 5.24: Percentage error of weld bead chemical composition, grain size and microhardness properties for rutile-acidic flux system

Flux Mixture				Predicted Values										Actual values										Error									
TiO_2	SiO_2	MgO	Al_2O_3	C	Si	P	S	Mn	Mo	Ti	Cr	GS	MH	C	Si	P	S	Mn	Mo	Ti	Cr	GS	MH	C	Si	P	S	Mn	Mo	Ti	Cr	GS	MH
40	10	25	10	0.053	0.633	0.011	0.002	0.439	0.270	0.057	0.017	8.5	215	0.051	0.697	0.012	0.003	0.456	0.280	0.057	0.017	9.2	167	4.5	9.2	11.8	12.5	3.7	3.6	1.0	3.9	7.2	22
40	15	20	10	0.044	0.637	0.011	0.003	0.380	0.289	0.052	0.021	8.6	228	0.044	0.647	0.016	0.005	0.396	0.301	0.053	0.022	8.9	232	1.5	1.5	29.2	30.9	4.2	4.0	3.3	5.4	3.3	1.7
35	15	25	10	0.054	0.739	0.012	0.003	0.472	0.235	0.059	0.017	8.5	202	0.053	0.658	0.014	0.004	0.488	0.258	0.062	0.017	8.6	222	0.3	12.2	12.3	20.0	3.2	8.7	4.8	5.0	1.1	9.0

Error (%) = (EV)-(AV) x 100/ (EV); where EV and AV are exact and approximate values

To ensure the reliability as well as the repeatability of the predicted responses, the confirmatory experiments were performed by randomly selecting flux mixture components to validate the regression models. Three flux mixtures randomly selected from basic, rutile-basic, and rutile-acidic flux systems and it observed that the error percentage for most of the properties is almost 5% (Table 5.22-5.24). Error percentage for carbon and molybdenum is more than 5% for a basic flux system (Table 5.22). Table 5.23 shows that the error percentage for phosphorous, sulphur and manganese is more than 5% for rutile-basic flux system while for rutile-acidic flux system error percentage is more for silicon, phosphorous, sulphur and microhardness.

5.3 CORROSION ANALYSIS AND DISCUSSION

Corrosion behavior of API X70 steel specimen in different service environments performed by the method of weight loss. The chemical composition of X70 steel is given in Table 4.7 (Section 4.5, Material & Experimentation). Four different exposing environments such as freshwater, seawater, sodium thiosulphate solution (10^{-2} mol/l, pH=3) and sodium thiosulphate solution (10^{-3} mol/l, pH=5) were taken for the corrosion study. ASTM standard D1141-98 (2013) was used to prepare the seawater solution.

5.3.1 Corrosion study of heat treated API X70 steel due to weight loss in different environments

Twenty four specimens were taken for the weight loss study. Each specimen has an of dimension 12 x 10 x 22 mm. The suitable heat treatment procedure was carried out for all the specimens to observe the effect of heat treatment on corrosion in different environments [Sharma et al., 2019]. Table 5.25 represents the steps of heat treatment with specimen distribution.

Table 5.25: Distribution of heat treated specimens in various exposing environments

Heat treatment	*Austenizing Temp./time (^{o}C/min)*	*Tempering Temp./time (^{o}C/min)*			*Test Solution*			
		300^o	*450^o*	*600^o*	*FW (pH=7)*	*SW (pH=8.2)*	*5%NaCl+10^{-2} STS (pH=3)*	*5%NaCl+10^{-3} STS (pH=5)*
BM	----	-----	-----	-----	2 S	2 S	2 S	2 S
HT-1	1000^{o}C/30 min	1hr	1 hr	1 hr	2 S	2 S	2 S	2 S
HT-2	850^{o}C/30 min	1hr	1 hr	1 hr	2 S	2 S	2 S	2 S

Note: BM: Base metal; FW: Fresh water; SW: Sea water; 10^{-2} mol/l and 10^{-3} mol/l sodium thio-sulphate solution; HT-1: Heat treatment cycle 1; HT-2: Heat treatment cycle 2; S: no of samples; STS: Sodium Thio-sulphate solution. HT-1: 1000^{0}C austenization (30 min) then immediate water quenching followed by three tempering treatments at 300^{0}C, 400^{0}C and 600^{0}C for 1 hr. HT-2: 850^{0}C austenization (30 min) then immediate water quenching followed by three tempering treatments at 300^{0}C, 400^{0}C and 600^{0}C for 1 hr.

All specimens (table 5.25) immersed in four different solutions for thirty-day interval. Before immersion, the specimen was polished with 80-600 grit size emery papers, and the original weight of all specimens noted. The loss or gain of scale formed on the outer surface noticed by measuring the average weight change of all specimens after every three-day interval. After thirty days interval the outer surface of all specimen was visually analyzed (Figure 5.22-5.25). It showed the presence of various pits and scales developed in different testing solutions. For corrosion rate measurement the outer scale was removed from all the specimen using bristle wire brush. Then specimen cleaned, dried and re-weighed according to ASTM G1-03 (2011) standard. Equation 5.4 was used to find the corrosion rate.

Corrosion rate (mm/yr) = K * W/A*T*D (5.4)

Where, K= a constant = 87.6; W= weight loss in mg; A= area in cm^2; T= time in hours;
D= density of material in gm/cm^3 (7.85 gm/cm^3)

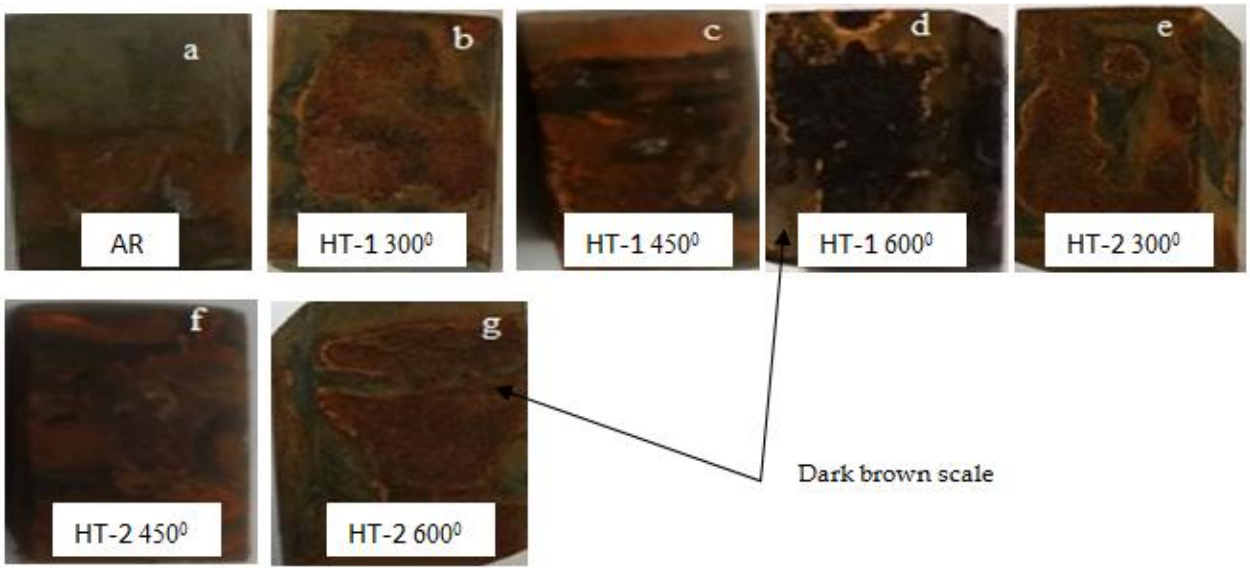

Figure 5.22: Visual examination of specimens immersed in fresh water solution after exposure of thirty days (Note AR: as received)

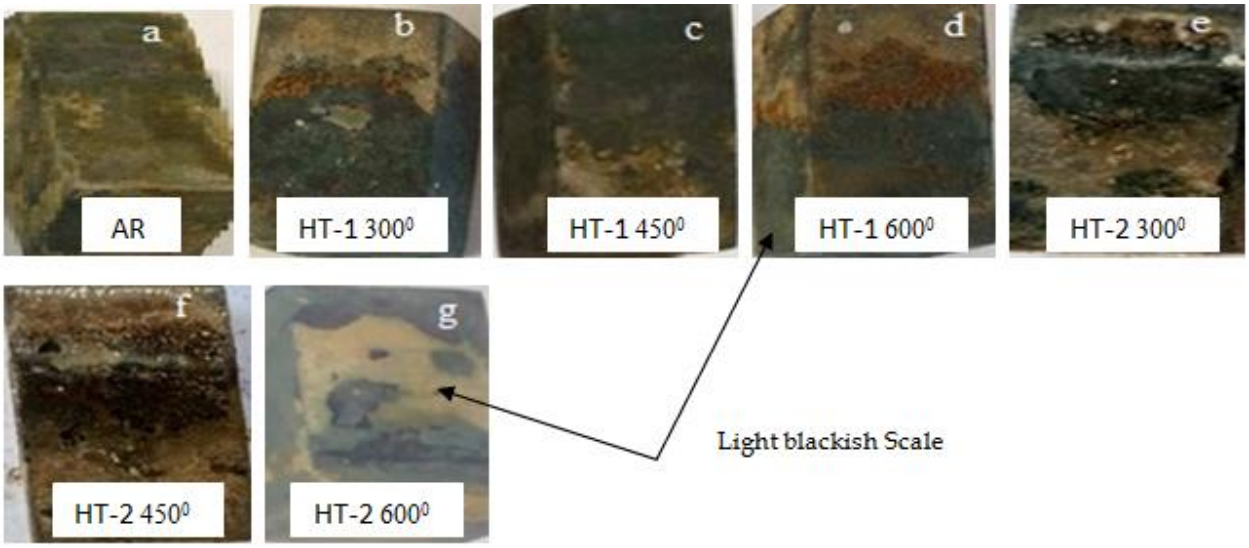

Figure 5.23: Visual examination of specimens immersed in sea water solution (pH=8.2) after exposure of thirty days

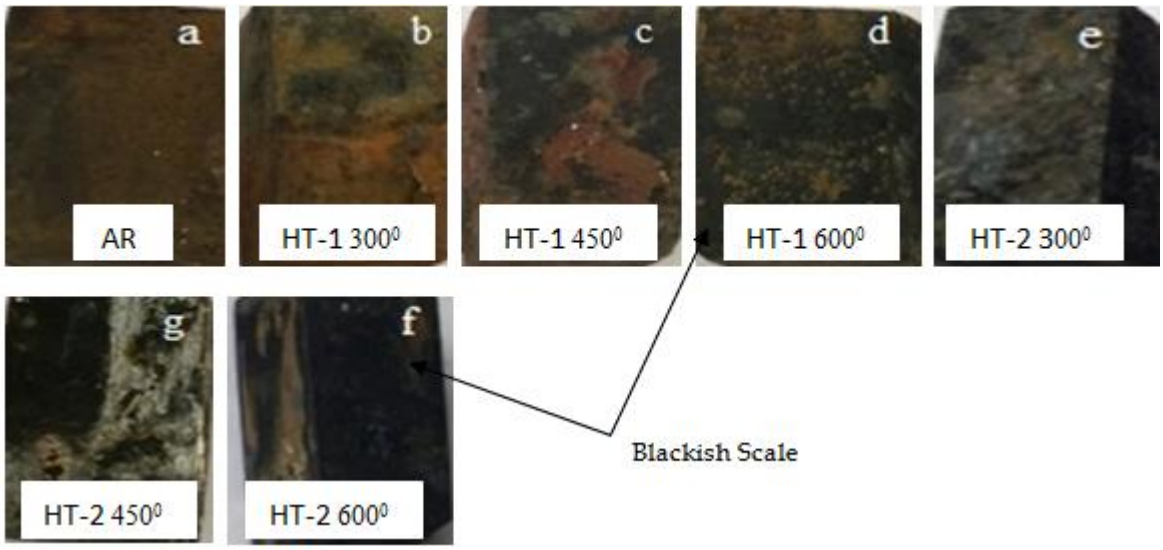

Figure 5.24: Visual examination of specimens immersed in 5%NaCl+10^{-3}mol/l sodium thiosulphate solution at pH-5 solution (pH=5) after exposure of thirty days

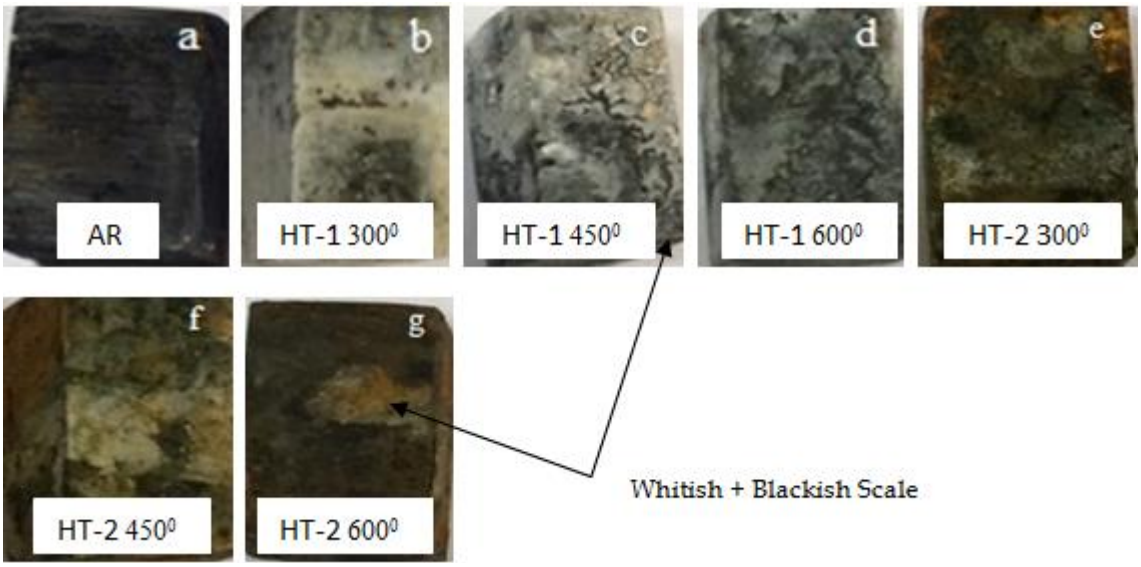

Figure 5.25: Visual examination of specimens immersed in 5%NaCl+10^{-2}mol/l sodium thiosulphate solution at pH-5 solution (pH=3) after exposure of thirty days

Figure 5.22-5.25 shows that with time, more scale developed on the surface of as received as well as heat-treated specimens. The depletion of parent metal material is more in as received compared to the heat-treated specimens in 5%NaCl+10^{-2}mol/l sodium thiosulphate solution due to the highly reactive behavior of hydrogen sulphide (H_2S) produced during the aqueous medium. It reported in the previous study that cathodic and anodic reactions become faster due to the presence of hydrogen sulphide in the solution or H_2S accelerate these corrosion reactions. Hydrogen sulphide is readily soluble in water. It is mildly acidic due to which it quickly attacks the metal surface resulting in pitting corrosion of the pipeline steels [Cheng et al., 2000, Tang et al., 2010]. Previous research shows that heat treatment and microstructure alteration of pipeline steel widely affect the corrosion resistance properties of steel in the hydrogen sulphide environment [Nagu et al., 2000, Ramunni et al., 2006]. Figure 5.26 shows the average percentage weight change as well as the corrosion rate of as received metal in a fresh and seawater environment after thirty days of exposure. Figure 5.27-5.28 shows the average percentage weight change and the corrosion rate of the HT-1 specimen in the freshwater and seawater environment.

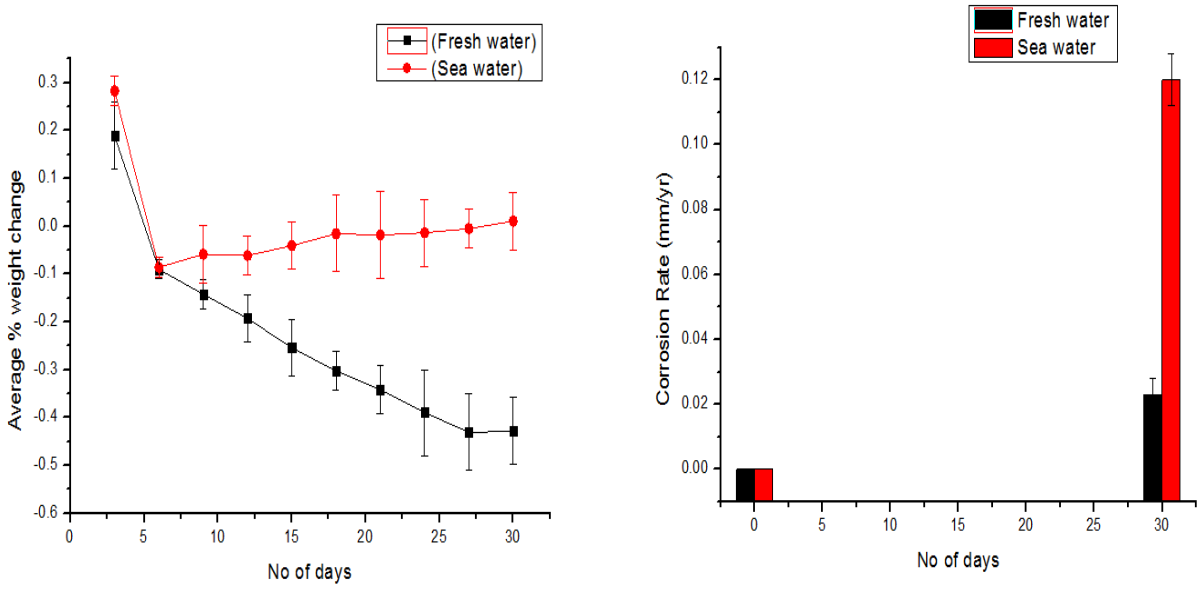

(a) Average weight change (b) Corrosion rate

Figure 5.26: (a) Average percentage weight change and (b) corrosion rate of as received metal in fresh and sea water after thirty days exposure

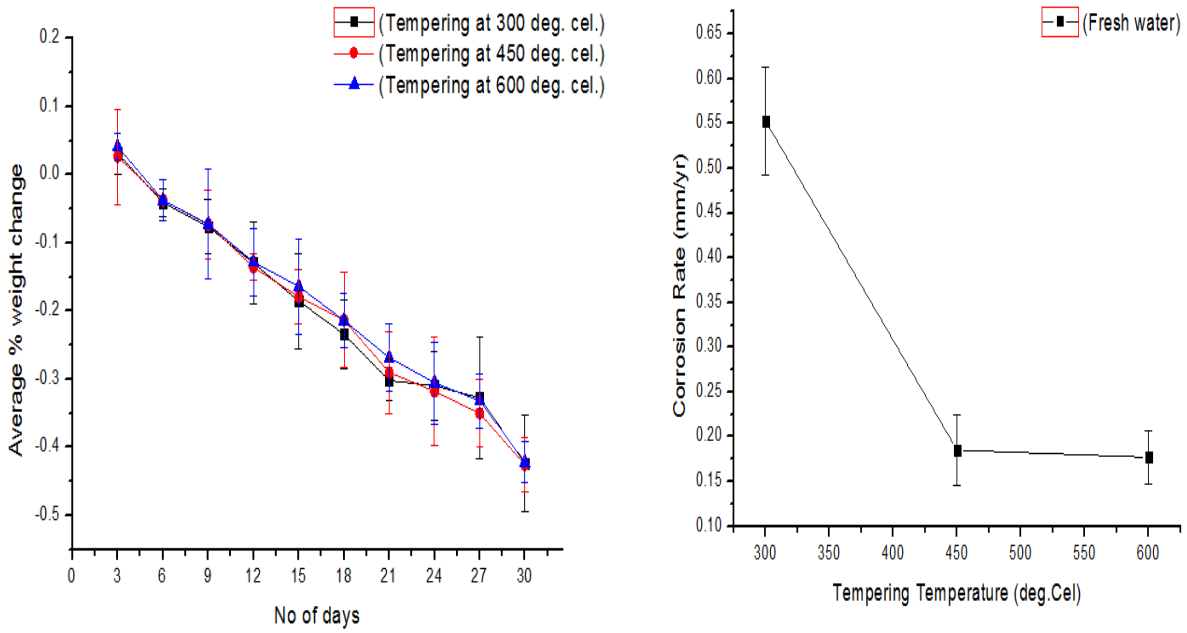

(a) Average weight change (b) Corrosion rate

Figure 5.27: (a) Average percentage weight change and (b) corrosion rate of HT-1 specimens (at tempering temp. 300°, 450° and 600° C) in fresh water after thirty day exposure

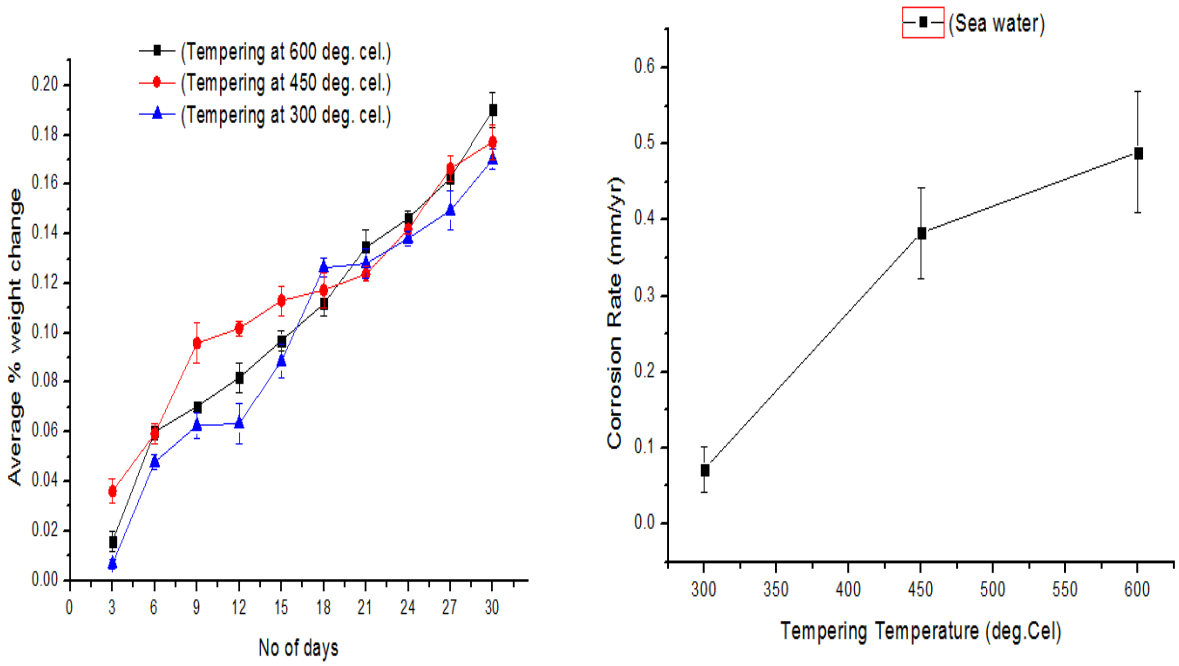

(a) Average weight change (b) Corrosion rate

Figure 5.28: (a) Average percentage weight change and (b) corrosion rate of HT-1 specimens (at tempering temp. 300°, 450° and 600° C) in sea water after thirty day exposure

Figure 5.29-5.30 shows the average percentage weight change and corrosion rate of HT-2 specimens in the fresh and seawater environment. Figure 5.31 shows the average percentage weight change and corrosion rate of HT-1 specimens in 5% NaCl + 10^{-2} Mol/l sodium thiosulphate solution (pH=3). It observed from Figure 5.27-5.31 that with an increase in exposure time, the average percentage weight change, as well as corrosion rate, increased for 300° C tempered specimen as compared to 450° and 600° C tempered specimen for HT-1 & HT-2. Table 5.26 shows the corrosion rate of all the specimens due to weight loss in different environments. More increase in the percentage weight change as well as corrosion rate (Table 5.26) was observed in 5% NaCl + 10^{-2} Mol/l (pH=3) and 5% NaCl + 10^{-3} Mol/l sodium thiosulphate solution (pH=5). It may be due to the more acidic behavior of sodium thiosulphate solution, which increases the cathodic and anodic corrosion reactions. It is reported in the previous study that the corrosion rate tends to increase in the aqueous medium (if hydrogen sulphide present in the medium) with decreasing pH value. At higher pH value (pH>6), the hydrogen sulphide forms unstable HS^- and S^{2-} in the solution [Kane, 1985]. Reduced solubility of solid sulphur and lesser reduction of hydrogen were observed due to the formation of iron sulphide which decreases the corrosion rate in alkaline mediums. At higher pH value (pH>7), the sulphide layer promotes passivation while this layer breaks down at a lower pH value (pH 4-6), and there is more dissolution of the metal surface that takes place [Cheng et al., 1998].

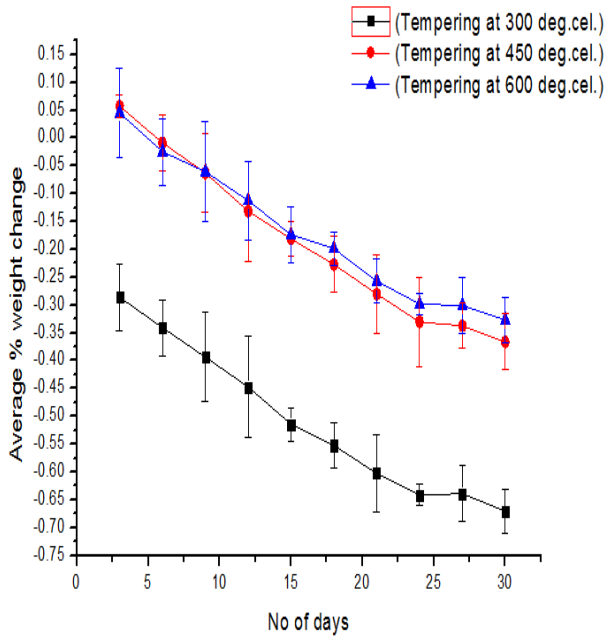

(a) Average weight change

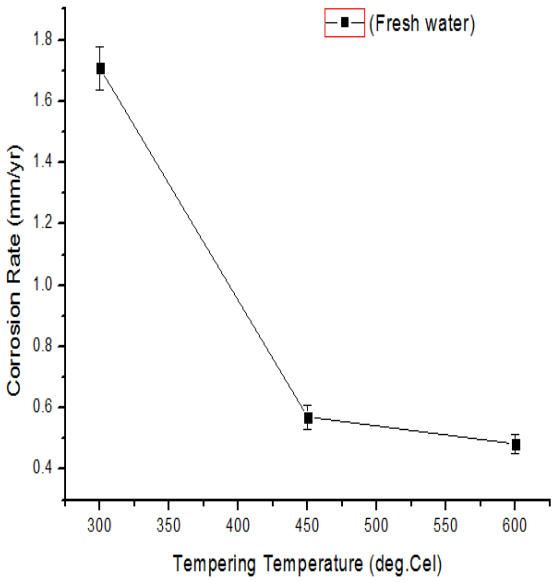

(b) Corrosion rate

Figure 5.29: (a) Average percentage weight change and (b) corrosion rate of HT-2 specimens (at tempering temp. 300°, 450° and 600° C) in fresh water after thirty day exposure

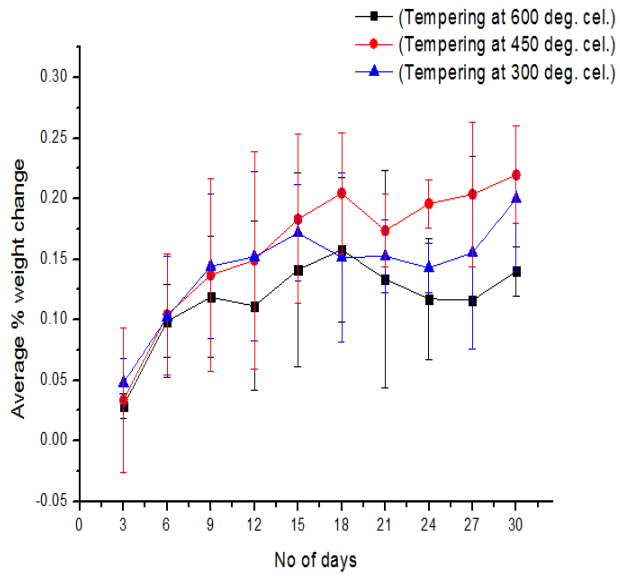

(a) Average weight change

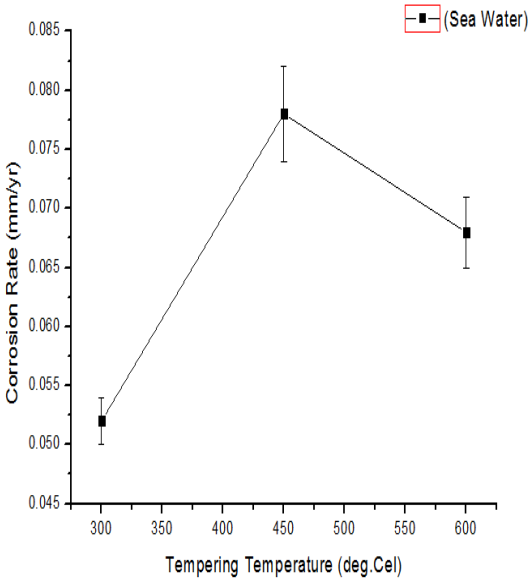

(b) Corrosion rate

Figure 5.30: (a) Average percentage weight change and (b) corrosion rate of HT-2 specimens (at tempering temp. 300°, 450° and 600° C) in sea water after thirty day exposure

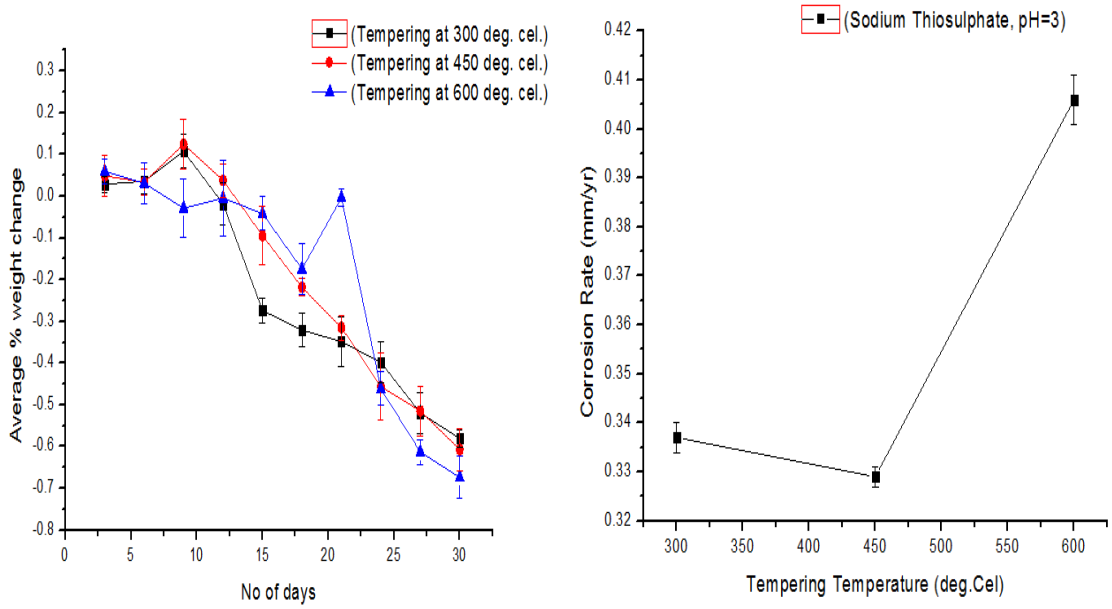

(a) Average weight change

(b) Corrosion rate

Figure 5.31: (a) Average percentage weight change and (b) corrosion rate of HT-1 specimens (at tempering temp. 300°, 450° and 600° C) in 5% NaCl + 10^{-2} mol/l sodium thiosulphate solution (pH=3)

Table 5.26: Corrosion rate of specimen due to weight loss in different test environments

S.No	*Solution*	*Material*	*Corrosion rate (mm/yr)*
1.	Fresh water (FW) (pH=7)	Base metal (BM)	0.023
		HT-1(300°C)	0.553
		HT-1(450°C)	0.185
		HT-1(600°C)	0.177
		HT-2(300°C)	1.708
		HT-2(450°C)	0.571
		HT-2(600°C)	0.483
2.	Sea water (SW) (pH=8.2)	Base metal (BM)	0.120
		HT-1(300°C)	0.072
		HT-1(450°C)	0.383
		HT-1(600°C)	0.489
		HT-2(300°C)	0.052
		HT-2(450°C)	0.072
		HT-2(600°C)	0.068
3.	5%NaCl+10^{-2} mol/l (pH=3) solution	Base metal (BM)	0.582
		HT-1(300°C)	0.337
		HT-1(450°C)	0.329
		HT-1(600°C)	0.406
		HT-2(300°C)	0.489
		HT-2(450°C)	0.371
		HT-2(600°C)	0.436

4.	5%NaCl+10^{-3} mol/l (pH=5) solution	Base metal (BM)	0.265
		HT-1(300°C)	0.343
		HT-1(450°C)	0.330
		HT-1(600°C)	0.324
		HT-2(300°C)	0.362
		HT-2(450°C)	0.339
		HT-2(600°C)	0.368

5.3.2 Mechanical properties of heat treated API X70 steel in different environments

A previous study reports that during the heat treatment process, there are crystallographic as well as phase transformation changes observed, which affect the mechanical and corrosion properties of the steel [Daramola et al., 2010]. The pipeline steels are required to have greater strength and toughness to work in sour service applications. API X70 pipeline steel generally has a ferrite-pearlite matrix with an extremely fine-grained microstructure, which shows a good combination of strength as well as toughness. Suitable thermomechanical heat treatments and the presence of micro-alloying elements provide the combination of good strength and toughness to pipeline steel. The addition of these microalloying elements brings the grain refinement in the microstructure of the steel. Fine precipitation within the grains improves the strength properties of pipeline steels [Yakubtsov et al., 2008, Zhao et al., 2003]. Microhardness and impact toughness of base metal, as well as heat-treated (HT-1 & HT-2) specimen, were observed in the different testing solutions. Mechanical properties of base metal and heat-treated (HT-1 & HT-2) specimens without immersing in the test solutions also noted. It observed from the study (Table 5.27) that the higher microhardness value was found for HT-1 & HT-2 (tempered at 300° C) without immersed specimen as compared to the HT-1 & HT-2 (tempered at 300° C) specimen immersed into the test solution. HT-1 & HT-2 specimen immersed in fresh and seawater shows lower microhardness value as compared to specimen immersed in sodium thiosulphate solution (Table 5.27). Base metal and HT-1 & HT-2 specimen tempered at 600° C shows the almost similar value of toughness as compared to other tempered specimens (Table 5.28). Figure 5.32 shows the microhardness value in fresh as well as seawater medium, while Figure 5.33 shows the microhardness behavior of HT-1 & HT-2 specimens in sodium thiosulphate solution. Figure 5.34 shows the impact toughness behavior of HT-1 & HT-2 specimens.

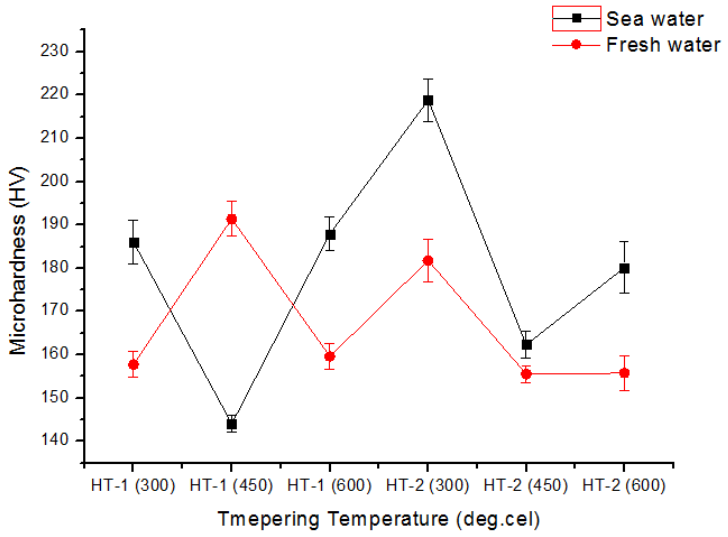

Figure 5.32: Relation between mirohardness vs. tempering temperature in fresh & sea water medium

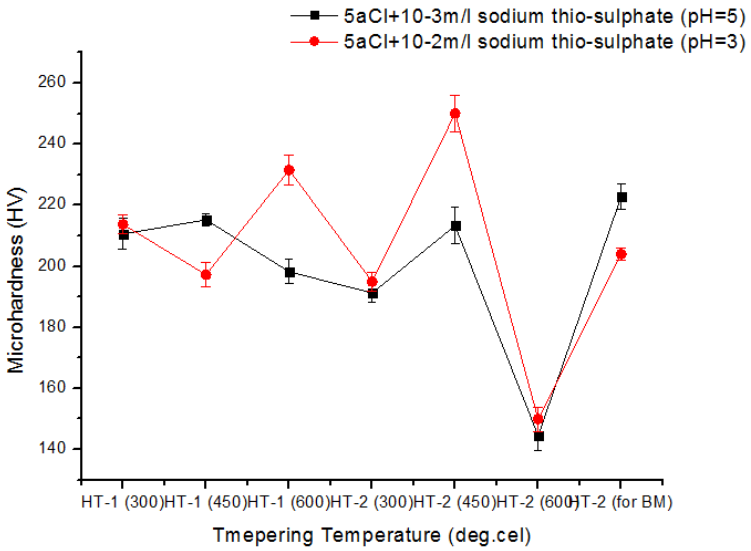

Figure 5.33: Relation between mirohardness vs. tempering temperature in sodium thiosulphate medium

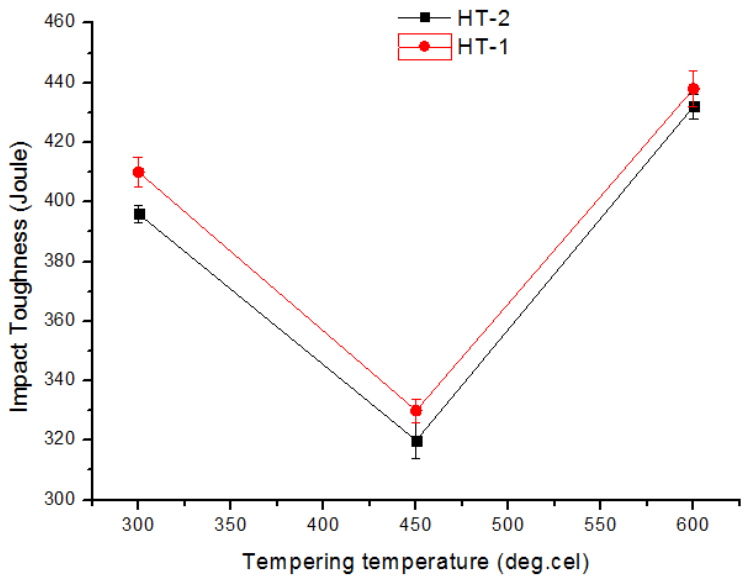

Figure 5.34: Relation between impact toughness vs. tempering temperature for HT-1 & HT-2 specimens.

Table 5.27: Average microhardness values for different specimens under various testing environments

Material	*Medium*	*Average microhardness (HV)*
Base metal (BM)	without immersion	194.09
HT-1(300°C)	without immersion	237.49

HT-1(450°C)	without immersion	193.13
HT-1(600°C)	without immersion	210.82
HT-2(300°C)	without immersion	238.04
HT-2(450°C)	without immersion	150.88
HT-2(600°C)	without immersion	150.73
HT-2 (300°C)	Fresh water	181.79
HT-2 (450°C)	Fresh water	155.54
HT-2 (600°C)	Fresh water	155.78
HT-1 (300°C)	Fresh water	157.77
HT-1 (450°C)	Fresh water	191.40
HT-1 (600°C)	Fresh water	159.60
HT-1 (300°C)	Sea water	186.04
HT-1 (450°C)	Sea water	144.04
HT-1 (600°C)	Sea water	187.95
HT-2 (300°C)	Sea water	218.81
HT-2 (450°C)	Sea water	162.33
HT-2 (600°C)	Sea water	180.17
HT-1 (300°C)	5%NaCl+10^{-2}mol/l sodium thio-sulphate (pH=3)	213.70
HT-1 (450°C)	5%NaCl+10^{-2}mol/l sodium thio-sulphate (pH=3)	197.23
HT-1 (600°C)	5%NaCl+10^{-2}mol/l sodium thio-sulphate	231.52

	(pH=3)	
HT-2 (300°C)	5%NaCl+10^{-2}mol/l sodium thio-sulphate (pH=3)	194.95
HT-2 (450°C)	5%NaCl+10^{-2}mol/l sodium thio-sulphate (pH=3)	250.07
HT-2 (600°C)	5%NaCl+10^{-2}mol/l sodium thio-sulphate (pH=3)	149.91
HT-1 (300°C)	5%NaCl+10^{-3}mol/l sodium thio-sulphate (pH=5)	210.58
HT-1 (450°C)	5%NaCl+10^{-3}mol/l sodium thio-sulphate (pH=5)	215.22
HT-1 (600°C)	5%NaCl+10^{-3}mol/l sodium thio-sulphate (pH=5)	198.23
HT-2 (300°C)	5%NaCl+10^{-3}mol/l sodium thio-sulphate (pH=5)	191.27
HT-2 (450°C)	5%NaCl+10^{-3}mol/l sodium thio-sulphate (pH=5)	213.29
HT-2 (600°C)	5%NaCl+10^{-3}mol/l sodium thio-sulphate	144.51

	(pH=5)	
HT-2 (for BM)	5%NaCl+10^{-2}mol/l sodium thio-sulphate (pH=3)	203.99
HT-2 (for BM)	5%NaCl+10^{-3}mol/l sodium thio-sulphate (pH=5)	222.84

Table 5.28: Impact toughness values of base metal and heat treated specimens (HT-1 & HT-2)

Material	*Tempering temperature*	*Impact toughness (J)*
BM		430.0
HT-1	300°C	410.0
HT-1	450°C	330.3
HT-1	600°C	438.0
HT-2	300°C	396.2
HT-2	450°C	320.2
HT-2	600°C	432.3

5.3.3 Electrochemical corrosion study and of heat treated specimens in different environments

Electrochemical corrosion behavior of heat-treated API X70 pipeline steel as well as received steel specimen observed in seawater (pH=8.2), 5%NaCl+10^{-2} mol/L sodium thiosulphate solution (pH=3) and 5%NaCl+10^{-3} mol/ L sodium thiosulphate solution (pH=5) using linear sweep voltammetry technique. The method of specimen preparation and heat treatment procedure is similar to that used in weight loss study (Section 5.3.1). Table 5.29 shows the corrosion rate of heat-treated API X70 steel specimens in various exposed environments. Tafel plots for HT-1 and HT-2 specimens exposed in different test environments were drawn to find the corrosion rate as well as corrosion potential. Figure (5.35, a-b) shows the Tafel plot of the as-received metal in different test environments, and there is more dissolution of metal in sodium thiosulphate solution (pH=3) as compared to the other test solutions. From table 5.29, it observed that for HT-1 specimen tempered at 300° C and 450° C shows more corrosion resistance as compared to 600° C tempered specimen in seawater medium (Figure 5.36, a-b) while in same medium HT-2 specimens gives opposite results (Figure 5.36, c-d). It reported in

the previous literature that microstructure having coarse grains exhibit a higher corrosion rate as compared to microstructure having fine grains [Nagu et al., 2000; Ramunni et al., 2006]. Previous literature suggests that tempered martensitic microstructure exhibit a higher corrosion rate as compared to polygonal ferrite microstructure due to the presence of large coarse grains [Hongwei et al., 2015, Park et al., 2008, Koh et al., 2004, Sharma et al., 2018]. Results obtained for HT-2 specimens in seawater medium are in close agreement with the previous literature. In 5% NaCl + 10^{-3} mol/L sodium thiosulphate solution (pH=5), HT-1 specimen tempered at 300^{o} C shows lesser corrosion resistance as compared to 450^{o} C and 600^{o} C tempered specimen while HT-2 specimen in the same medium shows the opposite effect. HT-1 and HT-2 specimen tempered at 450^{o} C in 5% NaCl + 10^{-2} mol/L sodium thiosulphate solution (pH=3) shows lesser corrosion rate as compared to 300^{o} C & 600^{o} C tempered specimen.

Table 5.29: Corrosion rate of API X70 heat treated specimens in different environments

Specimen	*α (mv/dec)*	*β (mv/dec)*	*E_{corr} Cal (mV)*	*J_{corr} (μA/cm²)*	*I_{corr} (μA)*	*C.R (mm/yr)*	*R_p (Ω)*
HT-1 300 ST, 10^{-2} pH=3	22.051	60.100	-857.60	2.159	6.910	0.025094	713.80
HT-1 450 ST, 10^{-2} pH=3	17.415	7.742	-516.2	1.120	4.20	0.0032104	590.52
HT-1 600 ST, 10^{-2} pH=3	62.201	76.071	-742.75	3.622	7.761	0.030468	514.9
HT-1 300 ST, 10^{-3} pH=5	54.88	31.090	-907.91	8.098	24.942	0.094099	345.57
HT-1 450 ST, 10^{-3} pH=5	19.529	42.744	-840.83	5.262	12.524	0.061146	464.82
HT-1 600 ST, 10^{-3} pH=5	60.319	24.051	-709.85	1.660	1.013	0.0021077	1595.8
HT-1 300 SW pH=8.2	18.824	27.437	-780.41	1.786	7.074	0.020758	685.39
HT-1 450 SW pH=8.2	46.862	21.595	-797.77	2.471	7.218	0.0208724	889.44
HT-1 600 SW pH=8.2	51.199	27.629	-895.00	25.227	87.287	0.29314	89.286
HT-2 300 SW pH=8.2	25.544	34.509	-781.29	1.591	5.348	0.014498	1191.8
HT-2 450 SW pH=8.2	25.147	35.238	-854.57	5.099	3.831	0.025700	538.67
HT-2 600 SW pH=8.2	48.51	12.79	-785.42	1.859	4.024	0.016007	729.60
HT-2 300 ST, 10^{-2} pH=3	45.693	41.346	-764.99	2.0839	8.668	0.024214	587.40
HT-2 450 ST, 10^{-2} pH=3	19.766	22.193	-769.69	2.462	5.205	0.020614	731.69
HT-2 600 ST, 10^{-2} pH=3	39.797	27.578	-839.89	2.013	7.813	0.023399	550.46
HT-2 300 ST, 10^{-3} pH=5	28.951	38.428	-830.36	2.466	5.131	0.028665	697.50
HT-2 450 ST, 10^{-3} pH=5	36.766	64.043	-670.41	1.513	4.359	0.017590	1012.7
HT-2 600 ST, 10^{-3} pH=5	60.546	41.039	-892.74	8.833	28.975	0.10265	366.62
BM, ST, 10^{-3} pH=5	28.205	22.968	-683.03	1.860	4.278	0.02160	1085.1
BM, ST, 10^{-2} pH=3	40.855	22.726	-845.26	5.612	23.573	0.065218	269.03
BM, SW pH=8.2	38.873	19.021	-773.83	4.474	10.292	0.051997	538.92

Note: α= anodic decay, β= cathodic decay, E_{Corr}= Corrosion potential, J_{Corr}= Corrosion current density, C.R= Corrosion rate, R_P = Polarization resistance; BM: base metal; ST: 5%NaCl+10^{-2}mol/l sodium thiosulphate pH=3 and 5%NaCl+10^{-3}mol/l sodium thiosulphate pH=5; SW: Sea water pH=8.2.

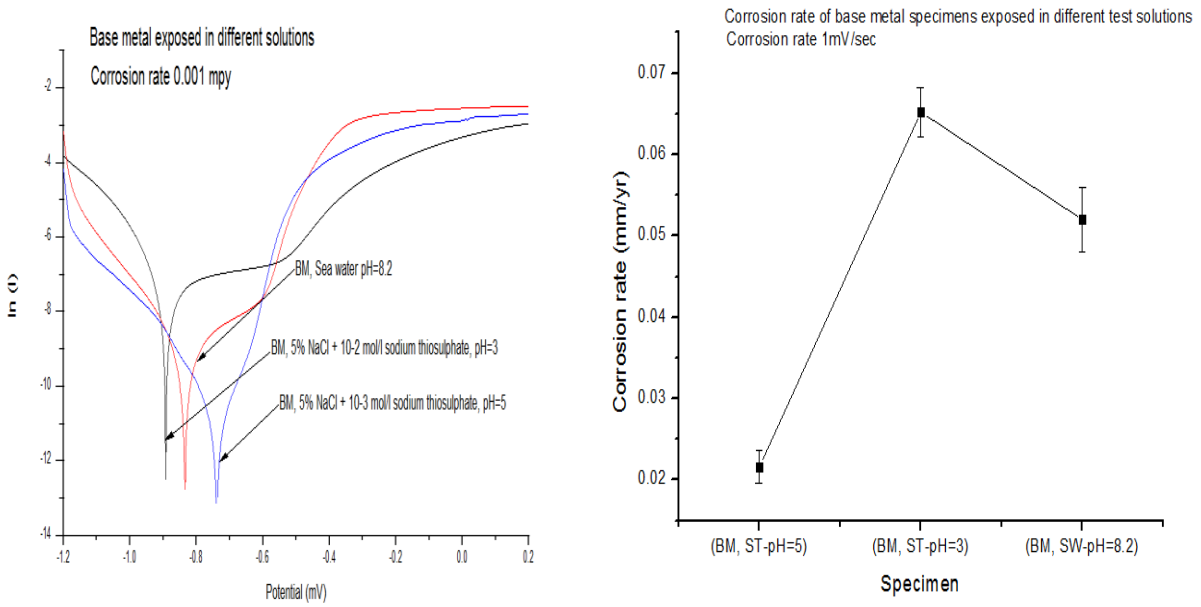

(a) (b)

Figure 5.35: (a) Base metal tafel plots in various test environments; (b) Corrosion rate of base metal in various test environments

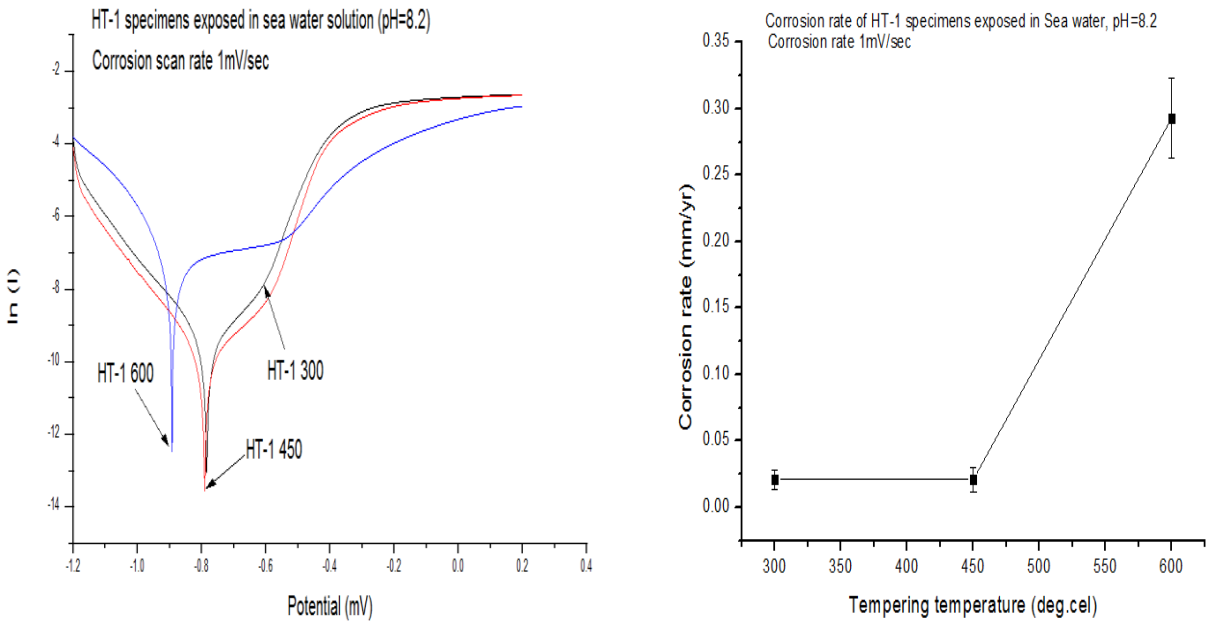

(a) (b)

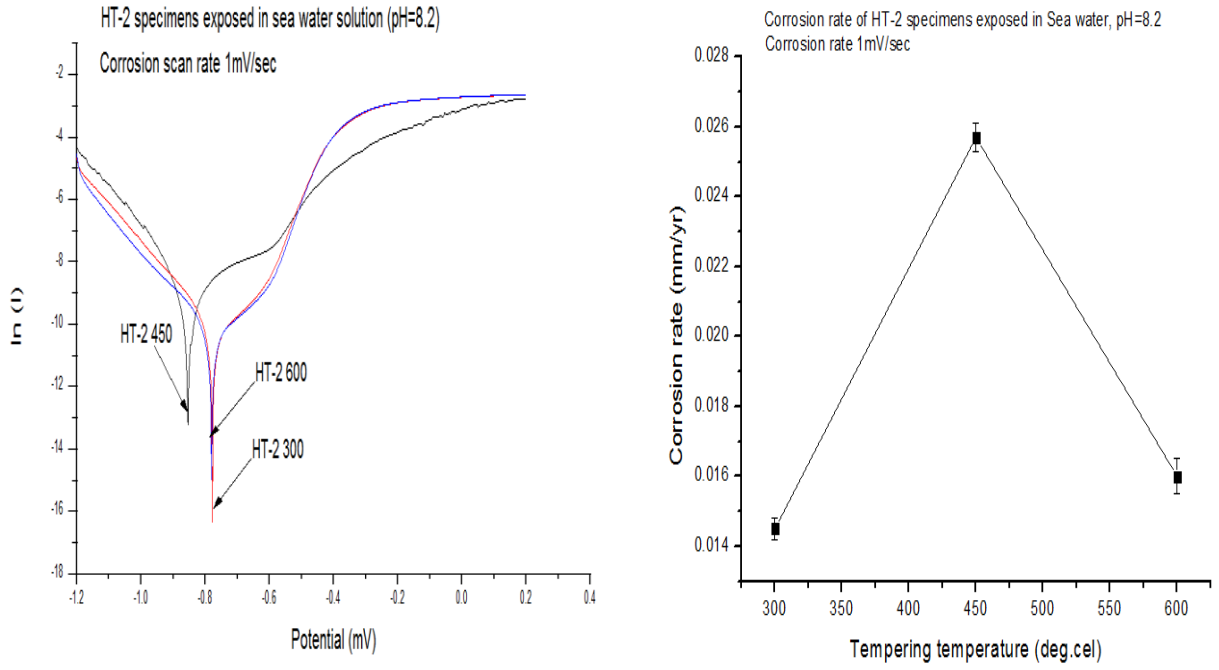

(c) (d)

Figure 5.36: (a-b) Tafel plot and corrosion rate of HT-1 specimens in sea water medium; (c-d) Tafel plot and corrosion rate of HT-2 specimens in sea water medium

5.4 SELECTION OF FLUX (FROM THREE FLUX SYSTEMS)

From twenty-one different multi-pass welds bead deposit, the slag detachability, porosity, and bead appearance observed in three flux systems (Section 5.2). Based on the qualitative analysis of multi-pass bead on plate weld deposits, two fluxes from each flux system selected for final submerged arc welding.

5.4.1 Selection of suitable fluxes from three flux systems

By visual examination of bead profile analysis during multi-pass bead on plate experimentation, two fluxes from each flux system i.e., F5B & F15B from basic system, F5RB & F7RB from rutile-basic and F3RA & F19RA from rutile-acidic systems selected which have good bead morphology, least porosity, and good slag detachability. A total of six fluxes was chosen for final submerged arc weld joint fabrication from three systems and compared with commercial flux.

5.4.2 Chemical analysis of weld specimens

Table 5.30 shows the chemical composition of the base metal, commercial flux (C.F) as well as seven weld specimens. Base metal generally comprises of carbon-manganese steel having other micro-alloying elements such as nickel, chromium, niobium, and titanium. From table 5.30, it observed that nickel and niobium content in the weld metal significantly decreased while other carbide forming elements such as chromium, titanium, boron, and copper content increased in the weld region as compared to the base metal. There is an increase in the sulphur content for all weld specimens in the weld region as compared to the base metal. Rutile-acidic flux F19RA shows a maximum rise in sulphur while basic flux F5B shows the least increase in sulphur content. Basic flux F5B and base metal exhibit almost similar value of carbon equivalent (C.E=0.32), while other fluxes show lower value as compared to F5B and base metal. The carbon equivalent value broadly decides the weldability of metals. Optimum value (C.E=0.33-0.4) of carbon equivalent indicates good weldability while a too high and too low value of carbon

equivalent shows poor weldability of metals. Figure 5.37 (a) shows the relation between carbon equivalent and weld specimens, while Figure 5.37 (b) shows the relationship between chemical compositions for weld specimens.

Table 5.30: Chemical behaviour of seven weld specimen

S.No	*%C*	*%Si*	*%Mn*	*%P*	*%S*	*%Cr*	*%Mo*	*%Ni*	*%Cu*	*%Nb*	*%Ti*	*%B*	*%Fe*	*%CE*
BM (API X70)	0.0638	0.321	1.64	0.0070	0.0011	0.0065	0.0012	0.318	0.0072	0.0577	0.0205	0.0004	97.5	0.32
FW (EA2TiB)	0.0291	0.0886	0.8717	0.0104	0.0072	0.0326	0.2169	0.0844	0.1301	0.0223	0.0040	0.0020	98.4	0.23
C.F	0.0516	0.3976	1.5407	0.0172	0.0051	0.0414	0.3568	0.0568	0.0701	0.0093	0.0217	0.0027	97.4	0.37
F5B	0.0466	0.4218	0.7823	0.0205	0.0038	0.0358	0.4077	0.0536	0.0639	0.0077	0.0163	0.0019	98.1	0.30
F15B	0.0620	0.4437	0.4771	0.0219	0.0069	0.0348	0.3758	0.0671	0.0607	0.0159	0.0235	0.0020	98.3	0.27
F7RB	0.0534	0.4382	0.3979	0.0143	0.0040	0.0317	0.3659	0.0701	0.0656	0.0158	0.0236	0.0019	98.4	0.21
F5RB	0.0601	0.3106	0.4220	0.0166	0.0052	0.0332	0.3956	0.0601	0.0634	0.0120	0.0201	0.0017	98.5	0.22
F19RA	0.0521	0.7225	0.3125	0.0163	0.0078	0.0319	0.4106	0.0699	0.0651	0.0198	0.0226	0.0029	98.2	0.20
F3RA	0.0696	0.7671	0.3804	0.0127	0.0061	0.0301	0.3570	0.0926	0.0614	0.0193	0.0177	0.0028	98.1	0.19

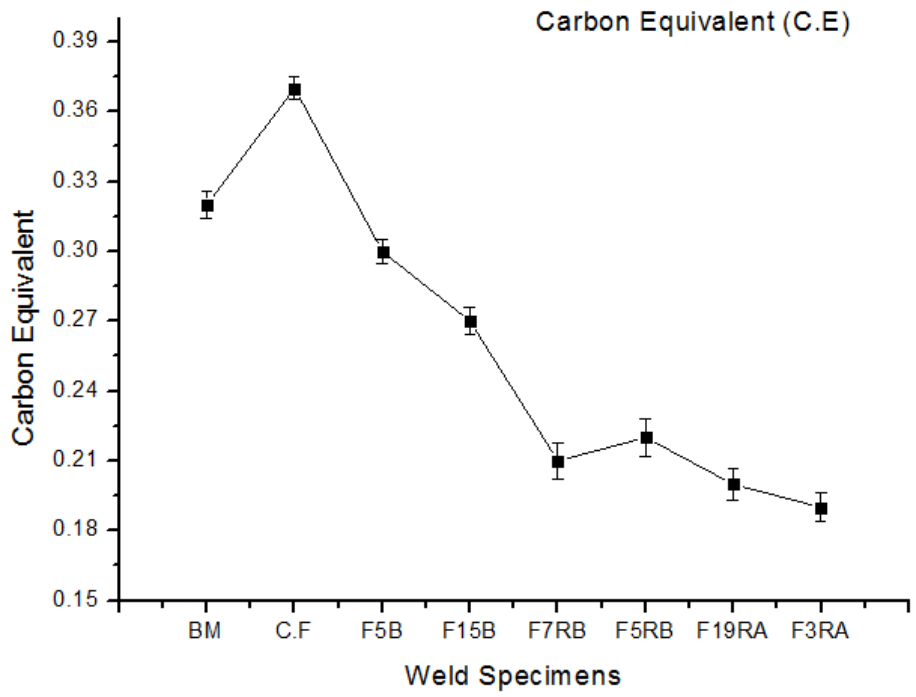

(a) Carbon equivalent

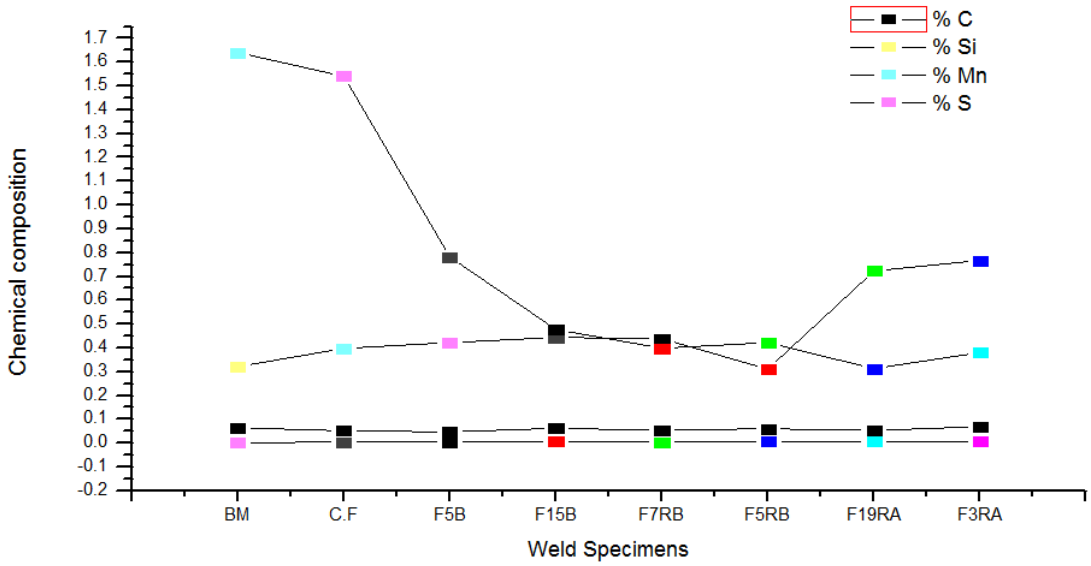

(b) Chemical composition

Figure 5.37: (a) Relation between carbon equivalent and weld specimens; (b) Relation between chemical composition (carbon, silicon, manganese & sulphur) and weld specimens

5.4.3 Microhardness and microstructure evaluation of weld specimens

The microhardness value of the base metal, weld region, and HAZ region of the seven weld specimen was studied, and the microhardness result shows that base metal has higher hardness as compared to the weld metal & heat-affected zone (HAZ) [Sharma et al., 2018]. Table 5.31 shows the microhardness results of base metal, weld metal, and heat-affected zone of seven

weld specimens. Figure 5.38 shows the microhardness graphs for base metal, weld region, and heat-affected zone. Microhardness value in the range of 180-240 HV observed for base metal, weld metal, and HAZ region. 230 HV and 190 HV hardness value found for weld metal, which is in the range of base metal hardness. A higher value of microhardness observed in the commercial weld joint as compared to the other weld joints. F15B weld joint shows comparable microhardness value with that of commercial weld joint (C.F). It was reported that an increase in hardness in the weld metal might be due to the presence of lower temperature transformation products such as bainite or widmanstaten ferrite in the weld region [Easterling, 1992, Sharma et al., 2018].

Table 5.31: Microhardness values of weld specimens

S.NO	Position	Parent metal	Weld metal	HAZ
F5RB	Max. hardness	213	210	203
	Min. hardness	200	209	195
F3RA	Max. hardness	230	212	221
	Min. hardness	224	190	206
F5B	Max. hardness	230	217	226
	Min. hardness	203	195	213
F7RB	Max. hardness	195	215	202
	Min. hardness	185	201	180
F15B	Max. hardness	240	223	227
	Min. hardness	200	190	195
F19RA	Max. hardness	232	209	219
	Min. hardness	225	208	220
C.F	Max. hardness	225	230	220
	Min. hardness	220	215	209

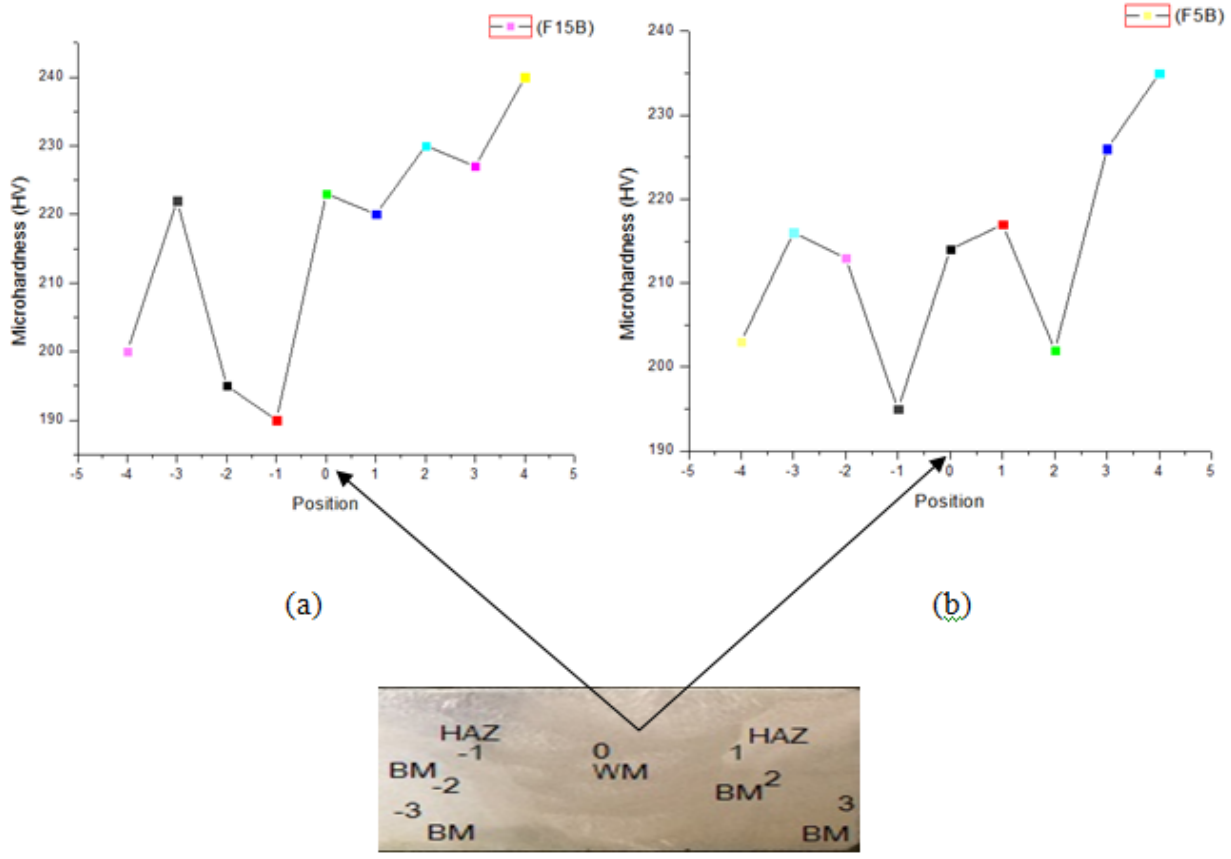

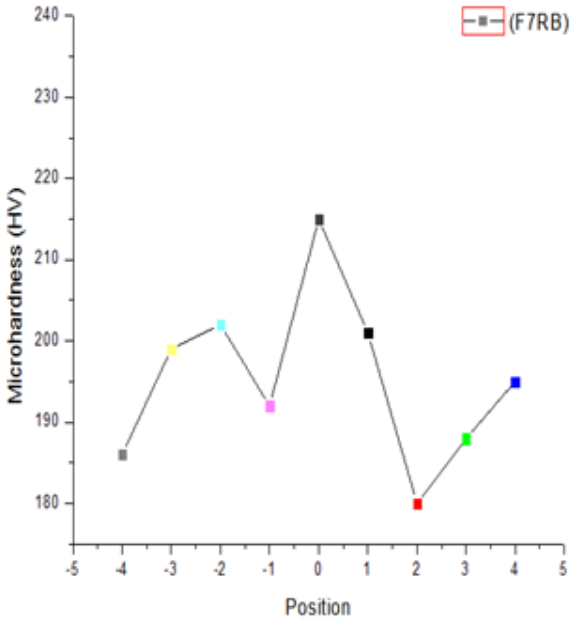
(F7RB)
Microhardness (HV)
Position

(c)

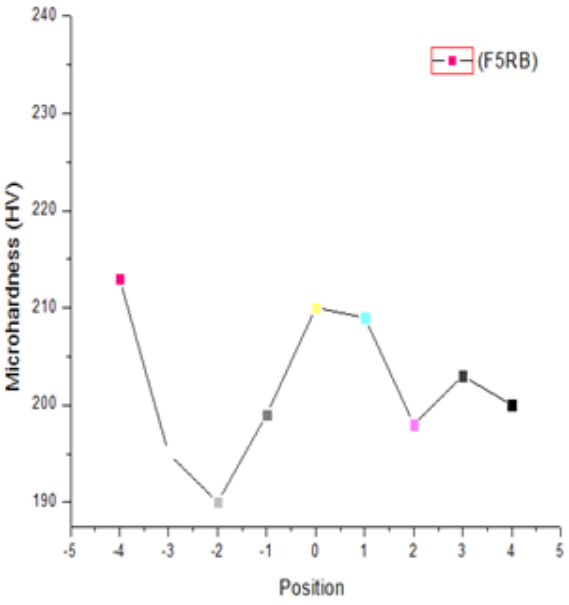
(F5RB)
Microhardness (HV)
Position

(d)

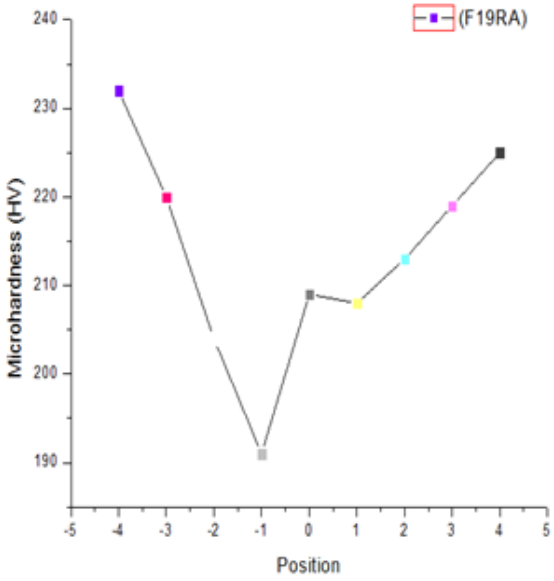
(F19RA)
Microhardness (HV)
Position

(e)

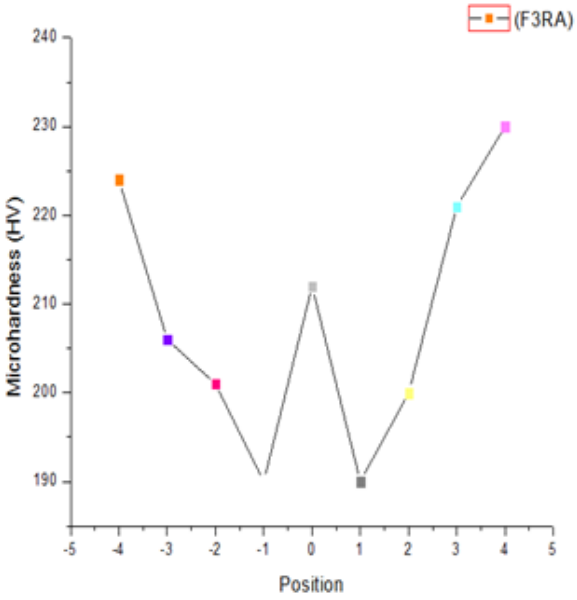
(F3RA)
Microhardness (HV)
Position

(f)

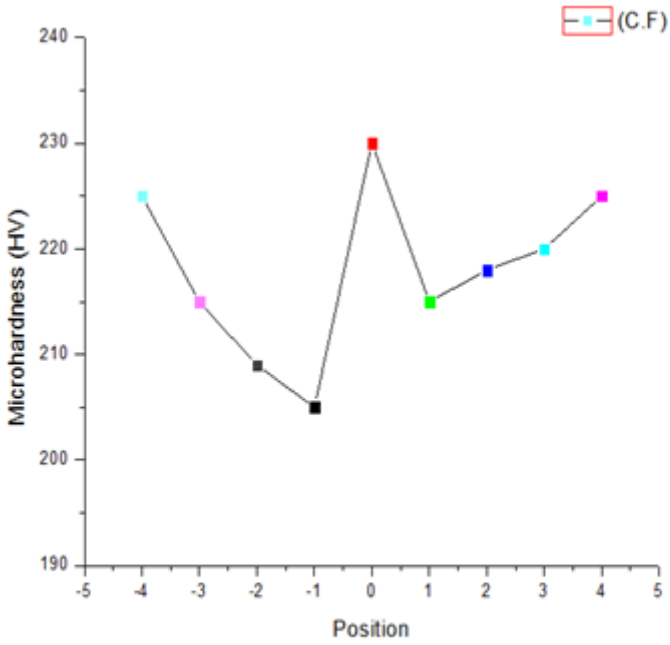

(g)

Figure 5.38: Microhardness plots for base metal, weld metal and heat-affected zone for different weld specimens

Figure 5.39 shows the variation of average microhardness with carbon equivalent for different weld specimen.

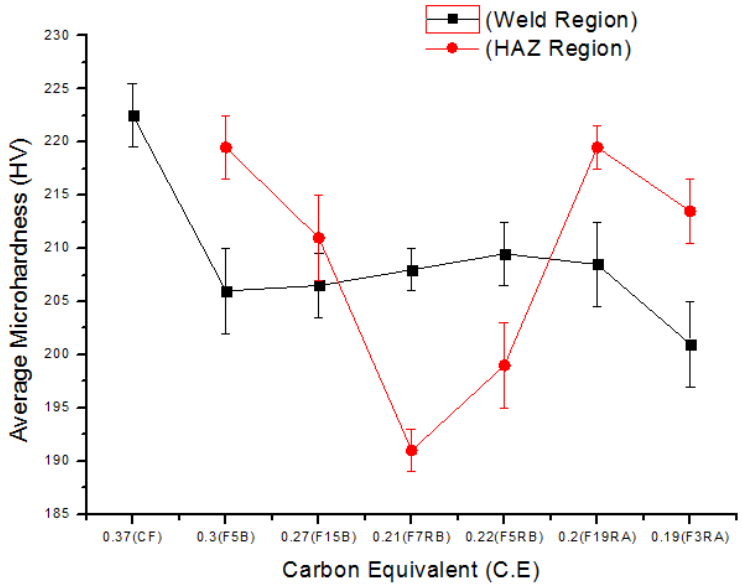

Figure 5.39: Relation between average microhardness vs. carbon equivalent for weld specimens

Figure 5.40 shows the microstructure of seven different weld specimens, which consist of the parent metal, fusion zone, and heat-affected zone. Parent metal mainly consists of fine-grained ferritic-pearlitic (F-P) microstructure and small bainite (B) inclusions. Acicular ferrite, polygonal ferrite (PF), grain boundary ferrite (GBF) microstructure was observed in the weld metal region while tempered martensitic (TM), coarse-grained heat-affected zone (CGHAZ) and fine-grained heat-affected zone (FGHAZ) microstructure and small inclusions of bainite were observed in all the heat-affected specimens. The coarse microstructure of the HAZ zone may be due to the

subsequent heating produced during the multi-pass thermal cycle generated during the submerged arc welding process. Due to multi-pass heating, the grains present in the heat-affected zone tend to grow and become coarse [Beidokhti et al., 2009; Rahim et al., 2009].

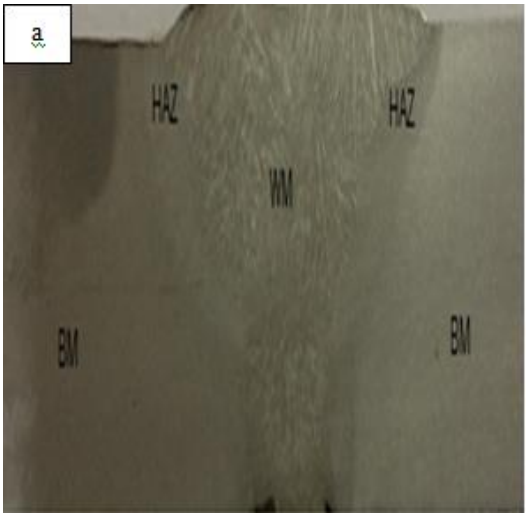

(a) Weld region

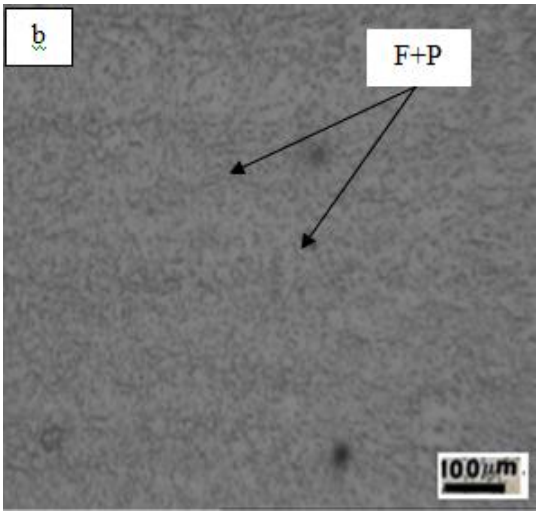

(b) Base metal

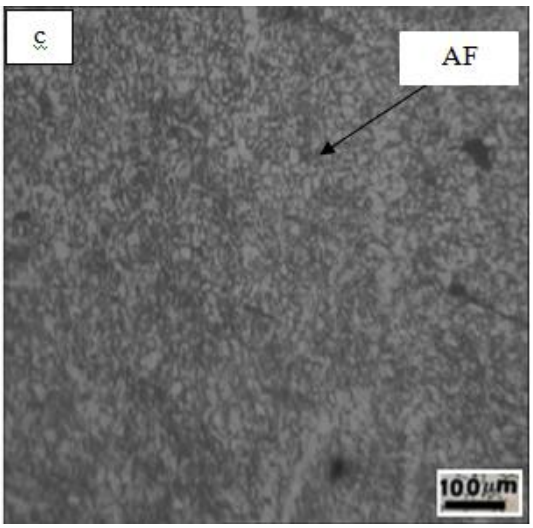

(c) C.F weld

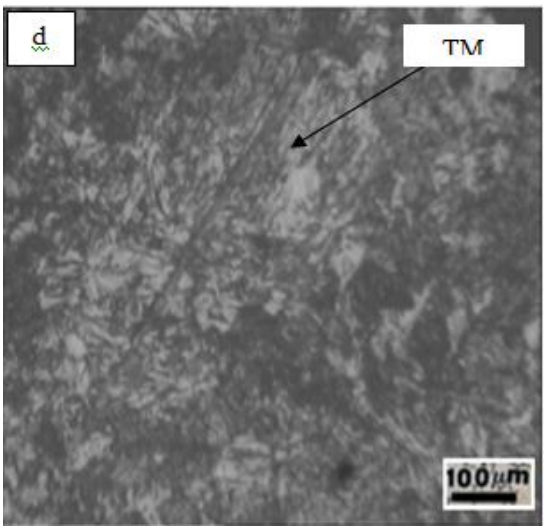

(d) C.F HAZ

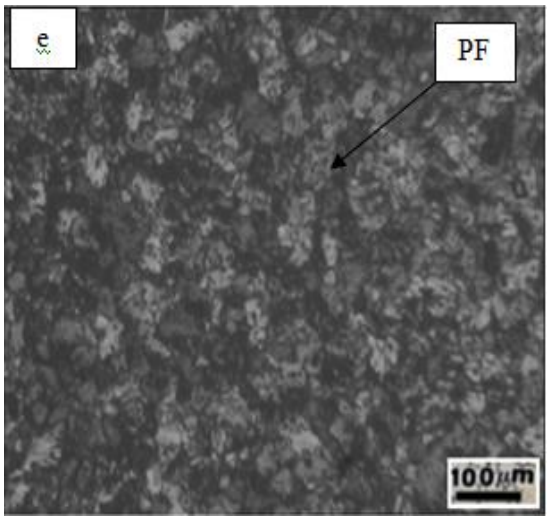

(e) F3RA weld

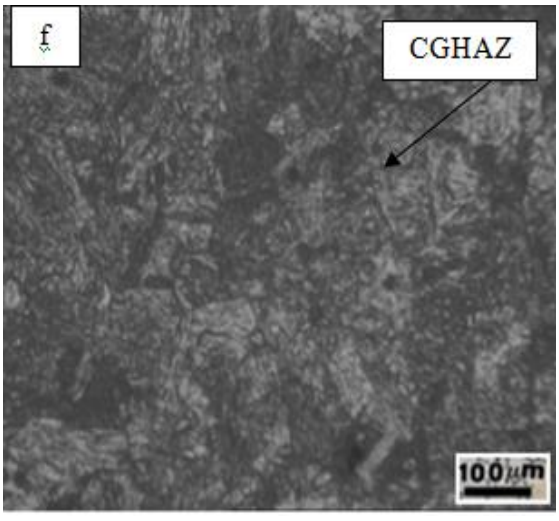

(f) F3RA HAZ

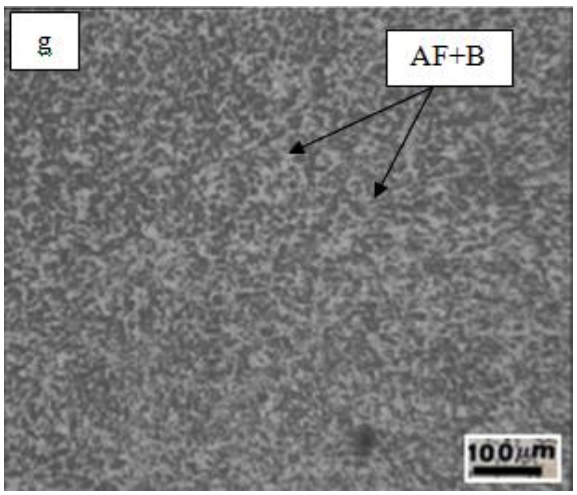

(g) F5B weld

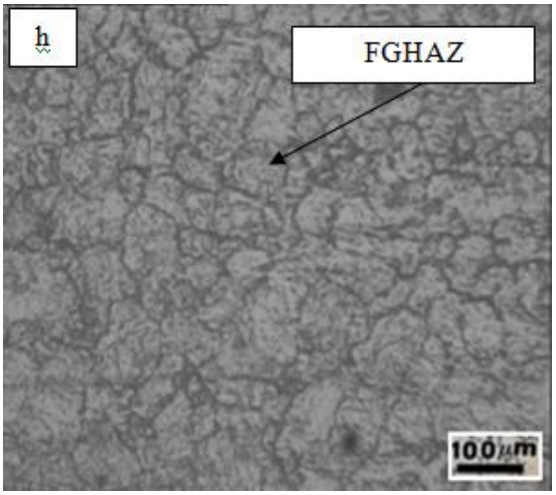

(h) F5B HAZ

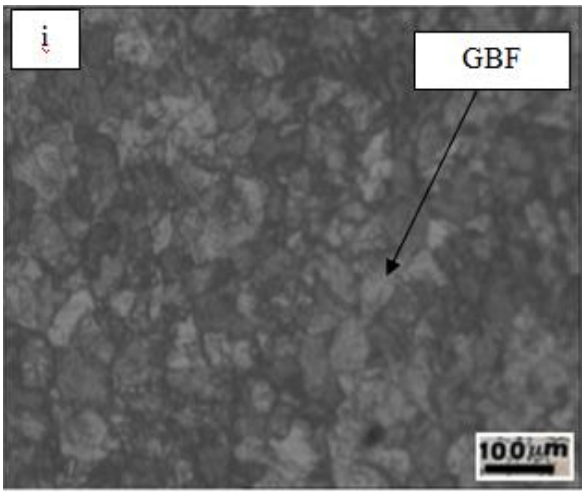

(i) F5RB weld

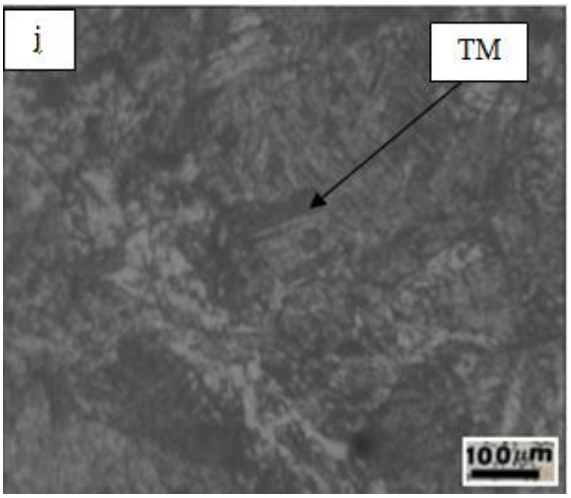

(j) F5RB HAZ

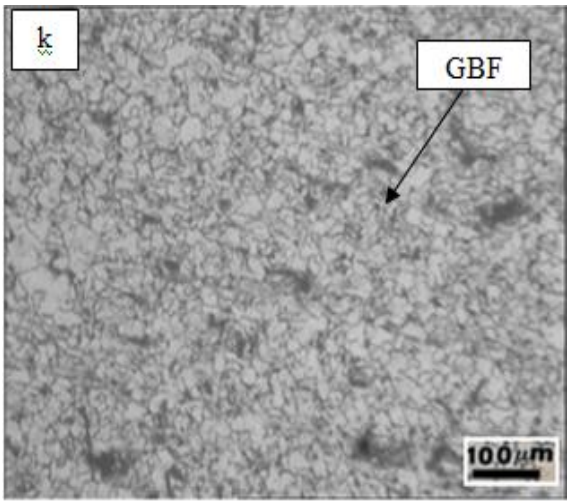

(k) F7RB weld

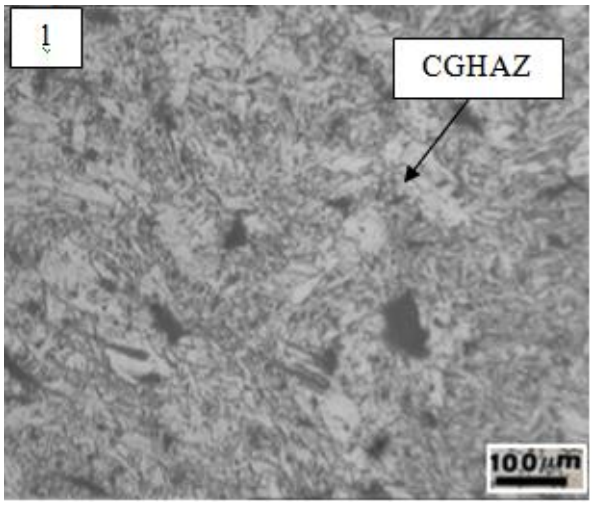

(l) F7RB HAZ

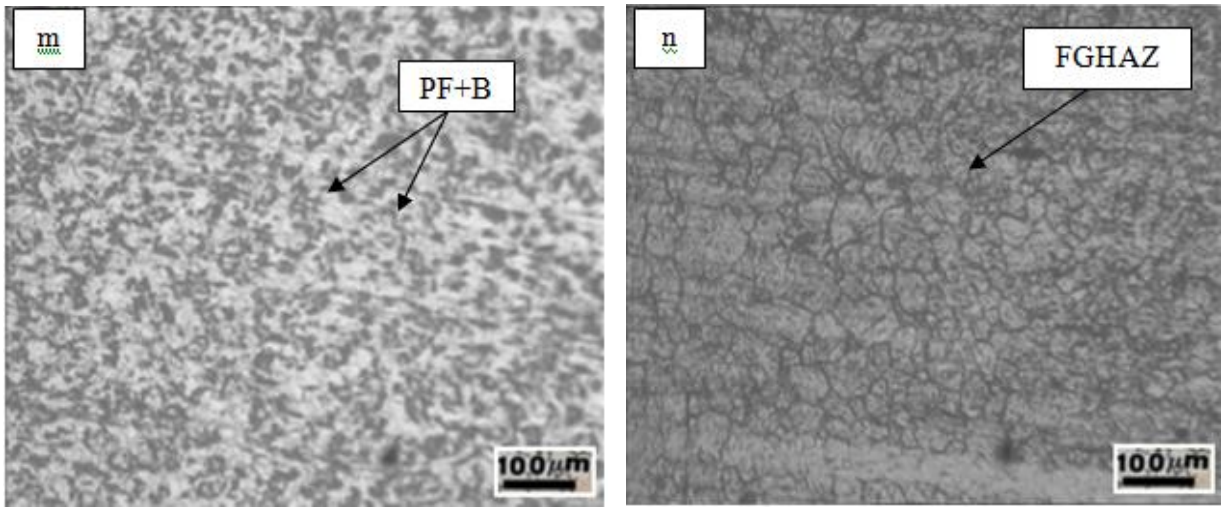

(m) F15B weld (n) F15B HAZ

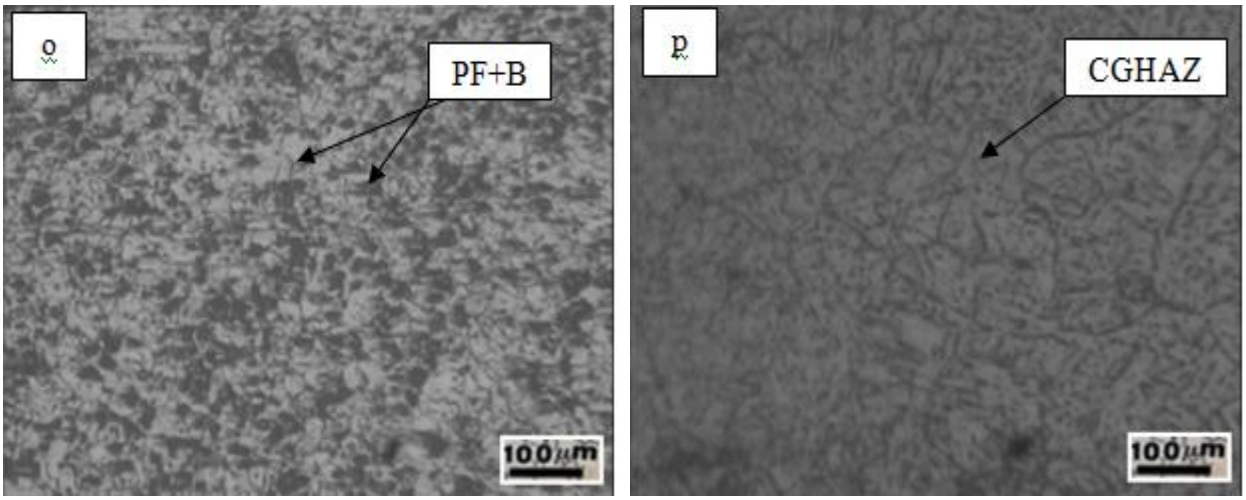

(o) F19RA weld (p) F19RA HAZ

Figure 5.40: Microstructure of various weld as well as heat-affected zone (HAZ) specimens at 100X magnification

5.4.4 Impact testing of weld and HAZ specimens at room temperature & -65° C

The impact toughness behavior of HAZ, as well as weld joints, were studied and noticed that impact toughness broadly depends upon the type of submerged arc welding fluxes i.e., basic flux, rutile-basic and rutile-acidic flux used. Basic fluxes show better impact toughness properties at room temperature as well as at low temperatures due to lower oxide content, which improves the impact toughness properties of weld metal [Sharma et al., 2018]. Table 5.32 shows the impact behavior of base metal and weld joints prepared by using selected fluxes. Base metal shows better impact properties at room temperature as well as -65° C, compared to the weld joints.

Table 5.32: Impact behaviour of different weld joints

S.No	Specimen	*Impact toughness (WM) (J)*		*Impact toughness (HAZ) (J)*	
		Room temp.	-65°C	Room temp.	-65°C
1	BM	443	39.6		
2	F5RB	89	5.0	439	44.4

3	F3RA	31	4.0	136	33
4	F5B	160	16.0	436	30
5	F7RB	20	3.0	413	43
6	F15B	70	4.0	428	33
7	F19RA	34	4.0	136	36
8	C.F	123	23	410	30

Basic flux (F5B) shows good impact toughness properties in the fusion zone as well as in the HAZ region both at room temperature and -65° C. F5B weld joint gives 160 J & 16 J of impact toughness in the weld region while 436 J & 30 J of impact toughness in the HAZ region even higher than the commercial weld joint (Table 5.32). Weld F3RA and F19RA exhibit lower impact toughness (Table 5.32) at room temperature as well as -65° C. Previous study reveals that higher acidic content or presence of high oxide inclusions in the weld metal gives poor impact toughness properties [Chai and Eagar, 1982, North et al., 1979]. Acicular ferrite microstructure was observed for the F5B weld specimen, while F5B HAZ specimen exhibits a fine-grained heat-affected region. Available literature suggests that the presence of polygonal ferrite (PF), Grain-boundary ferrite (GBF), and Acicular ferrite phases in the microstructure provide excellent impact properties. But, the acicular ferrite phase in the weld region is more dominant as compared to other phases [Beidokhti et al., 2015]. Figure 5.41 shows the variation of impact toughness in weld and HAZ region for different weld specimens at room temperature as well as -65° C. Figure 5.42 shows the relation between impact toughness behavior with a carbon equivalent of base metal and weld specimens at the room as well as -65° C.

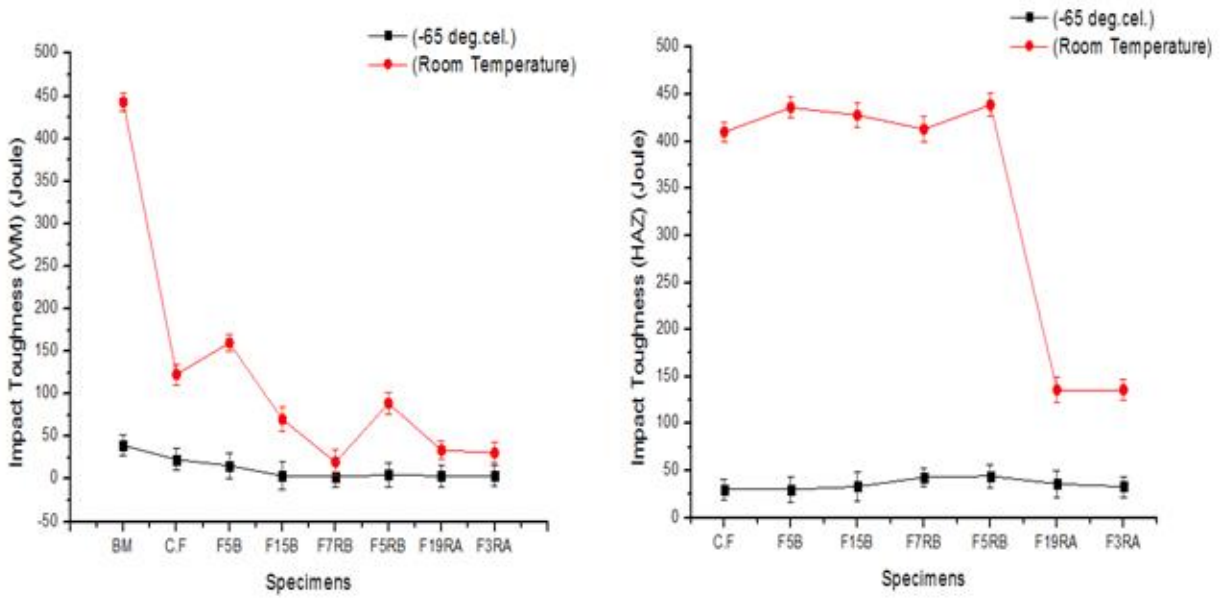

(a) Weld region (b) HAZ region

Figure 5.41: Impact toughness behaviour of base metal and weld specimens at in (a) weld region and (b) HAZ region

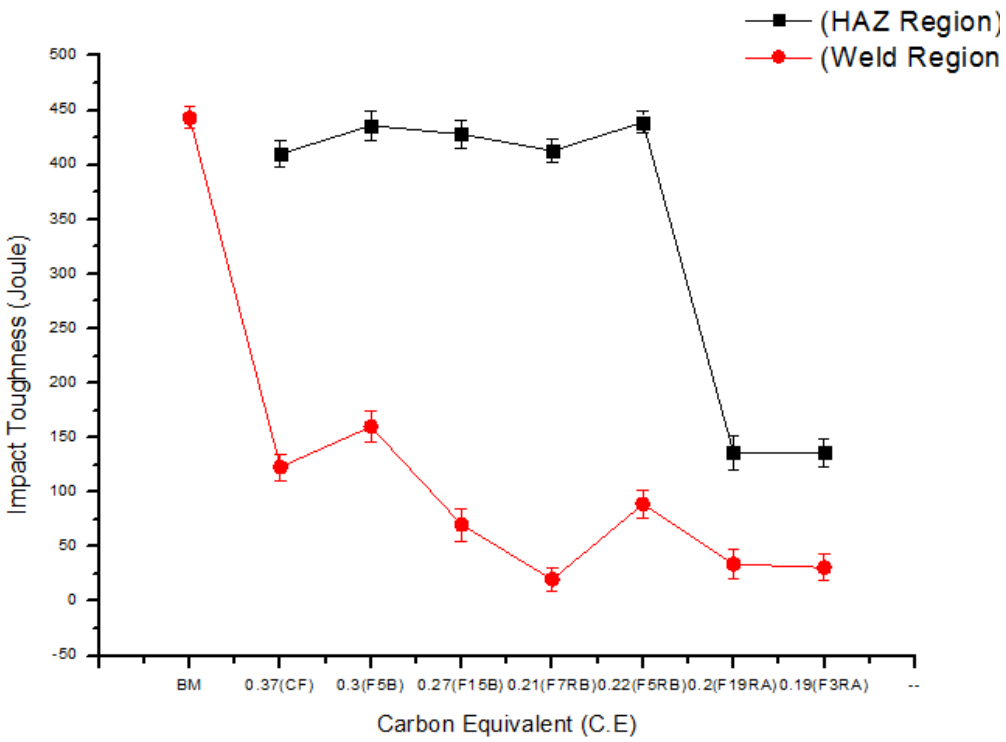

(a) Weld and HAZ region (Room Temp.)

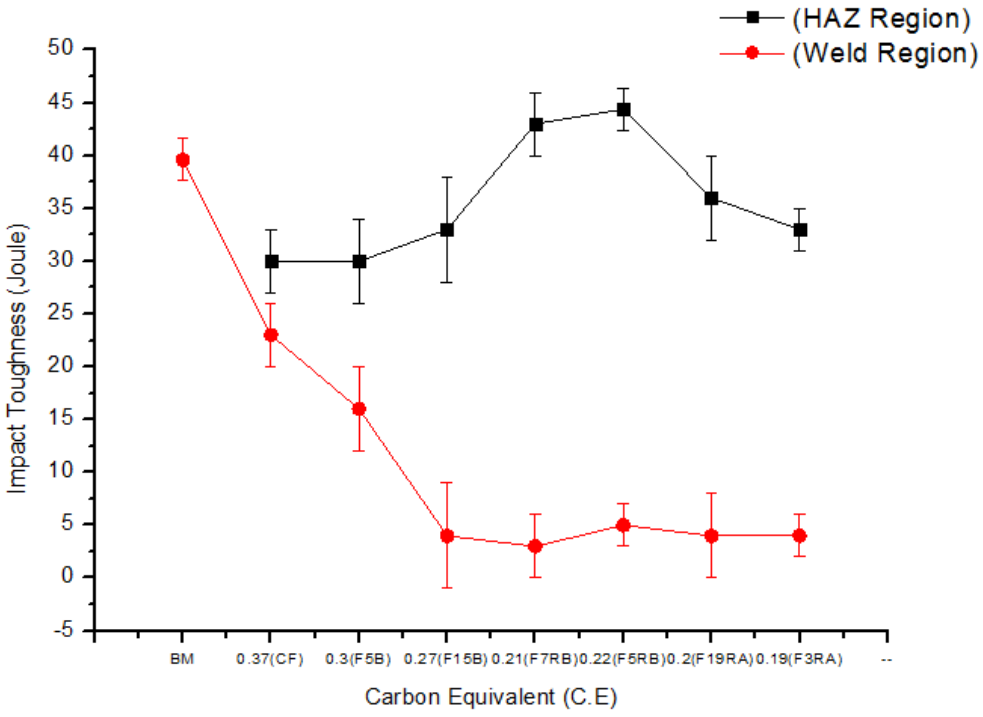

(b) Weld and HAZ region (-65° C)

Figure 5.42: Relation between impact toughness behaviour with carbon equivalent of base metal and weld specimens in (a) weld as well as HAZ region at room temperature (b) weld as well as HAZ region at -65° C

5.4.5 Tensile testing of weld specimens

For base metal as well as weld specimens, the tensile properties such as ultimate tensile strength, yield strength, and yield to tensile strength ratio were observed (Table 5.33). Base metal and weld joint prepared by commercial flux exhibits higher yield strength, ultimate

tensile strength and percentage elongation as compared to the remaining weld joints. Weld joint prepared by basic flux (F15B) shows comparable ultimate tensile strength and percentage elongation as obtained by commercial flux (Table 5.33). Weld joint prepared by rutile-basic flux (F7RB) shows the higher value of yield strength as compared to the remaining weld joints and almost near to the base metal's yield strength [Sharma et al., 2018]. Figure 5.43 (a-b) shows the relation between tensile properties as well as percentage elongation for weld joint specimens. Figure 5.44 shows the Force vs. Displacement graph for some of the weld specimens obtained from a similar test. F3RA & F19RA weld specimen gives lower tensile as well as impact toughness value as compared to the other weld specimen. A decrease in the tensile & impact toughness value of F3RA and F19RA is due to the acidic behavior of rutile-acidic flux. Available literature suggests that acidic fluxes give inferior mechanical properties as compared to the basic fluxes due to the presence of more oxide inclusion content [Bang et al., 2009]. Base metal shows higher tensile strength & toughness value as compared to other weld specimens due to the presence of fine ferritic-pearlitic microstructure. C.F and F5B weld specimen gives almost similar tensile and impact toughness value and higher than the remaining weld specimens. The high value of strength & toughness is due to the formation of acicular ferrite phase in the microstructure. Because it reported in the previous literature that the formation of acicular ferrite phase tends to improve the mechanical properties of weld metal. [Beidokhti et al, 2015].

Table 5.33: Base metal as well as weld metal tensile test properties

S.No	Specimen	YS (N/mm^2)	UTS (N/mm^2)	% E	YS/TS
1	BM	533	663	26.80	0.80
2	F5RB	411	517	22.0	0.79
3	F3RA	501	548.8	9.31	0.91
4	F5B	339.5	558.6	21.4	0.60
5	F7RB	527.8	528.6	17.4	0.99
6	F15B	454	561.8	23.57	0.80
7	F19RA	424.5	548.6	8.68	0.77
8	C.F	504	613	22.8	0.82

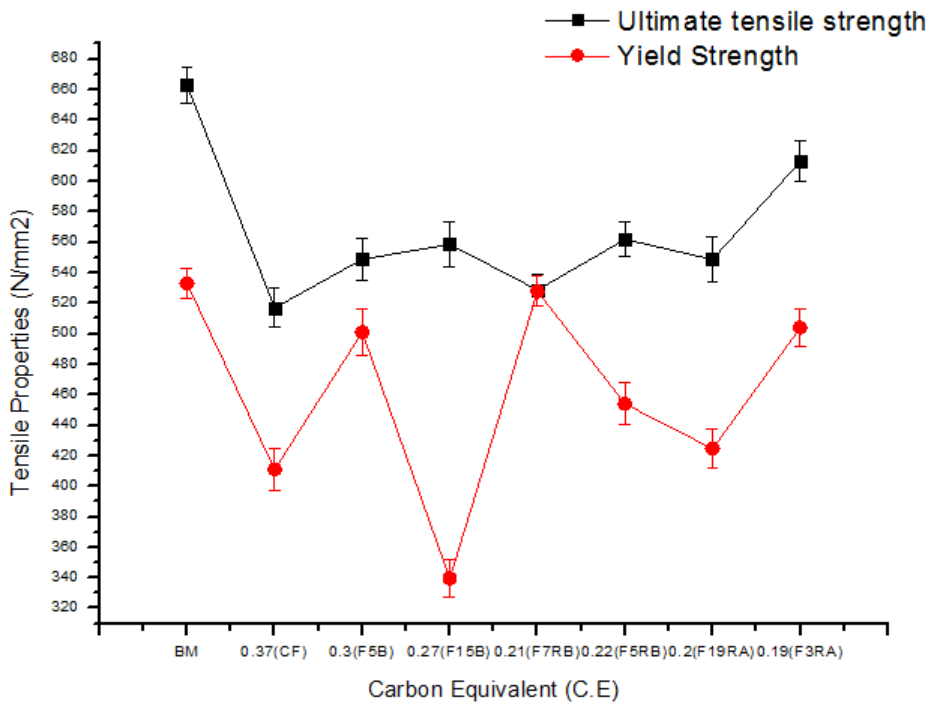

(a) Yield and Ultimate tensile strength

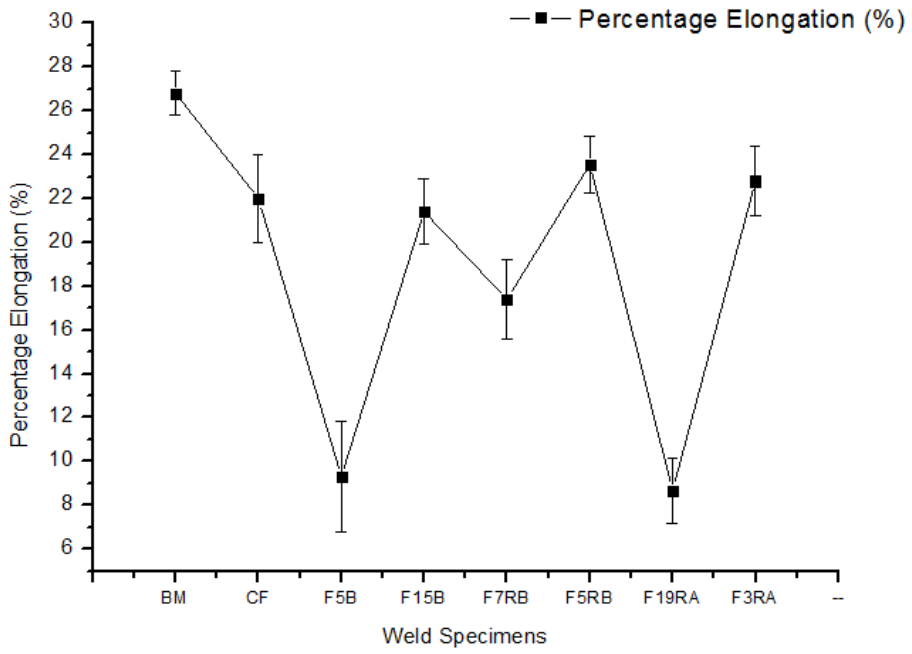

(b) % Elongation

Figure 5.43: (a) Relation between yield strength as well as ultimate tensile strength for weld specimens; (b) percentage elongation for weld specimens

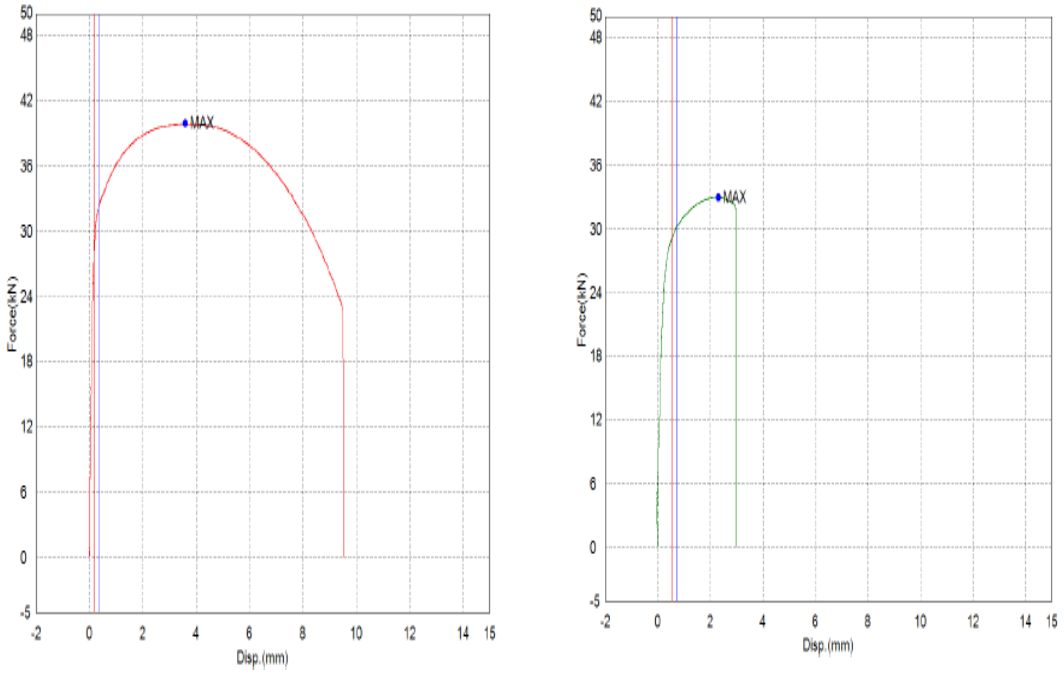

(a) Base metal (b) Weld F3RA

Figure 5.44: Force vs. displacement graphs for (a) base metal; (b) F3RA weld joint.

5.4.6 Hydrogen induced cracking of welds specimens

NACE TM0284-2003 standard used to study the hydrogen-induced cracking behavior of weld specimens. According to this standard test, specimens immersed in the solution (testing solution: sodium chloride plus acetic acid mixed in deionized water at ambient pressure) for 96 hours. After that, the microstructure analysis (at 100X magnification) of the specimens

performed to find any crack developed. A crack developed in the test specimen can be quantified by finding (Table 5.34) the crack length ratio (CLR), crack thickness ratio (CTR), and crack sensitivity ratio (CSR).

Table 5.34: Measured crack parameters for base metal and weld specimens

Weld Specimen	*∑a (mm)*	*∑b (mm)*	*W (mm)*	*T (mm)*	*CSR (%)*	*CLR (%)*	*CTR (%)*	*ASTM Grain size*
BM	4.8	0.50	33	22	32.91	14.50	2.27	6.5
C.F	4.5	0.50	33	22	30.97	13.63	2.27	6.2
F5B	5.0	0.40	33	22	27.54	15.15	1.81	6.4
F5RB	5.8	0.50	33	22	39.93	17.57	2.27	8.7
F3RA	6.4	0.62	33	22	54.64	19.39	2.81	8.5
F19RA	6.1	0.60	33	22	50.26	18.48	2.72	9.0
F7RB	5.6	0.40	33	22	42.40	16.96	2.50	9.0
F15B	5.2	0.45	33	22	32.14	15.75	2.04	6.0

Where a = length of crack, b = width of crack,W = specimen width and T = specimen thickness

Here W=33mm, T=22mm, ∑a and ∑b can be calculated from Section1 (S1) and Section2 (S2) shown in Figure 4.24 (b) (Section 4.6.6 Hydrogen induced cracking measurement of weld samples, in Chapter 4). Figure 5.45-5.46 shows the visual examination of specimen before and after immersion into the test solution.

Figure 5.45: Visual examination of specimens before immersion into the solution

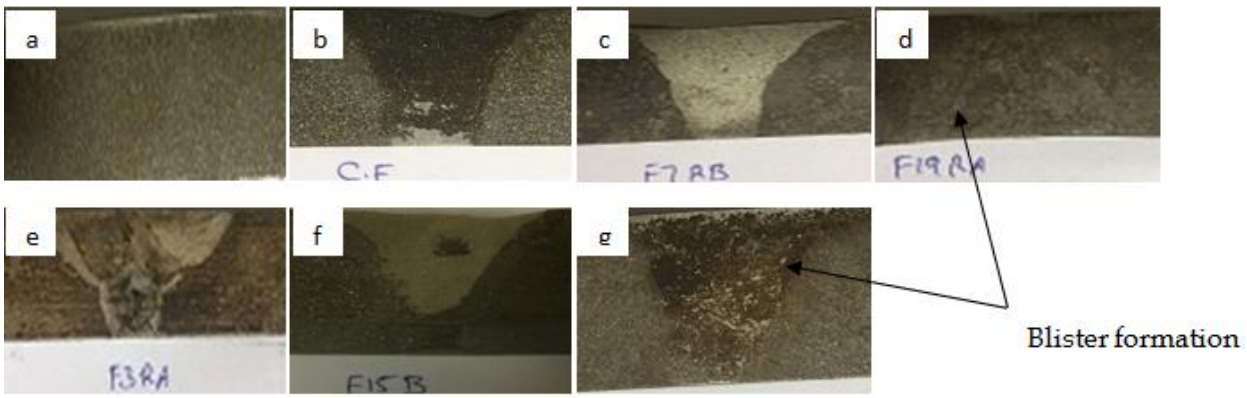

Figure 5.46: Visual examination of specimens after immersion into the test solution

After 96 hour exposure in the hydrogen sulphide solution, the microstructure analysis of base metal, as well as weld specimen, evaluated. Weld (F3RA & F19RA) prepared by using acidic fluxes show higher susceptibility towards hydrogen induce cracking as compared to the basic or

rutile-basic weld specimen. Figure 5.47 shows that base metal, as well as weld F5B and C.F gives minimum crack susceptibility as compared to the remaining weld specimen. Acicular ferrite with small inclusions of pearlite and bainite generally observed in all the weld specimens. There is a change in the microstructure due to variation in the grain size of the specimen after continuous exposure of weld specimens in the hydrogen sulphide environment [Sharma et al., 2018]. There is an increase in the grain size of some of the weld specimens (F3RA & F19RA) after the HIC test (Table 5.34) and show higher susceptibility towards cracking. Longitudinal (LC), as well as transverse cracks (TC), was developed in the weld specimens. Longitudinal cracks generally parallel to the weld centreline while TC extends perpendicular to the centreline (Figure 5.47). F3RA weld specimen exhibits transverse crack formation as compared to the other weld specimen. Transverse cracks generally developed in the low ductility areas. F3RA (%E=9.31) and F19RA (%E=8.38) specimens are having lower tensile strength as well as lower percentage elongation due to which they exhibit lower ductility. Higher crack susceptibility of acidic fluxes may be due to higher oxide content or lower carbon equivalent value (Table 5.30). Lower crack susceptibility was observed for weld F5B having an average grain size of 6.4 µm and mainly consisted of ferritic-bainitic microstructure. A previous study reveals that higher susceptibility of hydrogen cracking observed for specimens having intermediate average grain size as compared to the coarse or fine-grained specimen. It is because, at grain boundaries, there is faster diffusion of hydrogen or may be due to the entrapment of hydrogen at the nodes of triple points across the grain boundaries [Ichimura et al., 1991]. Base metal as well as F5B, F15B, and C.F weld specimen, shows fine acicular ferrite microstructure with small bainite inclusions.

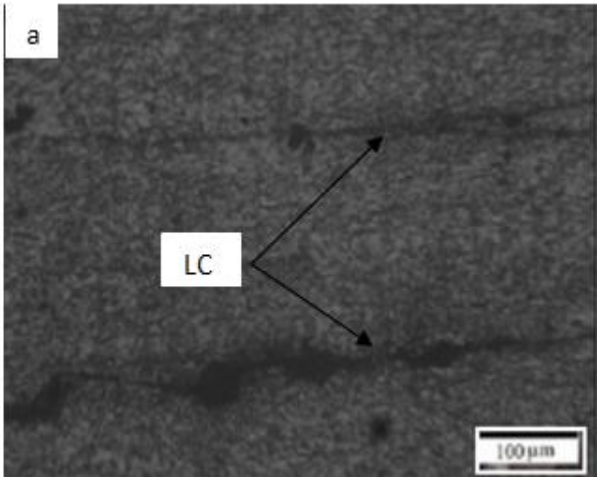

(a) Base metal

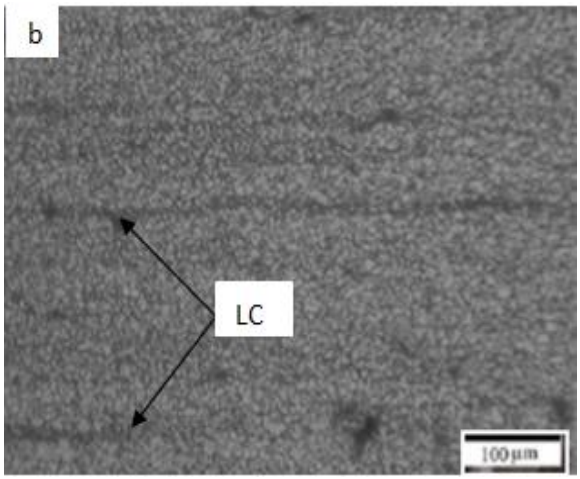

(b) C.F weld

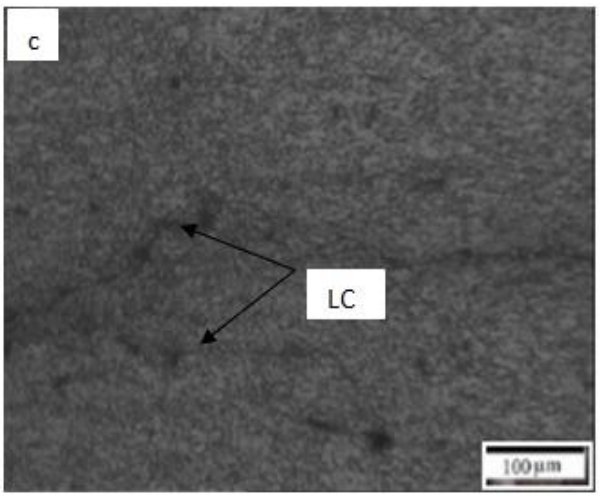

(c) F5B weld

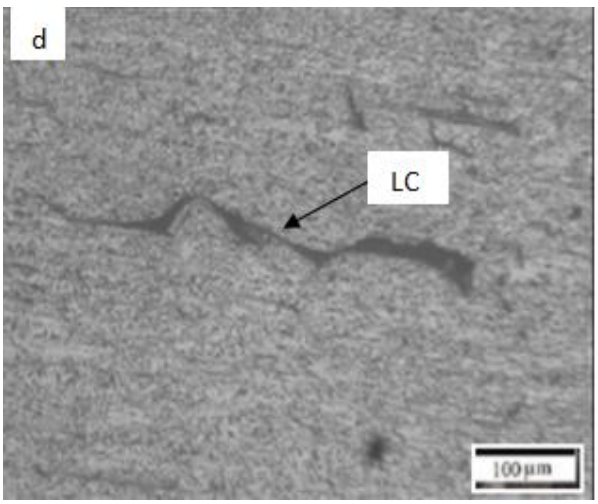

(d) F5RB weld

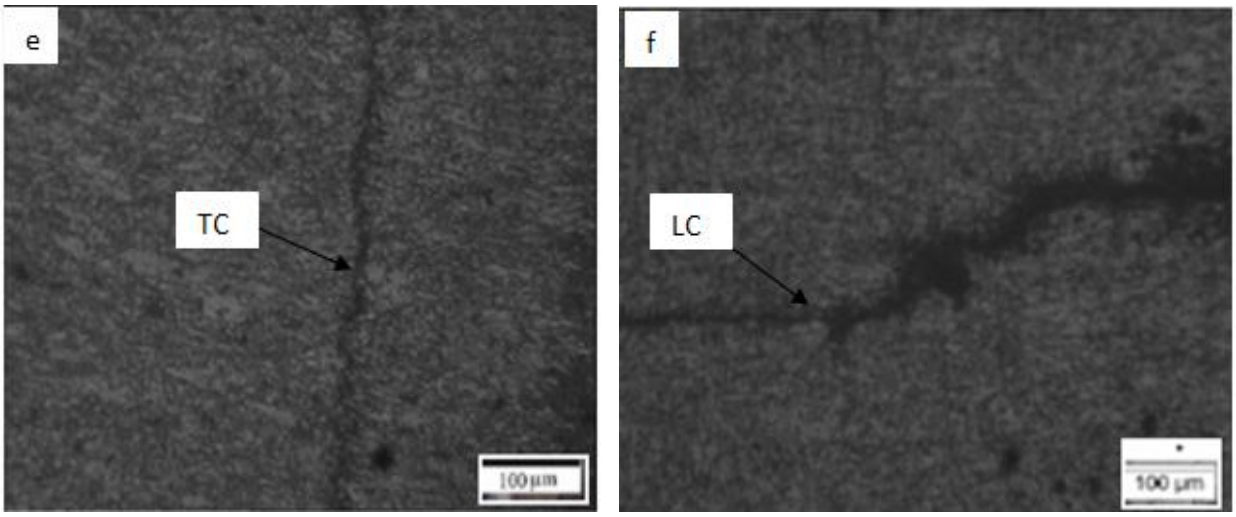

(e) F3RA weld (f) F19RA weld

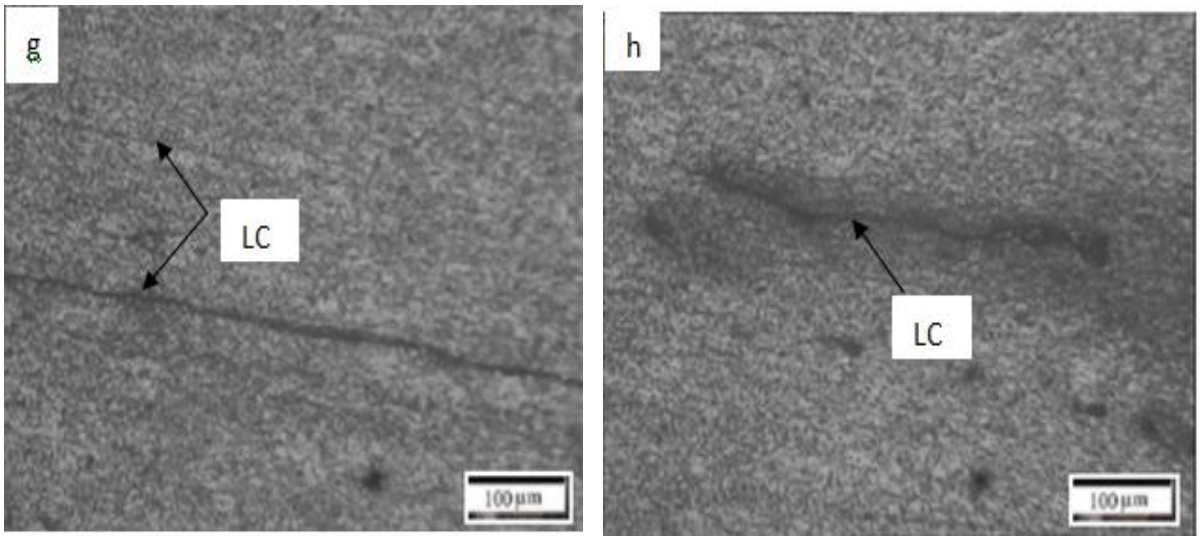

Figure 5.47: Microstructure analysis of hydrogen induced base as well as weld metal specimens

5.4.7 Electrochemical corrosion study of welds in different environments

Electrochemical corrosion behavior of weld specimens in different exposing environments was performed using Linear Sweep Voltammetry. Different exposing environments such as seawater and sodium thiosulphate solution (10^{-2} Mol/l, pH=3, and 10^{-3} Mol/l, pH=5) were taken for the corrosion study. Table 5.35 shows the electrochemical corrosion results of weld specimens in seawater and sodium thiosulphate solution. Figure 5.48 (a-c) shows the Tafel plots of different weld specimens in sodium thiosulphate and seawater medium. It observed that commercial weld (C.F), basic weld (F5B & F15B), and rutile-basic weld (F5RB) shows higher corrosion resistance or minimum corrosion rate (Table 5.35) as compared to the rutile-acidic welds (F3RA & F19RA).

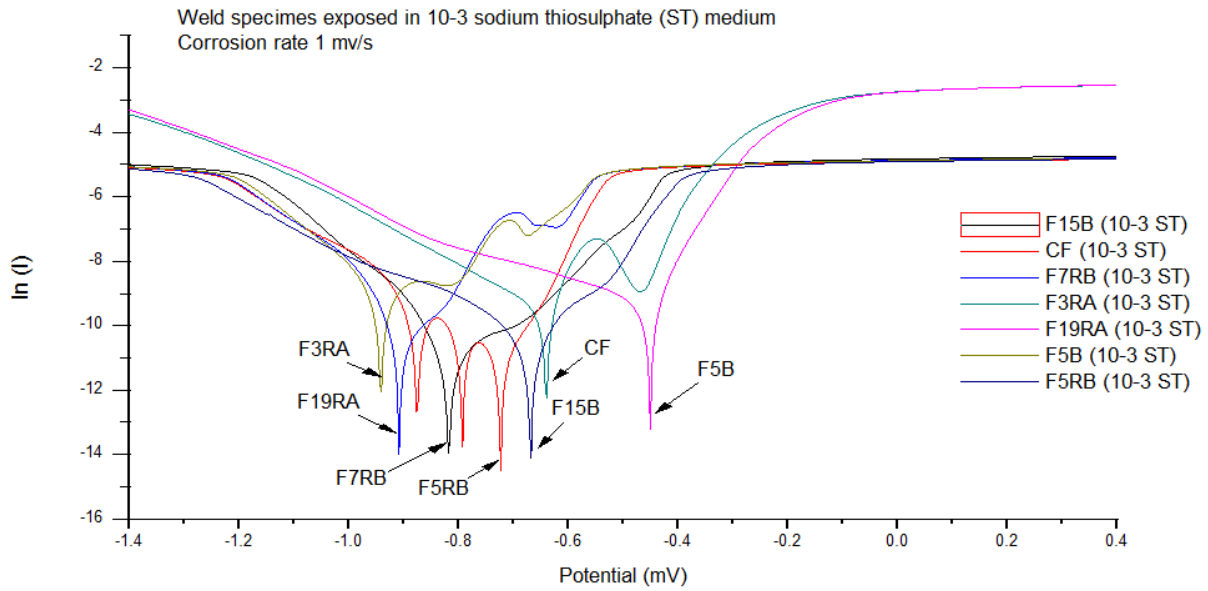

(a) Sodium thiosulphate solution (10^{-3} mol/l, pH=5)

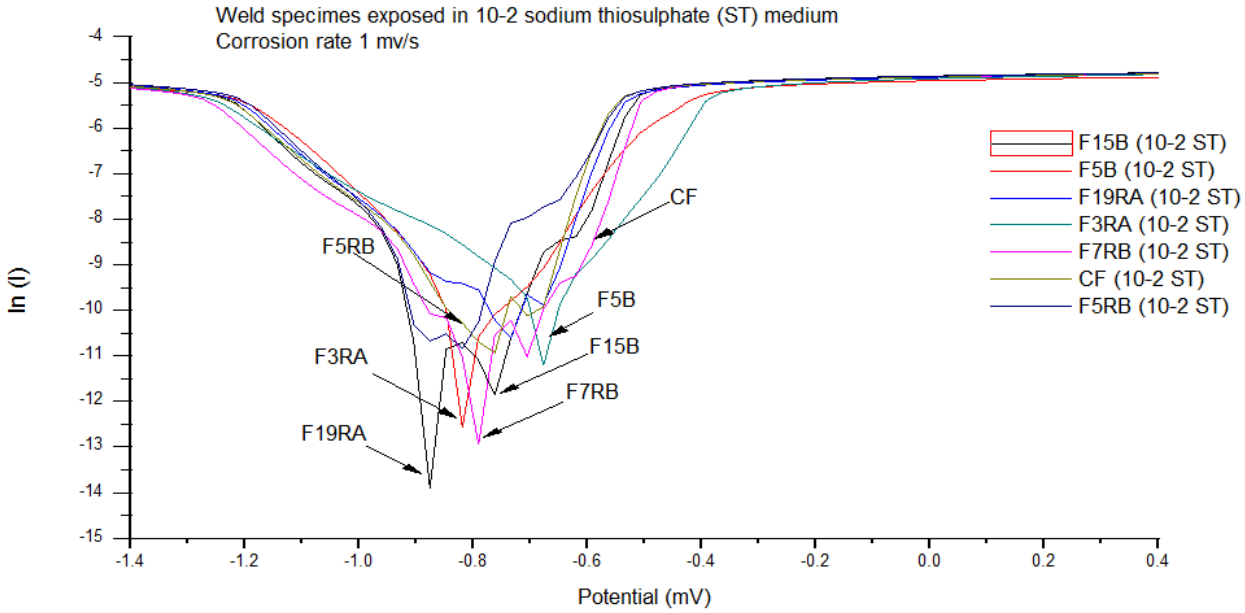

(b) Sodium thiosulphate solution (10^{-2} mol/l, pH=3)

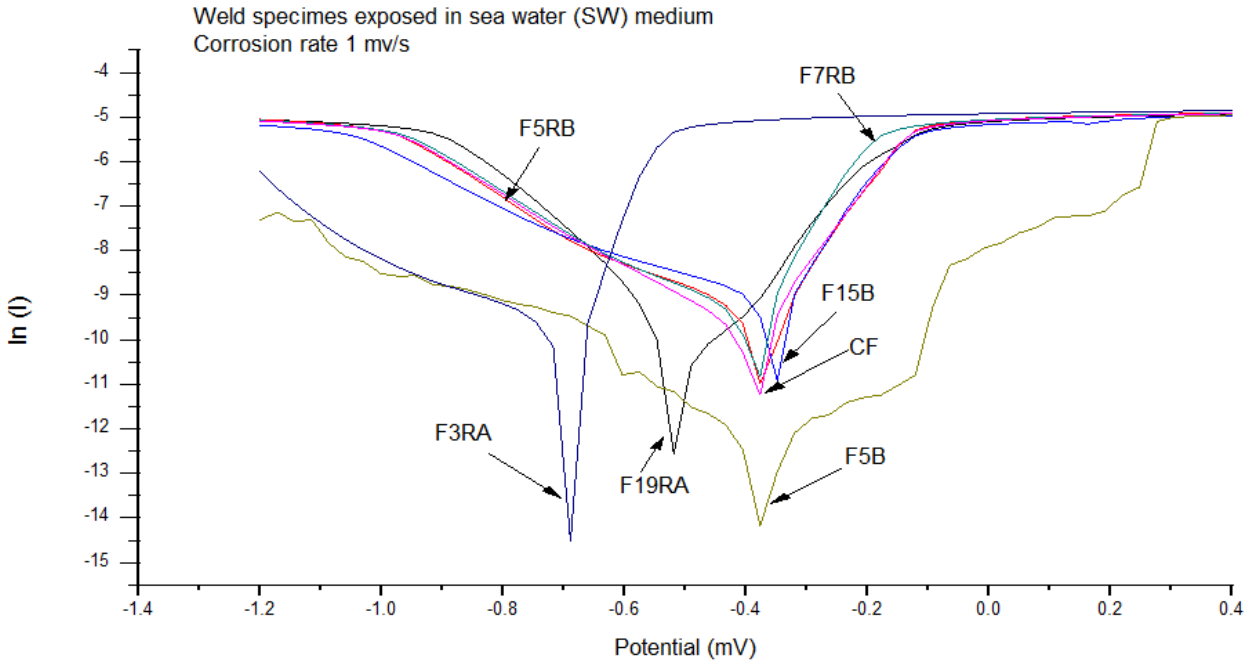

(c) Sea water medium (pH=8.2)

Figure 5.48: (a-c) Tafel plots of different weld specimens in sodium thiosulphate and sea water solution.

Higher the corrosion current density higher will be the corrosion rate and vice versa. F3RA and F19RA weld specimen shows higher corrosion rate (Table 5.35) in sea water and sodium thiosulphate medium (pH=3 or 5). Figure 5.48 (a-c) shows that almost similar corrosion rate beahviour was observed for commercial and F5B & F15B weld specimen.

Table 5.35: Electrochemical corrosion behaviour of weld specimens

S.No	α (mv/dec)	β (mv/dec)	E_{corr} Cal (mV)	J_{corr} (μA/cm²)	I_{corr} (μA)	C.R (mm/yr)	R_p (Ω)
F3RA (SW)	261.650	80.263	-693	11.775	35.560	0.1368	950.140
F19RA (SW)	171.360	116.300	-696	12.847	33.659	0.1492	983.500
F5B (SW)	178.120	155.750	-785	6.370	19.504	0.0743	15.616
F15B (SW)	247.800	56.358	-693	9.307	31.833	0.1081	626.430
F7RB (SW)	223..350	116.120	-679	14.662	44.280	0.1162	740.030
F5RB (SW)	110.590	109.160	-675	5.236	15.815	0.0608	1.508
CF (SW)	172.40	98.870	-672	12.040	36.361	0.1399	750.830
F3RA (10-2 ST)	165.310	221.780	-749	10.841	33.824	0.1259	360.00
F19RA (10-2 ST)	178.100	120.110	-720	12.511	22.131	0.1345	375.123
F5B (10-2 ST)	108.200	90.123	-920	13.413	5.531	0.0308	1.1260
F15B (10-2 ST)	82.895	127.230	-845	1.419	4.853	0.0164	4.4912
F7RB (10-2 ST)	134.490	157.930	-785	3.837	11.589	0.0445	2.7219
F5RB (10-2 ST)	135.510	84.731	-819	5.001	21.824	0.0589	1.0335
CF (10-2 ST)	134.870	201.620	-791	7.056	21.311	0.0819	1.6469
F3RA (10-3 ST)	249.180	81.252	-732	17.798	72.971	0.2068	364.670
F19RA (10-3 ST)	255.140	87.564	-734	17.342	77.342	0.2061	366.060
F5B (10-3 ST)	69.771	120.570	-901	7.587	19.880	0.0881	965.490
F15B (10-3 ST)	40.413	34.935	-781	5.110	20.954	0.0593	980.900
F7RB (10-3 ST)	239.880	50.084	-634	9.950	30.051	0.1156	598.800
F5RB (10-3 ST)	61.959	154.960	-824	3.552	10.728	0.0412	1.7918
CF (10-3 ST)	17.462	33.521	-770	1.224	3.698	0.0142	1.3482